LOW FREQUENCY VARIABILITY IN A SIMULATED ATMOSPHERE OCEAN SYSTEM

By

Robert L. Jacob

A dissertation submitted in partial fulfillment of the

requirements for the degree of

Doctor of Philosophy

(Atmospheric Science)

at the

UNIVERSITY OF WISCONSIN – MADISON

1997

Abstract

A new coupled ocean atmosphere model was constructed for the purposes of studying the low frequency internal variability of the atmosphere ocean system. Extant models of the atmosphere and ocean designed for execution on massively parallel computing platforms were combined via a new component called the coupler to form the new model. This model is the first to have a closed hydrologic cycle via a river runoff model, a simple sea ice model, and a relatively high resolution ocean model all in one simulation. No flux corrections or other restraints on the model climate are employed. The model climate compares well with other coupled models as seen in means and trends presented here. A simulation of over 600 years was performed.

An assessment of the model's low frequency variability was made with a rotated Empirical Orthogonal Function analysis of sea surface temperature in three frequency bands. The first mode of variability in the highest frequency band of interest (less than five years) was related to the model ENSO. In the midband frequencies (five to thirty years), a decadal mode in the Tropical Pacific is most prominent followed by an Antarctic mode and decadal variability in the gyres of the North Pacific and Atlantic. The multidecadal (thirty years and longer) variability is mostly in the form of a thermohaline oscillation in the North Atlantic with a period of nearly fifty years. Other low frequency variability centers occur near locations of model deep water formation.

Additional experiments were performed with the coupled model to determine

which of several new atmosphere parameterizations is most responsible for an improvement in the simulated Tropical Pacific over earlier model versions. The addition of a parameterization for deep convection is found to be most responsible.

Dedication

To the memory of my Mother and Father

Acknowledgements

I would like to thank my advisor, John Anderson, for giving me the opportunity to participate in this project and for his thoughtful guidance throughout. John always made himself available for consulting on even minor details and his clear vision of the big picture could always be called upon for inspiration. Hopefully I have acquired some of his wide-ranging expertise. I would also like to thank him for his amazing ocean model, without which this work would not have been possible.

The patience of my committee is most appreciated. Thanks to Professors John Young, Matthew Hitchman, Zhengyu Liu and John Magnuson for serving on the committee.

Development of FOAM would have been much slower without the uncanny abilities of Chad Schafer. Chad can fearlessly wade into thousands of lines of computer code he didn't write and make major changes without breaking the program. He wrote most of the code changes and additions required in the atmosphere model, developed a system of scripts to aid in running the model continuously, and made other valuable contributions too numerous to mention.

I would like to thank Ian Foster for providing this project with its connection to Argonne National Lab and the computer resources available there, also for his contributions to the development of FOAM and its atmosphere component. I would also like to thank Bruce Briegleb of NCAR and John Michalakes, Brian Toonen and Jace Mogill of Argonne for quickly answering questions about the

internals of the atmosphere model whenever they came up.

The river model of FOAM is based on the work of Mike Coe, who graciously gave me a copy of his stand-alone river model and patiently answered my many questions. Discussions with Ravi Nanjundiah clarified what was necessary to merge the river model with FOAM. Michael Tobis helped implement the R15 version of the parallel atmosphere model which was made possible by the work of Jim Tucillo at IBM.

On a more personal note, doing all of this without the love and support of Kristie Marks would be unimaginable. I would like to thank her for her patience and understanding throughout this process. Many thanks to our friends and family who where there for support or distraction, whichever was needed.

Much gratitude also goes to the Johnies of the tenth floor. Michael Tobis, Leigh Orf, Jim Boyle, Anne Notestein and former coworkers Gwen Jewett and Mary Tyree created an enjoyable and stimulating work environment. I was fortunate to have an officemate like Bob Gifford who always seemed to be studious or conversational at the same time that I was.

This work was supported by the DOE CHAMMP program.

List of Figures

List of Tables

Contents

Chapter 1

Introduction

1.1 Overview

The Earth's climate exhibits variability at many different time and space scales. The largest of these are driven by the solar forcing: the high frequency daily and seasonal cycle and the very low frequency alternations of glacier retreat and advance. Between these two extremes lies the internal variability of the climate system. Here we address variability that is not caused by external forces such as the solar geometry or volcanic activity but instead results from interactions between and within the components of the coupled system. The shortest time scale of interest is about one year. The most well known of these internal cycles is the El-Niño- Southern Oscillation (ENSO) phenomenon which has an irregular period of three to seven years and is fundamentally caused by the interaction of the atmosphere and ocean (Philander, 1990).

The full spectrum of internal climate variability is not yet known. One obvious reason for this is the lack of an instrument or proxy record with sufficient temporal and spatial resolution. This is especially true for any events with periods of decades or longer, what is normally called the low frequency variability of the climate. The existence of climate variability on long time scales has been proposed

based on paleoclimate evidence and other proxy records (Broecker *et al.*, 1985; Stocker and Mysak, 1992). Taken together, these data suggest rather broad band variability at periods of decades and longer. Instrumental data records have just recently achieved enough spatial and temporal span to reveal more information about decadal variability in the atmosphere-ocean system (Deser and Blackmon, 1993; Kushnir, 1994). In recent years a healthy interplay between observations and state-of-the-art coupled models has developed which is slowly leading to an understanding of the geophysical dynamics behind some low frequency variability.

(The term "variability" requires some clarification. In the literature, "variability" is used to describe everything from linear trends in a single variable, to discrete shifts in regional or global climate, to oscillatory behavior. ENSO, which is considered a low frequency oscillation to the synoptician, is high frequency noise from the perspective of decadal and interdecadal climate change.)

Most of the modeling work, summarized below, is motivated towards low frequency variability in specific regions: those with the best data coverage or where prior observational or theoretical studies has suspected low frequency internal variability. The work discussed here takes a slightly different perspective: how much low frequency internal variability is there in the global atmosphere-ocean system as a whole? Which modes are dominant over the globe and what are their characteristic patterns and frequencies? In other words, this study seeks an assessment or inventory of the ocean-atmosphere system's variability on decadal to century time scales which makes no prior assumptions about what form that variability might take.

Answering these questions by observations alone is limited by the inhomogeneity in space and time of measurements of the atmosphere-ocean system. In order to employ statistical techniques to delineate the low frequency variability, a long and globally comprehensive data set is preferred. A globally comprehensive data set could be simulated by a model of the atmosphere ocean system. But most coupled ocean atmosphere models are very expensive to run for long periods of time and so there are only a very small number of long runs available. Further, of the small number of models which have long integrations, all restrict the possible range of climate variability in some way, typically through the use of flux corrections.

To assess the low frequency variability in the coupled ocean-atmosphere system, a new coupled ocean-atmosphere model has been constructed which can be inexpensively integrated for many hundreds of years and which has more degrees of freedom than other modeling efforts. Massively parallel supercomputing is employed to achieve these combinations of long integration times and high model fidelity. Analysis of the resulting data set can provide an estimate for the total spectrum of internal variability in the ocean-atmosphere.

The following sections review past and current efforts to model internal variability in the atmosphere-ocean system. Additional observational evidence will be reviewed in the discussion of the results. Chapter 2 contains a description of the components of the new coupled model which is called FOAM, the Fast Ocean Atmosphere Model. A brief overview of the models simulation is given in Chapter 3 and results from a rotated Empirical Orthogonal Function (EOF) analysis of the sea surface temperature variability are presented in Chapter 4. During model

development, it was found that simulation of internal variability in the tropics depends greatly on parameterizations in the atmosphere and these issue are explored in Chapter 5. The conclusions are summarized in Chapter 6.

1.2 Low Frequency Variability in Ocean Models

The ocean has the ability to create and control variability on long time scales simply by virtue of its bulk thermodynamic properties (Mikolajewicz and Maier-Reimer, 1990). Much of the early modeling work on internal variability uses ocean-only models. Attention was first focused on the longest time scales: changes in the ocean's thermohaline circulation involving tens and hundreds of years. The thermohaline circulation (THC) is the slow meridional overturning circulation, driven by heat and freshwater fluxes, which accounts for most of the oceanic heat transport poleward of 45 degrees. Any changes in its magnitude could have profound regional and global effects. To a first approximation, the low frequency variability of the atmosphere-ocean system is bounded by the variability in the thermohaline circulation.

Understanding the possible variability in the THC began with the work of Henry Stommel who studied a simple analytical model of the ocean consisting of two well-mixed boxes of saltwater subject to both heat and salt forcing. This model circulation has two stable states and each can be reached from the other by applying perturbations (Stommel, 1961). Stommel speculated that this vulnerability may be present in the real ocean with obvious implications for climate variability but despite these provocative conclusions, his work went under appreciated for over

twenty years.

A series of researchers looking for a source mechanism of some of the oscillations seen in paleoclimate records settled on the thermohaline circulation and the freshwater forcing (Weyl, 1968; Rooth, 1982; Walin, 1985). Broecker *et al.* (1985) suggested that climate fluctuations evidenced from ice cores and other paleoclimate data around the North Atlantic was caused by anomalous freshwater fluxes periodically shutting down deep water production there. (The deep water production provides the downward branch of the thermohaline circulation.) This and the foregoing work finally prompted the first study of thermohaline variability in a primitive equation ocean circulation model by Frank Bryan (Bryan, 1986).

1.2.1 Box Geometry Ocean Models

F. Bryan was aware of the work of Stommel and Rooth. Rooth had pointed out that salinity and temperature anomalies have different feedback paths. Salinity has little effect on the precipitation and evaporation from the atmosphere while sea surface temperature (SST) is strongly linked to the heat flux. Almost all of the ocean modeling work before Bryan had used just one buoyancy variable or did not take into account the different feedback paths. To force salinity with little or no feedback while retaining the feedback on temperature, Bryan introduced the mixed boundary condition for ocean general circulation models (OGCMs). In the mixed boundary condition, the heat flux is still a linear function of the difference between the model's prognostic SST and some equivalent atmosphere temperature (usually taken to be observed SST (Haney, 1971)) while the freshwater flux is a constant

field. Bryan demonstrated that, as in Stommel's simple model, the thermohaline circulation in a full OGCM had multiple steady states that could be reached by perturbations in the freshwater forcing. Another phenomenon discovered in the model was the Polar Halocline Catastrophe: a collapse of the thermohaline circulation that occurred after the switch to mixed boundary conditions.

F. Bryan's seminal work spawned a large body of follow-up literature which sought to classify the number of steady states of the oceans thermohaline circulation and their stability under mixed boundary conditions. Subsequent researchers followed many of the precedents set by F. Bryan; employing mixed boundary conditions and an OGCM in a box-shaped basin. The ocean model of choice was an early version of the what became the Modular Ocean Model of the Geophysical Fluid Dynamics Laboratory (GFDL) based on the work of K. Bryan (1969) and Cox (1984). The horizontal resolution for all this work is typically coarse, from 3x3 to 4x4 degrees. Vertical resolution is anywhere from 12 to 15 levels.

The first follow-up work rapidly expanded the types and mechanisms of thermohaline variability. Marotzke *et al.* (1988) confirmed many of Bryan's results in a two dimensional model. Marotzke (1989) also found an oscillation in the model's thermohaline circulation where a state with no THC would periodically undergo violent flushing events with a strong THC after the ocean was destabilized by the vertical diffusion of heat.

A thorough study of thermohaline variability in Bryan-Cox type OGCMs, taking into account resolution, parameterization constants, forcing strength, etc., revealed decadal scale variability as well (Weaver and Sarachik, 1991b; Weaver and Sarachik, 1991a). This oscillatory behavior was caused by the advection of salinity

anomalies in high latitudes which alternately slow down and speed up the rate of deep water formation and the thermohaline circulation. The amount of variability was found to directly depend on the strength of the freshwater forcing portion of the mixed boundary condition (Weaver *et al.*, 1993).

The types of internal variability found in these box-geometry OGCMs under mixed boundary conditions spans the range from decadal, to interdecadal (Yin and Sarachik, 1995), to century scale and millennial (Chen and Ghil, 1995; Stocker, 1996) They have also been seen in non-Bryan-Cox models which use linear momentum advection (Winton and Sarachik, 1993). But in all cases the character of the mixed boundary condition, especially the strength and structure of the freshwater flux, plays a crucial role in the existence of the variability. For example, Chen and Ghil (1995) found interdecadal variability if the high latitude freshwater flux had net evaporation and decadal to interdecadal variability if it had net precipitation. Since there is no clear way to equate the box model freshwater forcing with the real freshwater forcing, even assuming the latter was measured well, extending these results to the real atmosphere-ocean system is problematic.

Estimating the variability in the atmosphere-ocean system with ocean-only models is complicated by this relation between the THC variability and the boundary conditions. Mixed boundary conditions are an ad hoc substitute for an atmosphere and may be overestimating the possibility for thermohaline variability (Zhang *et al.*, 1993; Tziperman *et al.*, 1994). Other boundary conditions besides mixed have been able to create thermohaline oscillations but again the interaction with the boundary condition determines the solution (Huang and Chou, 1994; Zhang *et al.*, 1995; Greatbatch and Zhang, 1995).

The box geometry itself may also be overestimating the THC variability (Winton, 1996; Greatbatch and Peterson, 1996; Winton, 1997). The latter problem is avoided in ocean models which employ realistic ocean bottom topography and basin boundaries. Despite concerns about the mixed boundary condition, THC variability studies have been extended to full-global ocean models which are also reviewed.

1.2.2 Global Ocean Models

In general there are fewer studies of thermohaline variability in full global OGCMs mostly due to the computational expense of long full global ocean runs. The Hamburg Large Scale Geostrophic (LSG) Model, a fully implicit OGCM which neglects the nonlinear momentum terms, was one of the first used to study long term internal variability thanks to its one month time step. With the standard LSG configuration, 3.5x3.5 with 11 vertical levels and realistic bottom topography, Mikolajewicz and Maier-Reimer (1990), (hereafter MMR90), found a 320 year oscillation in the thermohaline circulation. They were the first to add a new feature to the mixed boundary condition: a spatially coherent white noise forcing was added to the standard diagnosed freshwater flux to approximate the randomness of the atmosphere P-E field. (Just how much the atmosphere's freshwater forcing resembles a white noise process is debatable.) Their model showed little variability without it. MMR90 found support for a 300 year oscillation in the paleoclimate evidence. The existence of the 300 year oscillation found in the LSG model by MMR90 does not depend on the character of the noise (Barnet *et al.*, 1994) and

can exist without the random component if the base surface freshwater flux is strong enough (Pierce *et al.*, 1995). Users of the box geometry models also found oscillations on a similar time scale when a white noise field was added to their freshwater forcing (Mysak *et al.*, 1993; Weaver *et al.*, 1993).

Other global OGCMs with realistic topography, including those based on the Bryan-Cox model, were found to contain variability on decadal and longer time scales in the THC (Moore and Reason, 1993; Tziperman *et al.*, 1994; Drijfhout *et al.*, 1996). The fact that THC variability is still seen in more realistic models with bottom topography is encouraging but the results still depend on the exact formulation of the boundary conditions (Osborn, 1997; Maier-Reimer *et al.*, 1993; Tziperman *et al.*, 1994).

The possibility that thermohaline circulation changes may be responsible for low frequency climate variability is still considered a very real one. But estimates of that variability using ocean only models are connected almost entirely to the rather arbitrary boundary conditions. The mixed boundary condition augmented with noise in the freshwater forcing is just not an adequate substitute for a real atmosphere. The situation was summed up nicely in a recent review by one of the box model researchers:

> When variability is found under mixed boundary conditions, it will be taken as smoke: whether or not there is fire will be left to more complex coupled atmosphere-ocean models....[T]here is no 'correct' boundary condition for an ocean-only model since there is no single boundary condition that can give both the correct fluxes and the correct time change of fluxes: the only correct and consistent boundary condition is given

by a correct atmosphere consistently coupled to the ocean (Sarachik *et al.*, 1996).

An atmosphere model automatically provides all the correct feedbacks, variability, and magnitudes in the freshwater and heat flux forcing fields, at least to within the accuracy of the model parameterizations. For the purposes of thermohaline variability studies, the atmospheric general circulation model (AGCM) is, in effect, an elaborate parameterization scheme for the ocean's boundary conditions.

1.3 Low Frequency Variability in Coupled Models

So far there have been few applications of coupled ocean-atmosphere models to the study of thermohaline variability, mostly because of the computational demands. The few existing results are summarized next.

Most of the coupled ocean-atmosphere models developed over the past decade have been constructed to study CO_2 induced climate change (Meehl, 1990; Washington and Meehl, 1989; Manabe *et al.*, 1991; Cubasch *et al.*, 1992). When a coupled model is applied to anthropogenic climate change issues, the standard practice is to impose some increase in CO_2 and compare the resulting climatology with a control run. Typically the internal variability of the control run was regarded as an obstacle rather than a subject of study and the run times have been too short, on the order of a few decades, to provide useful statistics for low frequency variability studies.

In the late eighties and early nineties, coupled models for the study of El-Niño began to appear (Neelin *et al.*, 1992; Neelin *et al.*, 1994). In these applications the relatively high frequency variability of ENSO is the subject of study. The integrations are again of short duration and usually only the tropical Pacific ocean is actively modeled while the atmosphere is often greatly simplified. However, there have been reports of internal decadal and secular variability in at least one of the ENSO models (Zebiak and Cane, 1991). But again they are not the right tool for an assessment of the whole Earth's low frequency variability.

The number and variety of programs calling themselves coupled models is growing rapidly. They can be roughly classified as follows (Neelin *et al.*, 1994):

ICM Intermediate Coupled Model–approximate models, such as shallow water models, coupled together with parameterizations for fluxes, etc.

HCM Hybrid Coupled Model–one component, usually the ocean, is a full GCM and the other is some simple model such as an energy balance model.

To which we add:

FCM Full Coupled Model–both atmosphere and ocean are full GCMs which solve the primitive equations.

There will of course be models which don't fit neatly into any category. In this section we summarize the few low frequency variability studies available for FCMs.

A recent table of FCMs provided by Meehl (1995) is adapted and updated in Table 1. The models are grouped roughly according to the combined resolution of the component atmosphere and ocean models. The wide variety of coupled

models built and run by different groups, accompanied by close communication between those groups, is seen as an effective way to converge on the best possible model (Meehl, 1995).

Table 1: Some Current Full Coupled Models

Resolution	Group	Name	AGCM	OGCM	Comments
High	NCAR	CSM[1]	T42 L18 CCM3	2x2 L45 (GFDL MOM2)	no rivers,D
	MPI (Germany)	ECHO[2]	T42 L19 ECHAM3	2.8x2.8 L20 HOPE	no sea ice,D
	MPI	ECHO2[3]	T42 L19 ECHAM4	2.8x2.8 L20 HOPE-2	no sea ice
Medium	UW/Argonne	FOAM	R15 L18 PCCM3	1.4 x 2.8 L16	fully parallel,D
	CERFACS (France)	none[4]	T21 L30 ARPEGE	2x1.5 L31 OPA	no rivers, climo soil temps
Low	GFDL	none[5]	R15 L9 GFDL	4.5x3.75 L12 GFDL	F,D
	MPI	none[6]	5.6x5.6 L19 ECHAM1	4x4 L11 LSG	F,D
	GISS	none[7]	4x5 L 9 Model II	4x5 L13	no flux cor
	CSIRO (Aust)	none[8]	R21 L9 (and L4)	3.2 x 5.6 L12 GFDL	F
	Hadley Centre (UK)	none[9]	2.5x3.75 L19 UK	2.5x3.75 L20 GFDL	climo land surface forcing, no rivers, F

1. Boville and Gent (1997)
2. Latif *et al.* (1994)
3. Frey *et al.* (1997)
4. Guilyarid and Madec (1997)
5. Manabe *et al.* (1991)Manabe and Stouffer (1994)
6. Cubasch *et al.* (1992, von Storch *et al.* (1997)
7. Russell *et al.* (1995)
8. Gordon and O'Farrell (1997)
9. Johns *et al.* (1997)

F = Flux corrections employed
D = Decadal variability studied

Only recently have coupled models of any type been applied to the study of decadal and longer natural variability. A recent review by Latif (1996) summarizes the findings for the decadal and interdecadal scales in coupled models (of all types) in four categories: decadal variability involving the tropics, involving tropic–mid-latitude interactions, mid-latitude only modes, and decadal variability involving the mid-latitudes and the THC. A "D" in Table 1 appears in the comments section for any model reported to have internal decadal or interdecadal variability.

Using ECHO, Latif and Barnett (1996), hereafter LB96, have found interdecadal variability in the North Pacific and North Atlantic. Their proposed mechanism is a coupled mode involving interaction between the subtropical ocean gyres and atmosphere gyres (Latif *et al.*, 1996). (As noted by the above authors, the possibility of low frequency midlatitude coupled variability was first raised by Namias (1959) and Bjerknes (1964).) Similar modes have also been seen with the lower resolution MPI model consisting of ECHAM1 and LSG in the North Pacific (Robertson, 1996) and North Atlantic (Zorita and Frankignoul, 1997). But a general assessment of the either model's variability is still lacking.

The GFDL coupled model was one of the first models to study variability in the lowest frequencies thanks to the long integration periods available. Manabe and Stouffer (1988) found that an early version of the coupled model, with only annually averaged insolation, could be driven to two different states and remain there while fully coupled. One had a normal THC circulation and the other had none. This lent early support to ocean-only work which found multiple steady states of the THC including collapses of the thermohaline circulation.

The current version of the GFDL coupled model, which includes the seasonal

cycle, has undergone a very long integration. A series of papers have studied its CO_2 sensitivity and internal variability as 3 runs of the model, a control and 2 types of CO_2 increase, reached 100 years (Manabe *et al.*, 1991; Manabe *et al.*, 1992), 500 years (Manabe and Stouffer, 1994), 600 years (Delworth *et al.*, 1993), 1000 years (Delworth, 1996; Manabe and Stouffer, 1996; Knutson and Manabe, 1997), and 2000 years of simulated time (Delworth *et al.*, 1997). The model has found support for other ocean-only results such as the thermohaline strength dependence on freshwater perturbations (Stouffer, 1995).

A seminal study of low frequency variability in a coupled model is Delworth, Manabe, and Stouffer (1993), hereafter D93. Using the GFDL model, D93 found a 50 year oscillation in the THC of the model North Atlantic. The proposed oscillation mechanism involved density anomalies and associate gyre circulation anomalies which interact with the mean salinity field to alternately increase and decrease the THC. The SST differences between strong and weak phases resemble SST patterns found in observational data (Kushnir, 1994). This mode has been shown to be qualitatively similar to a linear damped oscillator driven by stochastic weather noise (Griffies and Tziperman, 1995). Latif (1996) cites a reproduction of this mode in an HCM and a 50 year oscillation has also been seen in the Climate System Model (CSM) (Capotondi and Holland, 1997).

The GFDL model has also had success in simulating the observed low frequency variability in surface air temperature (Manabe and Stouffer, 1996) and has also shown some evidence for decadal and multidecadal variability in the tropical Pacific, although its ENSO variability is lower than observed (Knutson and Manabe, 1997).

1.4 Summary and Motivation

The coupled model studies of low frequency variability provide obvious improvements over the ocean-only studies. But there is still a need for an objective assessment of the low frequency variability and there are reasons why a time series from any of the models discussed above may be inadequate.

A coupled model which has as many possible sources of unforced variability as the actual ocean-atmosphere system is sought. Low resolution models such as the GFDL are limited in their possible variability, especially the simulation of ENSO, by their ocean resolution. Their authors are the first to admit that confirming results from higher resolution models are needed (Knutson and Manabe, 1997). Thus one of the features needed in a new coupled model is higher ocean resolution.

Many of these low resolution models employ flux corrections (indicated with an "F" in Table 1). Flux corrections were formulated to reduce the initial drift a coupled model exhibits when the separately spun-up components are first coupled (Sausen *et al.*, 1988; Sausen and Ponater, 1990). Flux corrections essentially prevent any large, sustained variability by keeping the surface fluxes at the atmosphere ocean surface close to some predefined mean. They may also be a spurious source of variability (Neelin and Dijkstra, 1995; Chen and Ghil, 1995) and in general should not be used in any simulation where a new mean may be reached (Sausen and Ponater, 1990). So to allow a coupled ocean-atmosphere to range freely, flux corrections should not be applied.

The ECHO model does not have any sea ice component; it instead relaxes SSTs to climatology poleward of 60°. Some kind of simple sea ice model should be

included so that high-latitude sources of variability involving atmosphere-ocean-sea ice effects can be realized.

Another component often neglected in coupled models is the hydrologic cycle. An important part of the hydrologic cycle, the return of land-based precipitation to the ocean, is either neglected or handled by some non-physical means. Interaction between the full hydrologic cycle and the THC creates one of the the longest internal time scales available in the climate system (Rooth, 1982). In the new coupled model, the hydrologic cycle is closed with a river runoff model, an approach also taken in the coupled model of Russell *et al.* (1995).

The other coupled models of Table 1 either do not have a long enough integration available or are too computationally expensive to produce one. Long integration times at modest cost are achieved by using relatively inexpensive massively parallel supercomputers and component models designed to run efficiently on them.

A new coupled model called FOAM, for Fast Ocean Atmosphere Model, which contains all of these features has been constructed and is described next.

Chapter 2

Model Description

The goal of the FOAM project was to combine low resolution and massive parallelism to achieve climate model integrations that are both longer and contain more degrees of freedom than other efforts. All of this was to be accomplished at a modest computational cost.

In the taxonomy proposed by Neelin *et al.* (1992), FOAM is a high-vertical, medium-horizontal resolution OGCM coupled to a high vertical, low-horizontal resolution AGCM. This combination of resolutions makes FOAM a "medium resolution" coupled model. A medium resolution model is assumed to be the best choice to simultaneously provide a significant increase in climate simulation accuracy over low order models such as the GFDL CGCM while not incurring the computational cost of high resolution models such as ECHO or NCAR's CSM.

Significant improvements in the atmospheric physics over models such as GFDL is achieved by using CCM3, the third release of the NCAR Community Climate Model. The horizontal resolution of the atmosphere is the same as in the GFDL model but CCM3 has twice the vertical resolution and complete physics packages. The ocean dynamics are better represented in FOAM's ocean model which has 4 times the resolution of the GFDL model. FOAM's OGCM is based on the same physics as the Bryan-Cox model but the numerical methods were designed for

efficient execution on massively parallel processing (MPP) supercomputers. MPP was chosen for FOAM to achieve high throughput (simulated time per real time) at relatively low cost compared to the vector-parallel supercomputers used in most climate model applications.

Before further describing FOAM, a brief review of parallel computing is in order. A parallel computer is best thought of as a collection of individual computers, each with its own CPU and memory, and in some cases, its own disk space. The combination of a single CPU, its memory and disk is called a *node* of the system. Typical massively parallel computers contain hundreds or thousands of nodes. The memory available is then the product of the number of nodes and the memory on each. This gives effective memory sizes of tens to hundreds of gigabytes. More memory and processing power can be gained by adding more nodes.

When programming a geophysical fluid problem for parallel computers, the standard approach is to imagine the horizontal global domain laid out onto a horizontal grid of nodes, a two-dimensional decomposition. Each node then works only on its part of the finite difference mesh. When information is needed from a point which is logically adjacent to the local point but is really being handled by another node, some method of communication must be provided by both hardware and software to send and receive data between nodes. The software is usually an external library of new routines which must be integrated into the program by the programmer. FOAM uses the Message Passing Interface (MPI) standard library to communicate between nodes (Gropp *et al.*, 1994). The hardware can be special purpose switches or ethernet.

The total time the data passing takes per timestep is the biggest drawback

to parallel processing. The applications best suited to MPP are those that don't require a great deal of message passing or only passes data between nearest neighbors. Ideally an application will run twice as fast if one doubles the number of processors but communication costs generally prevent any given application from reaching this ideal. In well designed applications such as FOAM's ocean model, the speedup is near-linear.

In developing the coupled model existing parallel models were used wherever possible rather than making new models from scratch. The atmospheric component started out as PCCM2, a functionally equivalent version of CCM2 adapted for parallel computers by teams at Oak Ridge and Argonne National Laboratories. PCCM2 uses a two dimensional decomposition (Drake *et al.*, 1995) and MPI for the communication between nodes. The physics was later upgraded to CCM3 and the resulting model is referred to as PCCM3. The ocean model was developed at the University of Wisconsin-Madison. It is dynamically similar to the GFDL Modular Ocean Model (MOM) but contains a unique collection of numerical techniques designed for high efficiency on parallel computers. To link these two models together, a third component, called the coupler, was created. The coupler performs multiple duties such as implementing the land surface and sea ice models and calculating the fluxes of heat and momentum between the atmosphere and ocean models.

The coupler and ocean model also have two-dimensional decompositions. In practice, the coupler and atmosphere run on the same collection, or partition, of nodes while the ocean runs on a separate partition. The size of each partition can be varied according to the demands of each component and the desired throughput. The atmosphere typically require 16 nodes to keep up with ocean running on one

node despite the ocean having a factor of 8 greater resolution. Communication between and within the components is via MPI. Each submodel is described in more detail below.

2.1 Atmosphere Model

As mentioned above, the algorithmic basis for the atmospheric component of FOAM was CCM2, the well known climate model produced by NCAR and described in detail by Hack *et al.* (1993). Because FOAM was to employ massively parallel computers in its integrations the starting point was PCCM2, a functionally equivalent version of CCM2 which employs a 2D horizontal domain decomposition, a parallel version of the spectral transform and semi-Lagrangian transport (SLT), and special algorithms for balancing the load across the nodes (Drake *et al.*, 1995). The radiative and hydrologic changes to the physics from CCM2 to CCM3, described by Kiehl *et al.* (1996), have since been incorporated into FOAM. The atmospheric component of FOAM will be referred to as PCCM3 although it is not functionally equivalent to CCM3 and was developed directly from the the PCCM2 code. To describe FOAM's atmospheric component, an overview of PCCM2 is given first and then the portions of CCM3 which have been incorporated into FOAM are reviewed. For convenience important features and their associated references are recalled here but detailed descriptions and derivations of the equations and physics can be found in Hack *et al.* (1993) and (Kiehl *et al.*, 1996) for CCM2 and CCM3 respectively.

2.1.1 PCCM2

PCCM2 uses the spectral transform method to solve the primitive equations on a sphere. The spectral method is only used for the dry dynamics while the advection of moisture is handled with a shape-preserving semi-Lagrangian scheme which avoids the spectral-rain problems in full spectral models (Rasch and Williamson, 1990; Williamson and Rash, 1994). The vertical coordinate is a hybrid of sigma and pressure (Simmons and Strufing, 1983) with 18 vertical levels. The coordinate is sigma near the surface and becomes a full pressure coordinate near the top of the model. The momentum flux at the surface caused by gravity wave drag is parameterized following McFarlane (1987). PCCM2 can be made to run at several different resolutions but R15 was chosen, meaning that only the first 15 wavenumbers are retained in a rhomboidal truncation. The R15 resolution in physical space has 40 latitudes arranged in a Gaussian distribution centered on the equator and 48 longitudes for an average grid size of 4.5° by 7.5°. FOAM's PCCM2 uses a 30 minute time step and the recommended values for the horizontal diffusion coefficient given by Williamson *et al.* (1995) for an R15 CCM2 ($2 \times 10^{16} m^4 s^{-1}$).

Solar radiation is calculated with a δ-Eddington approximation using 18 spectral bands (Briegleb, 1992; Kiehl and Briegleb, 1991). CCM2 assumed an exact 365 day solar year but FOAM uses a 360 day year to simplify the statistical analysis by providing 12 30-day months. During the diurnal cycle, radiation calculations are done every hour (every other timestep) while the absorptivities and emissivities are calculated every 12 hours.

The radiative effects of clouds are parameterized using the scheme of A. Slingo

(1989) while the cloud fraction parameterization is a generalization of J. Slingo (1987). The values for the free parameters in the cloud diagnostic routine are also from Williamson *et al.* (1995).

All types of moist convection in PCCM2 are handled by the simple mass flux scheme developed by Hack (1994) instead of the more common moist adiabatic adjustment procedure of CCM1 and the GFDL coupled model. PCCM2 uses a non–local parameterization for transport in the atmospheric boundary layer (ABL) based on the work of Troen and Mahrt (1986) and Holtslag *et al.* (1990). The surface fluxes between the surface and the lowest model level use standard bulk transfer coefficients where the functional form of the coefficients depend on stability as determined by the sign of the surface layer bulk Richardson number (Louis *et al.*, 1982; Holtslag and Beljaars, 1989).

A complex land surface model known as BATS (Dickinson *et al.*, 1993) was an option in CCM2 but was not included in PCCM2 and so is also not available in FOAM. The land surface in PCCM2 is the CCM2 default and is modeled as a horizontally homogeneous (within a grid cell) medium with vertically varying thermal properties. The subsurface temperatures are assumed to obey a thermal diffusion equation with zero heat flux at the bottom. The number of soil layers is arbitrary with a default configuration of 4 layers. The type of soil is determined by taking the 21 categories of vegetation determined by Matthews (1983) and reducing them to only 5. Each soil type has a different heat capacity, density, thermal conductivity and different thicknesses for the 4 layers. The soil type which is dominant over a grid cell is assigned to the whole cell. A constant roughness length is also prescribed for each surface type. Albedos in two spectral bands and

for strong and weak zenith angle are also prescribed and used to calculate the total albedo following the method of (Briegleb *et al.*, 1986).

A simple sea ice model is included in PCCM2. Sea ice is present whenever the sea surface temperature is below -1.9°C. The sea ice temperature is forecast by treating it as another soil type with specified heat capacities etc. and a total thickness of 2m. If the forecasted temperature is above freezing it is reset to freezing. Albedos and a roughness length are also prescribed. The growth of sea ice, including the release of latent heat of fusion, is not modeled. The flux of heat into the bottom of the sea ice from the ocean is calculated from

$$F = \frac{\kappa_b}{h}(271.16 - T_b) \tag{2.1}$$

Where κ is the thermal conductivity, T_b is the temperature and h is the thickness of the bottom layer. This sea ice model, which was meant to be used with climatological SST, was adapted for use in the coupled model as described below.

The standard PCCM2 does not contain a land surface hydrology model. Instead a wetness factor D_w is prescribed and used in the latent heat flux calculation. However early versions of PCCM2 used during development contain a simple box model after Manabe (1969) and Budyko (1956) which was present in CCM1 (Williamson *et al.*, 1987). In this model, precipitation is added to a 15cm soil moisture box or to the snow cover if the ground and lowest two atmosphere levels are below freezing. The soil moisture is used to calculate the wetness factor D_w used in the latent heat flux calculation. (D_w equals 1 for land ice, sea ice, snow covered and ocean surfaces.) Evaporation removes water from the box (condensation may also occur if the sign of the moisture flux is downward) and any excess over 15

cm is designated as runoff. Snow cover modifies the properties of the upper soil layer for purposes of the albedo and surface temperature calculations. Snow melt is calculated from the forecast top soil layer temperature and the soil moisture and final soil temperature are adjusted accordingly. This hydrology model has been retained for use in FOAM.

As mentioned above in the overview of parallel computing, the number of nodes assigned to run the atmosphere are logically arranged in a grid and each node handles a subregion of the model domain. For a typical case of 16 nodes, the grid is a 4x4 array of nodes numbered 0 through 16. The physical space in PCCM2 is assigned to the nodes by first folding the world at the equator and then laying the resulting points over the node array. The resulting mapping of physical space to processor number is shown in Fig. 1. This non-intuitive decomposition is used

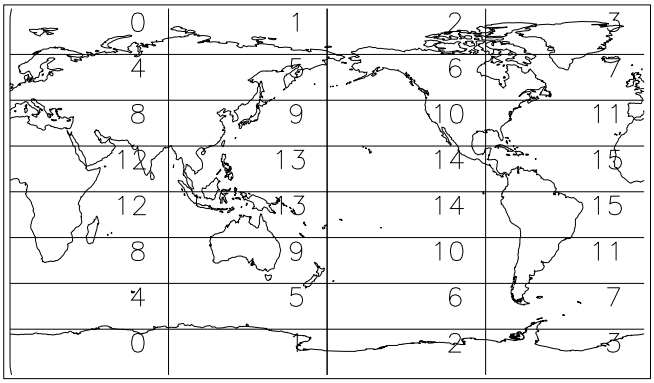

Figure 1: How the physical space is decomposed among a 4x4 array of nodes.

so that the parallel Legendre transform can take advantage of the symmetry in the associated Legendre polynomial (Drake *et al.*, 1995). Fig. 2 shows an abridged version of the calling sequence emphasizing the physics routines. As can be seen,

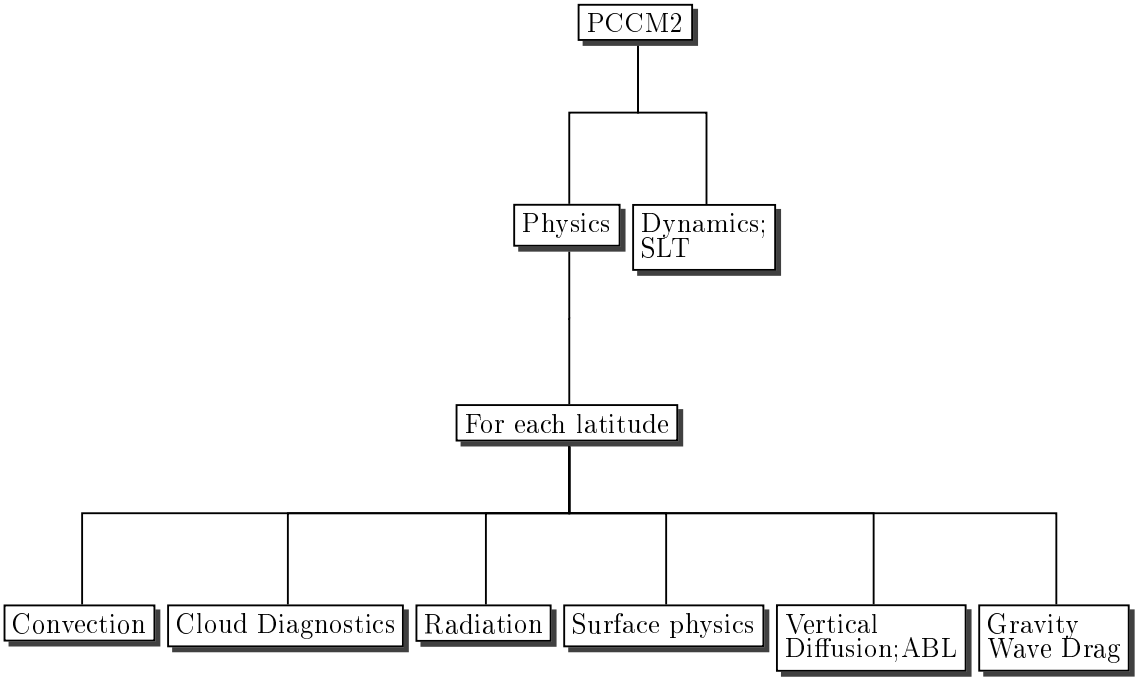

Figure 2: PCCM2 calling sequence for the physics routines.

the physics routines are called once for each latitude (and so the routines all employ one-dimensional arrays) alternating between Northern and Southern Hemisphere latitudes. This code structure had to be somewhat modified for coupling to an ocean model as described below.

2.1.2 PCCM3

CCM3 was released in the summer of 1996 after FOAM had been in development for over a year and a half using PCCM2. Rather then immediately move to CCM3, the model continued using PCCM2. But FOAM's consistent inability to produce a reasonable Pacific climate forced us to reexamine using CCM3. Luckily, most of the changes to CCM3 are in the physics routines which have identical structure and interfaces to the CCM2 versions which in turn are identical to the PCCM2

versions. (Most of the code changes in PCCM2 vs. CCM2 are in the dynamics since physical processes occur in vertical columns which don't require horizontal communication between nodes (Drake *et al.*, 1995).) The most significant CCM3 changes identified by Kiehl *et al.* (1996) were merged with PCCM2 to produce PCCM3. The Pacific climate improved significantly as discussed in Chapter 5 and the long simulation analyzed here was immediately started.

The dynamics formalism and parallel versions of the numerical methods in PCCM3 are identical to those of PCCM2. PCCM3 also uses the same resolution, R15.

PCCM3 has added new features to the radiation scheme. The longwave radiation now includes the effects of minor CO_2 band trace gases such as CH_4, N_2O, CFC11 and CFC12. The shortwave radiation routine now includes the effects of aerosol, assuming a constant background of 0.14 optical depth. Cloud formation now includes ice crystals and their different radiative properties. Cloud drop size takes account of the different sizes observed over land and ocean (Kiehl, 1994). There have been "minor" changes to the way convective and layered clouds are diagnosed (Kiehl *et al.*, 1996).

The other major changes involve the hydrologic cycle. The scheme of Hack (1994) is now only used for shallow and middle tropospheric moist convection. Deep convection in PCCM3 is now handled with a Zhang and McFarlane (1995) parameterization. The atmospheric boundary layer in PCCM3 has a new formula for calculating the boundary layer height as described by Vogelezang and Hotslag (1996). The surface fluxes over the ocean have new bulk transfer equations which do not assume a constant roughness length but are still stability dependent (Kiehl

et al., 1996). Finally the evaporation of stratiform precipitation is now included by use of the parameterization by Sundqvist (1988)

CCM3 has other changes which have not yet been included in PCCM3. These include a new Land Surface Model (Bonan, 1996) which calculates the fluxes of heat and momentum over land and a small change to the form of the hydrostatic matrix. The former is a significant change but was not included because of the time needed to incorporate this entirely new code into the coupler as had been done with the PCCM2 land surface model. LSM and the remaining CCM3 changes will be included in the next version of FOAM.

2.2 The Ocean Model

The ocean model was developed at the University of Wisconsin. It is a finite difference, hydrostatic, incompressible, z-coordinate model which solves nearly the same set of equations originally set down by Bryan (1969). FOAM's ocean model is thus very similar in concept to the Modular Ocean Model developed at GFDL (Cox, 1984; Pacanowski *et al.*, 1991). As in MOM, the equation of state is obtained from the polynomial expansion at each model level of the UNESCO equation of state (Bryan and Cox, 1972).

The ocean model uses the vertical mixing scheme of Pacanowski and Philander (1981) but with a steeper Reynolds number dependency derived from the observational analysis of Peters *et al.* (1988).

The horizontal discretization used is a simple A-grid (Arakawa, 1988). Spatial mode splitting on the A-grid is prevented through the use of a ∇^4 numerical

dissipation. The grid used is a 128 x 128 point Mercator grid (approx. 1.4° by 2.8°). A spatial filter similar to the sort used in atmospheric models (Williamson *et al.*, 1987) is used to maintain numerical stability in the Arctic.

The bottom topography as represented in the model is shown in Fig. 3. The topography is somewhat tuned to allow currents, such as the Mindanao, to flow through various important straits at the resolved space scales. "Wells" on the bottom have been filled in but the topography is otherwise not smoothed.

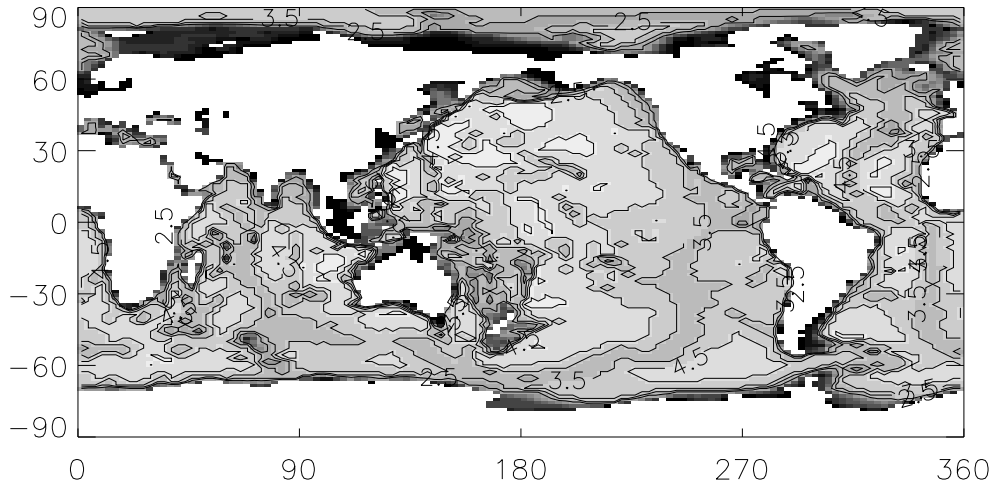

Figure 3: Topography for the ocean model. Land mask is shown in white

The z-coordinate is stretched to provide maximum resolution in the upper layers. 16 layers are used as shown in Table 2. A z-coordinate was chosen over an isopycnal model because of the importance of the SST field in a coupled model and the later models' problems in representing the SST.

The above makes for a rather pedestrian ocean model. The unique feature of FOAM's OGCM is a combination of numerical methods selected to provide

Table 2: Ocean model level thicknesses and depths.

level	thickness (m)	depth (m)
1	20	20
2	30	50
3	50	100
4	50	150
5	100	250
6	150	400
7	200	600
8	200	800
9	200	1000
10	200	1200
11	200	1400
12	350	1750
13	750	2500
14	1000	3500
15	1000	4500
16	1000	5500

maximum performance and scalability on MPP computers. First, the barotropic splitting method of Killworth *et al.* (1991) is employed to divide the ocean dynamics into a fast two-dimensional barotropic part and a slower three dimensional part. The ocean thus has a free surface instead of a rigid lid. The slower, three dimensional dynamics are in turn divided into relatively fast gravity balanced dynamics and slower, diffusive and surface forcing processes (Pollard and Millard, 1977; O'Brien, 1986).

An additional speed-up in the representation of the barotropic dynamics is obtained through a rescaling of the restoring force at the free surface as described in Tobis (1996). The scaling factor of 9 used in the runs reported here decreases the load for barotropic dynamics calculations by a factor of 3.0 (*ibid.*).

The resulting ocean model has a time step representing the barotropic pressure

balance of 15 minutes, the remaining pressure balance has a 2 hour time step, and advective and diffusive processes are represented at a 6 hour time step. The resulting efficiency is such that the atmospheric model, despite its much lower resolution, dominates the computational load of the full coupled model system.

2.3 The Coupler

The routines collectively known as the coupler contain nearly all the original work necessary to couple the separate atmosphere and ocean models. The coupler will thus receive a more detailed description then the ocean and atmosphere components.

2.3.1 General Considerations for a Coupler

When coupling an atmosphere and ocean model together there are two major questions to answer, one scientific and the other computational. These are: what shall be the physical model of the interaction and how can that model be programmed and interfaced with the separately developed ocean and atmosphere models?

The first question and part of the second was already answered by PCCM2. As described above, PCCM2, and really any atmosphere model, already has a model of interaction with the land/ocean surface. Sensible heat, evaporation and momentum fluxes are calculated using standard bulk transfer formulas which depend on the difference between state variable values at the lowest atmosphere model level and the surface. Since the currents are assumed to be zero for the momentum flux calculation and the saturation specific humidity is used for the surface value

in the evaporation calculation, the only variable needed is SST. When PCCM2 is run by itself, SST comes from a linear interpolation between the monthly mean climatology compiled by Shea *et al.* (1990).

One obvious way to couple the two models is to substitute the climatology SST with the ocean model's SST and pass the fluxes to the ocean model. This task is typically accomplished through a program called the "flux coupler" or just "coupler". In a flux coupler, state variables are passed in from the component models and the calculated fluxes are passed back. This intuitive approach has been taken by other groups constructing climate models and is very amenable to parallelization (Meehl, 1995).

Despite the conceptual simplicity, the calculations performed by the flux coupler are complicated by the different resolutions of the atmosphere and ocean models. Typically the ocean model has more resolution than the atmosphere model because the important dynamic motions occur on smaller scales. In general, the ocean and atmosphere grids may have zero collocated points. In the case of heat flux for example, a coupler has to ensure that the total heat flowing from the atmosphere is equal to the total heat entering the surface when the two interfaces have different resolutions. Some coupled models avoid this complexity by using the same horizontal resolution for the ocean and atmosphere or ensuring the ocean resolution is an integer factor of the atmosphere's.

The component models may also have different time steps. In the case of FOAM, the ocean model timestep for surface forcing is six hours while the atmosphere employs a half-hour timestep. So a coupler also may have to average fluxes over one or more time periods and must ensure that the component models are

synchronous. The main task of a flux coupler then is to calculate fluxes over different time intervals when the state variables are on different grids while ensuring that the total fluxed quantity is conserved. FOAM's coupler accomplishes all of these goals.

2.3.2 Additional Responsibilities in FOAM

When designing the coupler there were four main concerns in addition to those mentioned above. Interfacing the coupler with the atmosphere and ocean models, which were not written to be part of a coupled model, should not require too much alteration of those models' codes. The coupler needs to be flexible so that the resolution and the parallel decomposition of either the atmosphere or the ocean could be changed. Any physical processes (between the ocean and atmosphere) which weren't already modeled by the components, such as the transport of runoff by the river model, would be handled by the coupler. Finally the coupler needed to be a parallel program so it could interact efficiently with the parallel ocean and atmosphere models.

As it was originally conceived, the coupler would only have to interpolate fluxes and transport runoff. The land model and surface flux routines already implemented within PCCM2 would remain untouched. However each model, atmosphere and ocean, has its own land mask, a list of what points are land and what points are ocean. Suppose the atmosphere considers a coastal cell, which is really half land and half ocean, to be all land. The ocean model, with its finer resolution, recognizes that some of the points are ocean. In calculating the sensible heat flux

what should the surface temperature be? There are similar complications from the difference in roughness length between the land and the ocean when calculating the surface wind stress.

Rather than creating code to handle coastlines separately the land surface model of PCCM2 is implemented on the ocean grid. The box hydrology model, sea ice model, and albedo calculations are also implemented in the coupler at the ocean model resolution. This approach presents a simple picture of the coupled system: the low resolution atmosphere lies above the high-resolution land-ocean surface. The slight increase in execution time involved in running the land model at a higher resolution was not significant.

Thus in addition to the new river model, the coupler in FOAM is made responsible for all land surface processes. The calculation of fluxes between the surface and the lowest atmosphere level are also handled by the coupler using an efficient and flexible method for different grid resolutions described next.

2.3.3 Flux Calculation Method

For calculating the fluxes on the different grids, the task was greatly simplified by resolving the land, sea ice, and ocean models at the same resolution. The coupler then only has to handle two grids. The coupler first considers the surface of the globe as being divided up into rectangles or tiles. The center of each tile is at a computational point of the model and the four edges are halfway between each of the neighboring computational points. Each pole serves as the edge for the most poleward computational point. Thus from the atmosphere's point of the view the

surface is made of 40x48 tiles and the ocean sees the surface as 128x128 tiles. The tile boundaries form another grid which is offset from that defined by connecting the computational points. The ocean model is the fine grid and the atmosphere is the coarse grid. Although the computational grids coincide nowhere, the tile grids for the atmosphere and ocean coincide at the equator and at the poles.

In the discussion to follow, the word "grid" refers to the tile grid. A flux calculation will be illustrated using sensible heat for the flux and the temperature of the surface and the lowest atmosphere model level as the state variables.

The total amount of heat passing through a surface can be calculated from the sum of the fluxes through each tile:

$$SH^T{}_A = (\sum_{I=1}^{Nx}\sum_{J=1}^{Ny} F_{IJ}A_{IJ})\Delta t. \tag{2.2}$$

Where $SH^T{}_A$ is the total sensible heat transfered in Joules, N_x and N_y are the number of points in the x and y directions on the course grid, A_{IJ} is the area of tile at (I,J) on the coarse grid and F_{IJ} is the sensible heat flux through that tile, and Δt is the length of a timestep. FOAM's coupler conserves fluxed quantities on the different grids by ensuring that the sum is identical when calculated on each grid:

$$\sum_{I=1}^{N_x}\sum_{J=1}^{N_y} F_{IJ}A_{IJ} = \sum_{i=1}^{n_x}\sum_{j=1}^{n_y} f_{ij}a_{ij}. \tag{2.3}$$

Where n_x, n_y, a_{ij} and f_{ij} are as above but for the fine grid.

To guarantee that Eq. 2.3 holds, the coupler calculates fluxes on a third grid of tiles called the overlap grid. This third set of tiles is made by laying the atmosphere grid on top of the ocean grid as in Fig. 4a. The boundaries of the atmosphere tiles can be thought of as slicing the ocean tiles into smaller pieces. The overlap grid

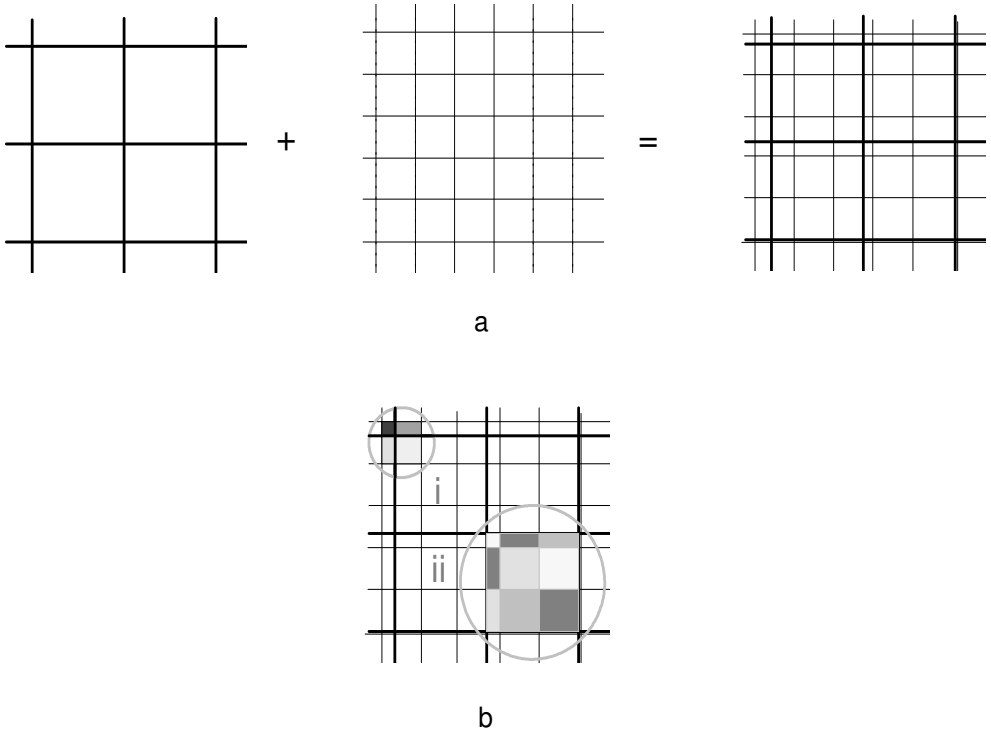

Figure 4: (a) Forming the overlap grid. (b) An ocean (region i) and atmosphere tile (region ii) composed of overlap pieces.

of tiles is an array of dimensions $(N_x + n_x)$ x $(N_y + n_y)$. To easily map elements of the overlap grid to the fine grid, the coupler indexes each overlap piece by adding a dimension to the fine grid array. The triplet i, j, k identifies the k'th piece that the ocean tile i,j is split into.

To calculate the sensible heat flux, it is first assumed that the temperature anywhere on an atmosphere or ocean tile is equal to the temperature of the computational point at the center of the tile. Thus the temperature of a surface tile piece, T_{sijk} is equal to T_{sij}. The air temperature is taken to be the temperature T_{ALM} where L,M are functions, $L = L(i, j, k)$, which map the index of overlap tile i,j,k to the index of the atmosphere tile that lies over it. The sensible heat flux through an overlap tile is then:

$$SH_{ijk} = Const(T_{si,j,k} - T_{AL,M}) \tag{2.4}$$

The flux through an ocean tile can be constructed by taking the area-weighted sum of the flux through each overlap piece:

$$f_{ij} = \frac{\sum_{k=1}^{Np_{ij}} SH_{ijk} w_{ijk}}{a_{ij}}, \tag{2.5}$$

where Np_{ij} is the number of pieces that ocean tile i,j is divided into and w_{ijk} is the area of piece i, j, k. This process is illustrated in Fig. 4 as region i. Region ii shows how the flux through an atmosphere tile can also be constructed from the pieces of the overlap grid:

$$F_{IJ} = \frac{\sum_{K=1}^{Np_{IJ}} SH_{ijk} w_{ijk}}{A_{IJ}}. \tag{2.6}$$

Now Np_{IJ} is the number of pieces an atmosphere tile I,J is split into and i, j, k are functions $i = i(I, J, K)$, etc., which map atmosphere tiles to overlap pieces.

Substituting Eqs. 2.5 and 2.6 into Eq. 2.3 yields:

$$\sum_{I=1}^{N_x}\sum_{J=1}^{N_y}\sum_{K=1}^{Np_{IJ}} SH_{ijk}w_{ijk} = \sum_{i=1}^{n_x}\sum_{j=1}^{n_y}\sum_{k=1}^{Np_{ij}} SH_{ijk}w_{ijk}. \tag{2.7}$$

Typically Np_{ij} is no more than 4 while Np_{IJ} can be as much as 20. When expanded, the left hand and right hand sides of Eq. 2.7 have the same number of terms summed in a different order. As long as the set of terms is the same on each side, as long as each piece of overlap tile is used once and only once, the two sums will be the same and the quantity will be conserved.

All the weights and mapping arrays are calculated ahead of runtime and stored in memory. A separate program begins with the latitudes and longitudes of the two computational grids. The tile grids are constructed and a search algorithm determines if a tile boundary from the coarse grid lies within a fine grid tile. A general case where a fine grid tile is divided into four pieces by the edges of four overlying coarse tiles is illustrated in Fig. 5. The index of the coarse tile is noted

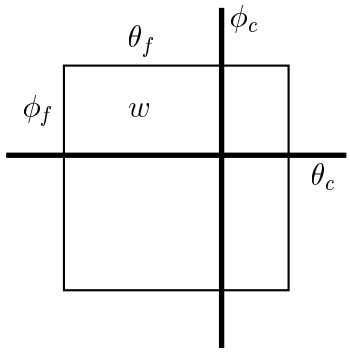

Figure 5: A fine grid tile divided into four pieces.

and the area overlap w is calculated by:

$$w = \int_{\phi_f}^{\phi_c}\int_{\theta_c}^{\theta_f} \cos\theta \, d\theta \, d\phi \tag{2.8}$$

where the factor R^2 (R = radius of the Earth) has been omitted and θ follows the meteorological convention for spherical coordinates.

The result of the search and area calculations is a list for each ocean tile which describes how many pieces it is divided into, the index I,J of the atmosphere tile that lies above each piece and the area w_{ijk} of the piece. The second mapping, which describes which overlap tiles compose an atmosphere tile, can be constructed from the first.

The method outlined above is the simplest way to simultaneously calculate a flux and conserve it between two different grids with a minimum number of floating point operations. Most of the savings in computation comes from eliminating the need to interpolate state variables from the coarse to the fine grid. The mapping functions and weights can be easily recalculated if the resolution of the atmosphere or ocean model is changed, another goal for FOAM's coupler.

2.3.4 Interfacing with the Atmosphere Model

By making the coupler responsible for the land model, the coupler completely replaces the surface physics routines in PCCM2. So to interface the coupler with the atmosphere model, the coupler accepts the same input and returns the same output variables as the PCCM2 surface routines at the same point in the calling sequence.

The non-coincidence of the two grids required the biggest change in the PCCM2 code. A given latitude band of ocean tiles may lie under two neighboring bands of atmosphere model tiles. So the atmosphere values from two latitudes need to be

known to calculate the flux through that ocean latitude band. But PCCM2 calls the entire physics package once for each latitude and the surface physics occurs about two-third of the way through that calling sequence (see Fig. 2). Thus before the coupler, which replaces the surface physics, can be called, the atmosphere state over the entire globe must be known. It was thus necessary to split the calling tree for the PCCM2 physics so that all the physics before the surface calculations could be done for the entire globe, then the coupler could be called, and then the remainder of the physics could be calculated as shown in Fig. 6. One goal of FOAM

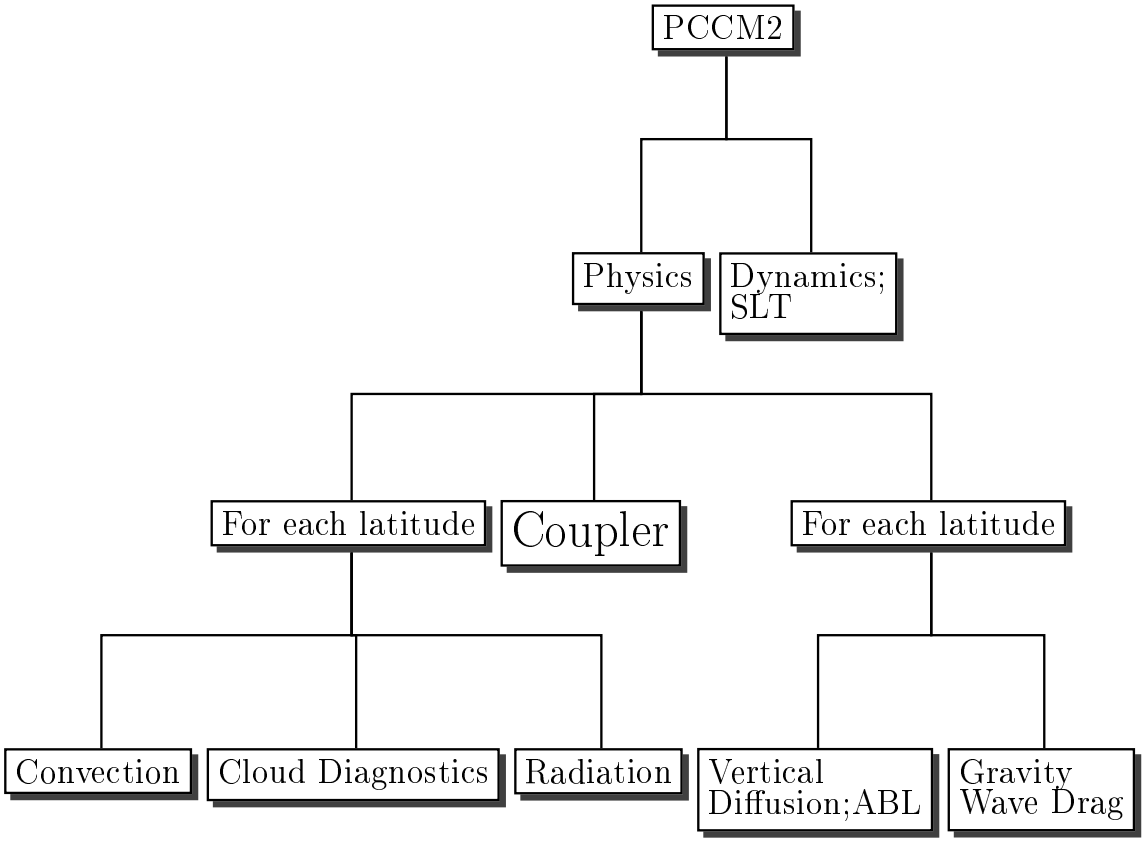

Figure 6: Split of PCCM2 calling tree for coupler. Compare with Fig 2.

was to leave as much of the PCCM2 code untouched as possible but this action was unavoidable given the different resolutions of the atmosphere and ocean. CCM3

which unlike CCM2 was designed to be coupled with an ocean model, contains a similar split (Acker *et al.*, 1996).

Originally it was envisioned that the coupler would run on a separate partition of nodes while the atmosphere and ocean models ran on their own separate partitions; each model exchanging data via MPI. This allows the coupler to have its own data decomposition on its collection of nodes. But this approach proved to be too slow because of the time it took to gather and communicate the entire atmosphere model state needed by the coupler. Instead the coupler in FOAM is a subroutine of the atmosphere model. This allows variables to be "communicated" by reference to FORTRAN common blocks which the atmosphere and coupler share—essentially cutting the communication time to zero.

Not all of PCCM2's interaction with the surface was confined to the surface model subroutines. The surface albedo and longwave radiation were both calculated in the radiation subroutines in PCCM2. In FOAM, the radiation model retrieves albedos and upward longwave radiation calculated by the coupler through reference to a common block of memory. The coupler calculates those quantities on the ocean grid and forms averages over an atmosphere grid tile using the same weights and index mappings as discussed in Section 2.3.3.

To complete the interface, the downward radiation and precipitation from the atmosphere model are interpolated onto the ocean grid. Again the weights and mappings already calculated can be used to construct the flux through ocean tiles which lie under more than one atmosphere tile. The resulting fields become part of the input into the surface temperature calculation and the hydrology model, respectively.

2.3.5 Interfacing with the Ocean Model

Interfacing the coupler with the ocean model required far less code modification. Like the atmosphere, the ocean model also already had an interaction with the surface in the form of a restoring boundary condition on temperature and salinity and monthly varying momentum flux. The only modifications were to include MPI calls to receive the fluxes from the coupler while passing back the new temperature field and then to convert those fluxes to forcings for the ocean model variables.

Since the ocean model has a time step of 6 hours, the coupler accumulates fluxes of heat, momentum and freshwater over this length of time and then passes the average flux to the ocean model. The total heat flux TH in W/m^2 provided by the coupler is:

$$TH = SR - LW - SH - LH \tag{2.9}$$

Where SR is the total downward radiation at the surface which was provided by the atmosphere and already interpolated to the ocean grid by the coupler. LW is the longwave radiation from the surface, SH is the sensible heat flux and LH the latent heat flux.

The total freshwater flux FW in kg/m^2s for the ocean model is:

$$FW = P - E + Rnf - SI \tag{2.10}$$

Where P is the precipitation calculated by the atmosphere model and interpolated to the ocean grid by the coupler, E is the evaporation, Rnf is the river runoff and SI represents the water loss (gain) due to sea ice formation (melting). (For melting the minus sign in Eq. 2.10 becomes a plus.) Average momentum fluxes τ_x and τ_y (in N/m^2) are also provided by the coupler. (When sea ice is present, the stress

calculated by the coupler is between ice and air. To represent the stress between sea ice ocean, the coupler values are divided by an empirically determined factor to reduce the magnitude before passing them to the ocean.)

After the fluxes are received by the ocean model, they are converted to tendencies appropriate to the ocean model variables:

$$\frac{\partial T}{\partial t} = \frac{TH}{\rho h C_p} \tag{2.11}$$

$$\frac{\partial S}{\partial t} = S\frac{FW}{\rho h} \tag{2.12}$$

$$\frac{\partial u}{\partial t} = \frac{\tau_x}{\rho h} \tag{2.13}$$

$$\frac{\partial v}{\partial t} = \frac{\tau_y}{\rho h} \tag{2.14}$$

Where ρ is the density of sea water (taken to be 1030 kgm^{-3}), h is the depth of the top level and C_p is the specific heat of seawater (taken to be 4100 $JK^{-1}kg^{-1}$).

Eqs. 2.11, 2.13 and 2.14 are straightforward while Eq. 2.12 is derived beginning with the definition of S:

$$S \approx \frac{m_s}{m_w} \tag{2.15}$$

where m_s is the mass of salt and m_w is the mass of water. Taking the partial derivative with respect to time and assuming equality leads to:

$$\frac{\partial S}{\partial t} = -\frac{m_s}{{m_w}^2}\frac{\partial m_w}{\partial t}. \tag{2.16}$$

Using Eq. 2.15,

$$\frac{\partial S}{\partial t} = -S\frac{1}{m_w}\frac{\partial m_w}{\partial t} \tag{2.17}$$

and substituting $\rho A h$ for m_w yields:

$$\frac{\partial S}{\partial t} = -S\frac{1}{\rho h}\left(\frac{1}{A}\frac{\partial m_w}{\partial t}\right). \tag{2.18}$$

Eq. 2.12 follows by equating the quantity in parentheses in Eq. 2.18 with FW.

On the coupler side of the interface, the sea surface temperature received from the ocean is merged with the land surface values calculated by the coupler to form the total surface temperature field. The SST is examined to set the new sea ice distribution using the same condition as in PCCM2: sea ice is present if the temperature is below -1.9°C. The SST and sea ice distribution are held constant over the following 6 hours of atmosphere/surface interaction.

2.3.6 Modifications to the Hydrologic Cycle Model

The hydrologic cycle model provided by PCCM2 was missing two important pieces: there was no way to return calculated land runoff to the ocean and there was no model for the effect of sea ice formation on the ocean salinity. The former is needed to prevent long term salinity drift in the model and to close the hydrologic cycle. The latter is important in deep water formation which is an important part of the thermohaline circulation. The coupler supplies these missing pieces in the form of an explicit river model and a crude parameterization of sea ice formation.

River Model

The river model is based on the work of Miller *et al.* (1994). First a river flow direction is set for each land point in the 128x128 grid. Although this can in principle be done by examining the topography, in practice many of the river directions had to be set by hand so that the resulting basin boundaries resemble the observed. A lake model or internal drainage was not included so each point on the land was given a path to the ocean. The ocean's land mask was adjusted

so that small enclosed seas which receive significant river outflow such as the Aral and Caspian Sea are resolved by the ocean model while comparably sized bodies of water which drain into the global ocean, such as the Great Lakes, are not resolved. (These inland seas are too small to be dynamically active at the chosen resolution but vertical mixing and horizontal diffusion can still act.)

The flow F_{out} in $m^3 s^{-1}$ out of a cell is determined by $F_{out} = V \cdot u/d$ where V is the total river volume in the grid cell, u is an effective flow velocity which is taken as a constant .35 ms^{-1} (Miller *et al.*, 1994) and d is the downstream distance. Precipitation and evaporation do not act directly on the river water and the temperature of the river water is not taken into account. Its salinity is assumed to be zero.

The change in river volume is given by:

$$\frac{dV}{dt} = \frac{\text{rnf}\ a}{\Delta t} + \sum F_{in} - F_{out} \tag{2.19}$$

Where each F_{in} is the F_{out} of a neighboring cell whose river direction flows into the cell being computed. rnf is the excess soil moisture (in m) after all precipitation, snow melt and evaporation has been taken into account, a is the area of a land tile and Δt is the atmosphere/coupler time step.

$\sum F_{in}$ for an ocean point near the coast can be calculated as the sum of the F_{out} from neighboring land points and converted back to a flux by dividing by the area of that ocean point. This river freshwater flux is then added to the local precipitation and evaporation rates as Rnf in Eq. 2.10 to close the hydrologic cycle.

An additional input to the river model comes from a restriction in the maximum

snow depth. The hydrologic cycle model in PCCM2 had no upper bound on snow depth. Early tests showed runaway snow depths on the Antarctic and Greenland Ice sheets as snow piled up with no process to remove it. Rather than implement a land ice formation model, the coupler adds any snow depth greater than one meter liquid water equivalent to the runoff input to the river model and subtracts the same quantity from the snow depth. This is, in effect, a simple parameterization of glacier calving—the main mechanism for removing water from the Antarctic ice sheet.

Sea Ice

The simple sea ice model of PCCM2 (Section 2.1.1) needed two modifications to interact with the ocean model. For sea ice formation, the ocean cools, mostly by radiative heat loss, until the temperature gets below -1.9°C when, as before, 2m of sea ice instantly appear at that grid point. While sea ice is present, the heat loss by the ocean is calculated from Eq. 2.1:

$$F = \frac{\kappa_b}{h}(SST - T_b) \tag{2.20}$$

where now the prognostic SST (in Kelvins) has replaced the constant 271.16. F replaces TH in Eq. 2.11 while sea ice is present.

Early test runs of the coupled model revealed that without any way to grow more sea ice and hold the ocean temperature above freezing by latent head release, the Arctic and surrounding waters cool so much that northern hemisphere sea ice begins to expand well beyond the normal southern boundaries. Since the ocean can continue to lose heat by conduction, it is necessary to impose a minimum on

temperature in the ocean. A value slightly below freezing is chosen, -1.92°C, so that numerical noise won't cause the sea ice to "flicker".

The condition that sea ice disappears when the temperature gets above -1.9°C is preserved. Since the penetration of radiation through sea ice is not modeled the only way the SST may warm from above is by conduction (Eq. 2.20). (The SST may also warm by temperature advection.) To allow enough heat to conduct through the ice during the thawing season, the constraint on sea ice temperature, which is not allowed to go above freezing in PCCM2, is removed in FOAM. The subsequent warming produces enough ice melting to approximate the seasonal cycle in sea ice. (see Fig. 20).

For the effect of sea ice on salinity, the formation of sea ice is treated as a flux of two meters of water out of the ocean over an ocean time step. Two meters was chosen because that is the thickness of the ice for purposes of the four layer temperature calculation. While sea ice is present, snow, snow melt, and rain (if any) is allowed to accumulate on top of the ice. When sea ice disappears, the freshwater flux into the ocean is then 2m plus the accumulated snow and snow melt. If snow or water accumulates on the ice above the 1m and 15cm limit, it is allowed to pass through to the ocean underneath.

2.3.7 Parallel Implementation

As discussed earlier, in PCCM2 or 3, most of the actual parallel programming is not in the physics routines since they all occur in a vertical column. FOAM's coupler however does require some explicit consideration of the parallel nature of

the model. Because the coupler is a subroutine of the atmosphere, the land surface fields handled by the coupler must have the same data decomposition on the nodes as the atmosphere (see Fig. 1). Because the two grids do not coincide, the exact boundaries of the regions in the atmosphere and on the surface handled by a node are slightly different. An example from the Southern Hemisphere region handled by node 5 in the standard 16 node configuration (Fig. 1) is shown if Fig. 7. When

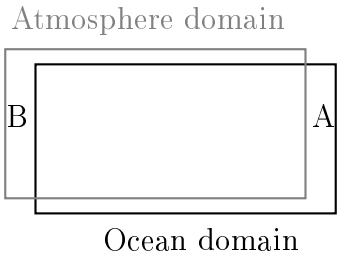

Figure 7: Non-coincident domains on a node.

calculating the fluxes in region A, some of the needed atmosphere data will be on another node. So an exchange of atmosphere state variables must be made using the parallel libraries. Similarly, when calculating the variables to pass back to the atmosphere at the end of the coupler's calling sequence, the overlap grid data under region B will be on other nodes and so another communication is necessary. Interprocessor communication is also needed in the river model so that grid points can receive inflow from neighboring points which are on other nodes.

2.3.8 Summary

FOAM's coupler performs the basic task of calculating fluxes based on state variables from two component models. The flux calculation method is conservative and easily implemented as a parallel program. The coupler in FOAM is given

many additional duties such as running the land surface and hydrology models. The coupler is integrated with the parallel atmosphere and ocean models so that the two models are synchronously coupled together through the fluxes of heat, water and momentum. The parallel coupler code and flux calculation method allows for easy switching between different resolutions in the components and different numbers of processors per component. The coupler is called once each atmosphere timestep but adds very little to the total time needed to compute a timestep. The couplers calling tree is summarized in the flow chart of Figs. 8 and 9.

2.4 Initialization and Model Spinup

The question of how one starts the integration of a fully coupled ocean atmosphere model does not have an objective best answer. Ideally, one would assimilate a global snapshot of the atmosphere and ocean or start each model synchronously from a rest state. As discussed above, concern over transients from the beginning of a coupled model integrations motivated many of the mixed boundary condition studies using ocean only models. FOAM takes the usual approach of spinning up each component separately from some initial state before coupling together. Transients are not a concern because FOAM is intended to be integrated long enough for them to decay.

Each component model—atmosphere, ocean and coupler—derives its initial conditions from separate sources. The atmosphere model is initialized as in CCM2, with assimilated data corresponding to conditions on September 1, 1981. The

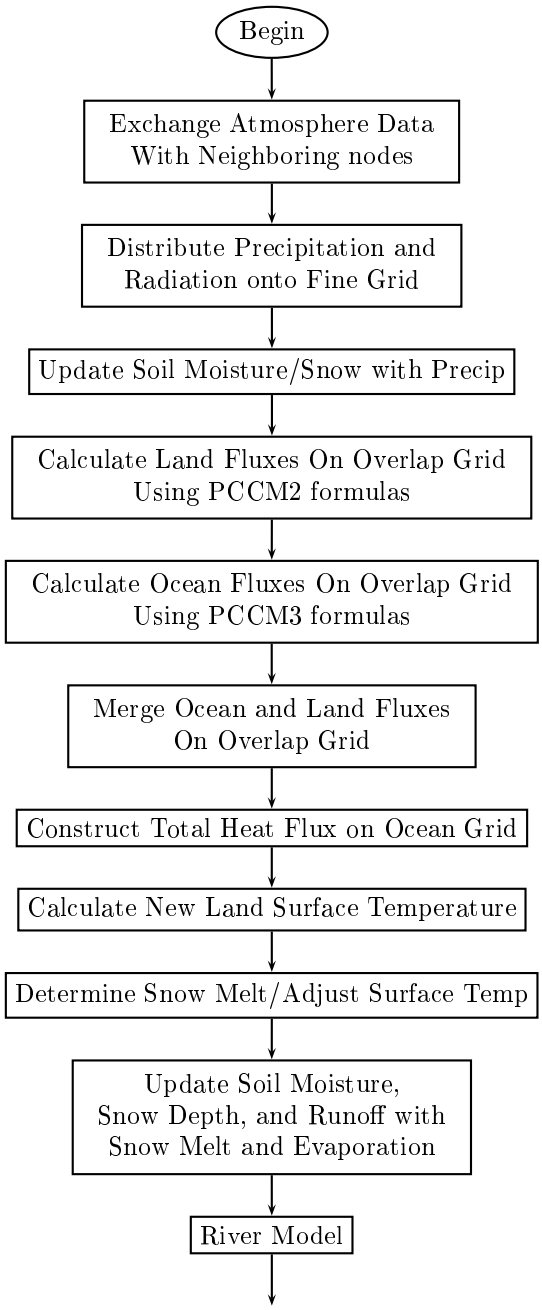

Figure 8: Coupler Flow Chart

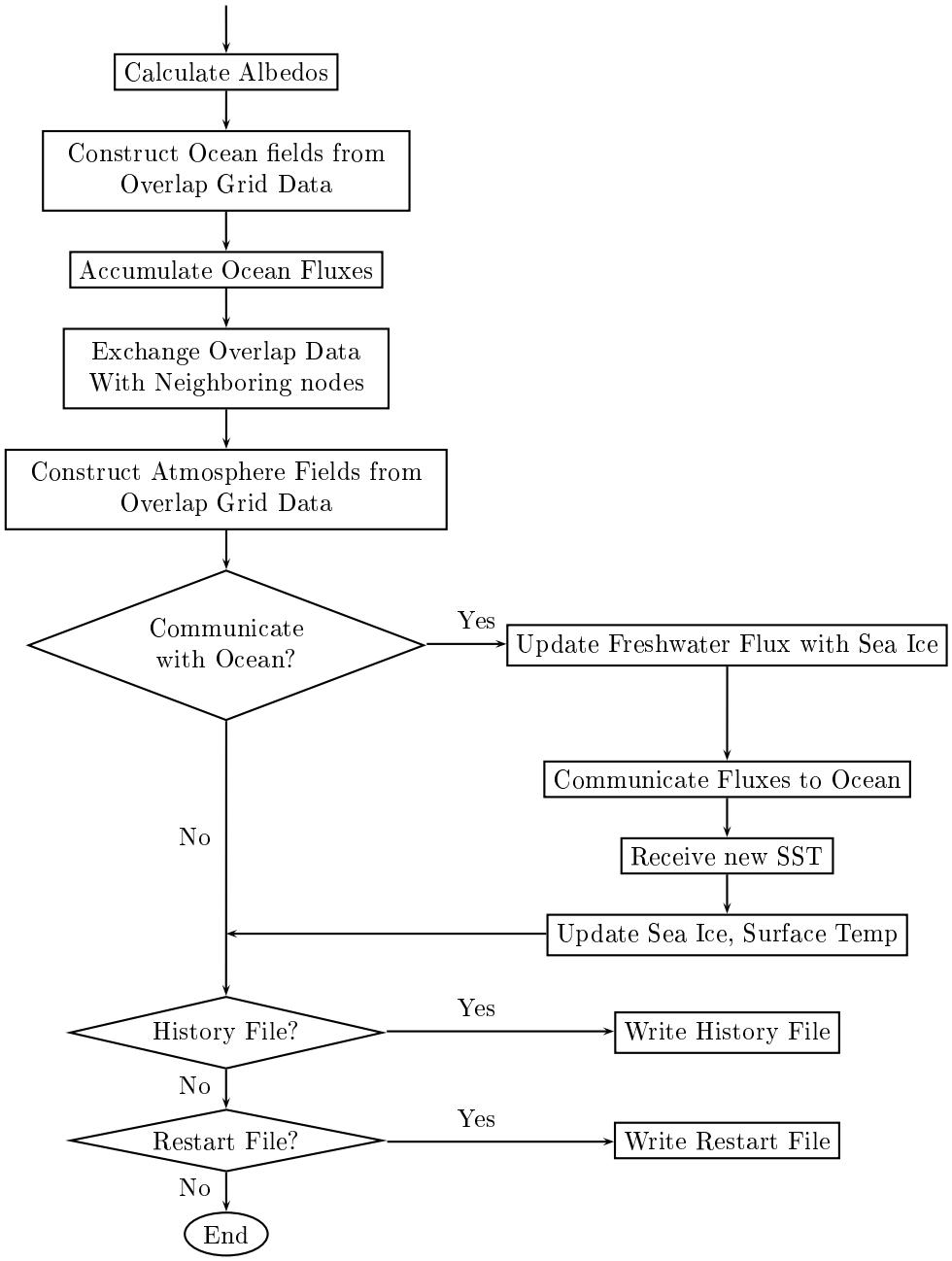

Figure 9: Continuation of Coupler Flow Chart

surface model in the coupler was derived from the atmosphere model so the atmosphere's lower boundary condition initial data is used to initialize the coupler. Since the coupler's grid resolution of 128^2 does not correspond to any of the available atmosphere resolutions, data is averaged from a higher resolution atmosphere data set, in this case T170 (512x256). The mapping between the T170 grid and 128x128 grid is computed with the same program that generated the R15–128^2 mappings. From the T170 data, initial surface temperature, snow depth, and soil moisture fields can be set. The initial river volume is zero everywhere.

The ocean model is initialized with a horizontally uniform, vertically stratified rest state. The temperature and salinity at each level are set equal to the values used as the base in the equation of state approximation.

Each model undergoes a separate spinup. The atmosphere and coupler are run together with SSTs interpolated to the current model time from the Shea *et al.* (1990) monthly climatology. After the first step, the current time is reset to January 1st so that large values of the model day counter can be conveniently converted to a season (i. e. so that day 360 and multiples thereof do not correspond to August). The atmosphere-coupler system were integrated together for two years after reseting the internal clock. This reset was done using the PCCM2 version of FOAM. Since the restart files are compatible, rather than perform the reset again, the PCCM3 version of the atmosphere-coupler model was integrated an additional year prior to coupling (see Fig. 10).

The ocean model spinup was forced with monthly climatological wind stress (Hellerman and Rosenstein, 1983). SST was restored to monthly climatological SST's using the same field as in the atmosphere-coupler model with a 30 day time

constant. Sea surface salinity was restored to the annual mean of Levitus (1982) also with a 30 day time constant. For the synchronous coupled run discussed here, the ocean model was first integrated for 57 years. This is not long enough for the deep ocean to reach equilibrium but was sufficient for the upper ocean to reach equilibrium.

To couple the models together, the three restart files (atmosphere, ocean and coupler) corresponding to the same point in the solar calendar, usually January 1, are taken from the end of each spinup run and used to start the fully coupled model. In the next section, we begin discussion of the results from the fully coupled integration.

Chapter 3

Trends and Mean Properties of FOAM

The R15-128[2] PCCM3 version of FOAM described previously was integrated synchronously for 643 model years. A schematic timeline of the integration is shown in Fig. 10. Because this is a new coupled ocean-atmosphere model, an overview of the model climate is presented in the following sections. This does not constitute a complete description of the simulated climate but instead provides data for the most commonly compared features to provide a basis for comparison to other models.

Since the atmosphere controls the model's sense of time, and it was already integrated for 3 years uncoupled, the final year of the run is considered year 646. To avoid confusion, we'll refer to specific years using the atmosphere's time frame. (Thus "Year 100" is really coupled year 97).

As stated above in the model description, a FOAM year was defined to be exactly 360 days long to simplify statistical analysis by providing 12 30-day months. During the run a history file was output every 30 days by each of the three components. Some statistics from the run are given in Table 3. As can be seen in Table 3, FOAM has generated a large amount of output. The large amount of

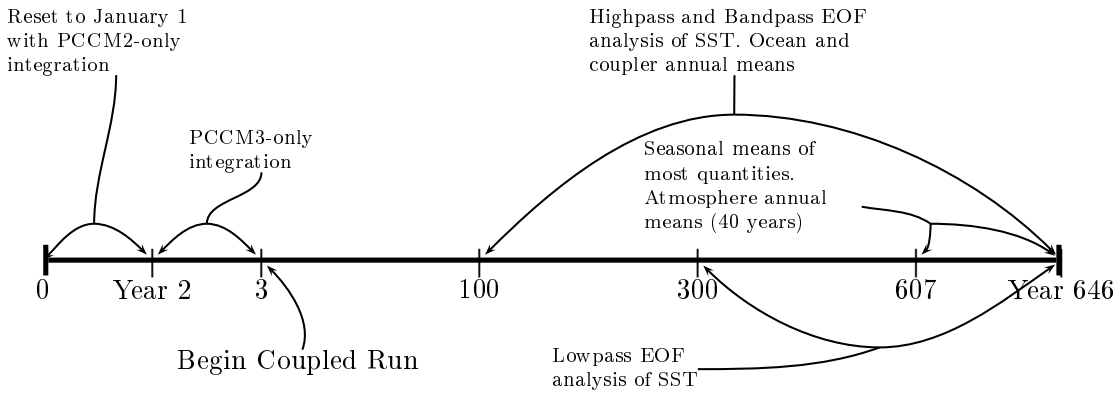

Figure 10: Timeline of FOAM integration showing analysis periods.

Table 3: Statistics from coupled integration.

Total simulated years	643
Atmosphere model time steps	11,111,040
Ocean model time steps	925,920
Number of history file sets	7716
Bytes per history file set	8 MB
Total history output	60.25 GB

data naturally leads one to use a data reduction method of analysis. The widely used method of Empirical Orthogonal Function analysis, or Principal Component analysis, is chosen. EOF analysis can reduce the 7716 monthly data sets or 643 annual average data sets to a small set of patterns which account for the maximum amount of variance. In Chapter 4 an EOF analysis of SST using the periods indicated in Figure 10 is presented. This chapter features an overview of the integration with full-length time series and annual means of relevant quantities.

3.1 Time Evolution

Here the evolution of FOAM over its integration period is summarized with selected globally and annually averaged fields. Fig. 11 shows the time series of temperature at two depths and heat flow into the ocean. The SST remains relatively steady after Year 100 while the temperature at 1000m shows a steady increase. A similar behavior—steady SST and increasing temperatures at depth—has been seen in CSM (Boville and Gent, 1997). Note that while there is a net heat flow out of the ocean, most of the ocean surface (60S - 60N) receives an influx of heat and the sequestering of this heat by deepwater formation is responsible for the temperature increases at depth. Including the spinup, the ocean has only been integrated for 700 years so the deep ocean is still seeking a thermodynamic equilibrium.

Most of the heat loss resulting from the net heat flow out of the ocean comes from ocean areas poleward of 60° (see Fig. 11). Despite this forcing, the Arctic and Southern oceans do not experience large amounts of cooling due to the minimum imposed on ocean temperature to supplement FOAM's sea ice model (see Section 2.3).

The time series of annual averaged salinity and two measures of the freshwater flow are shown in Fig. 12. There is a slight upward trend in SSS in response to the net loss of freshwater by the ocean. There are upward trends at all levels. These trends are not surprising since FOAM is integrated without any flux corrections and relies on the interaction between the different models' parameterizations to achieve a "natural" equilibrium. However they are somewhat disappointing since some effort was made to provide closure to the hydrologic cycle (through the inclusion of

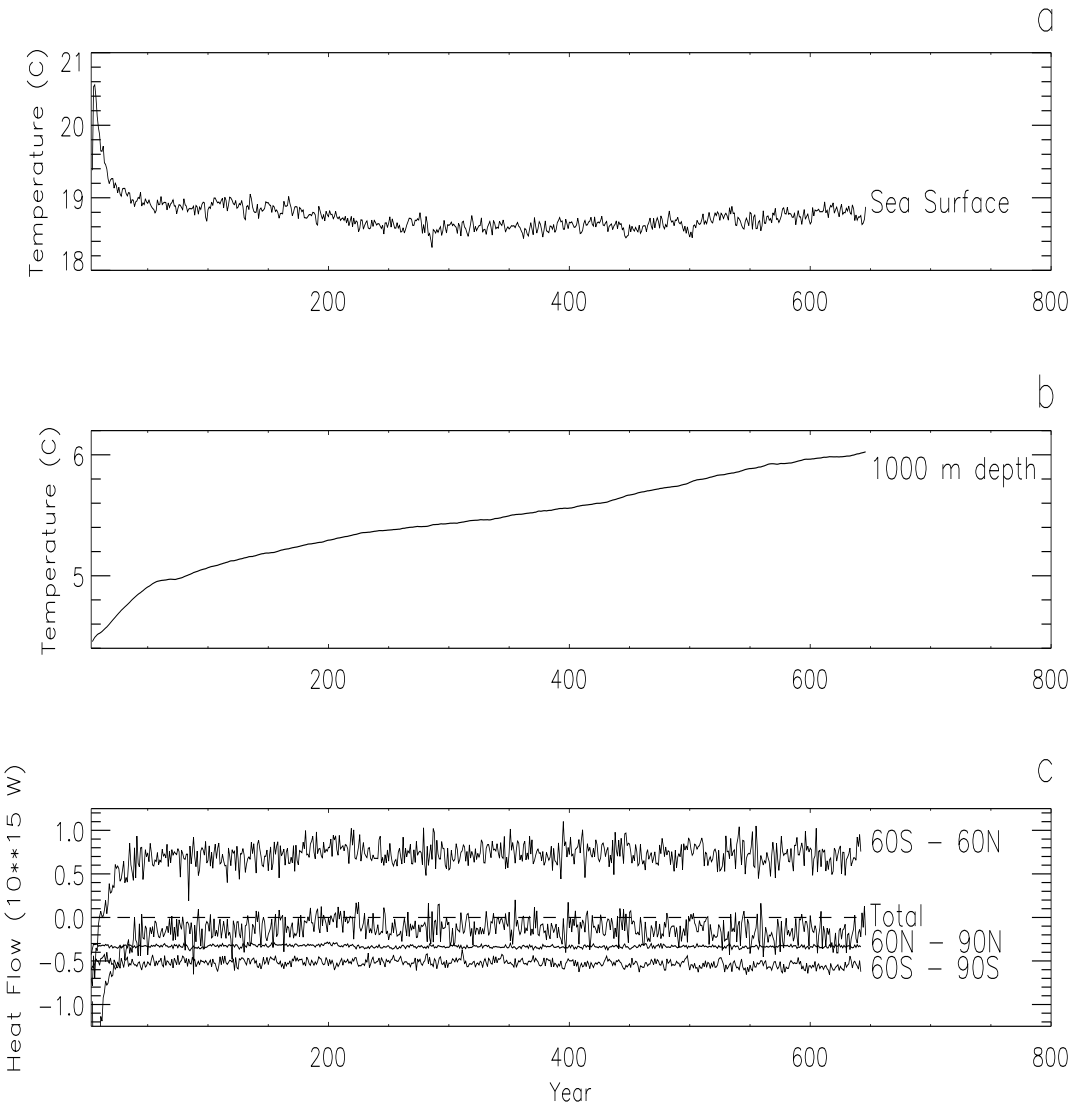

Figure 11: Time series of global and annual average temperature (a) on the surface and (b) at 1000 m depth. (c) Annual average heat flow into the ocean for 3 regions and for the whole ocean surface.

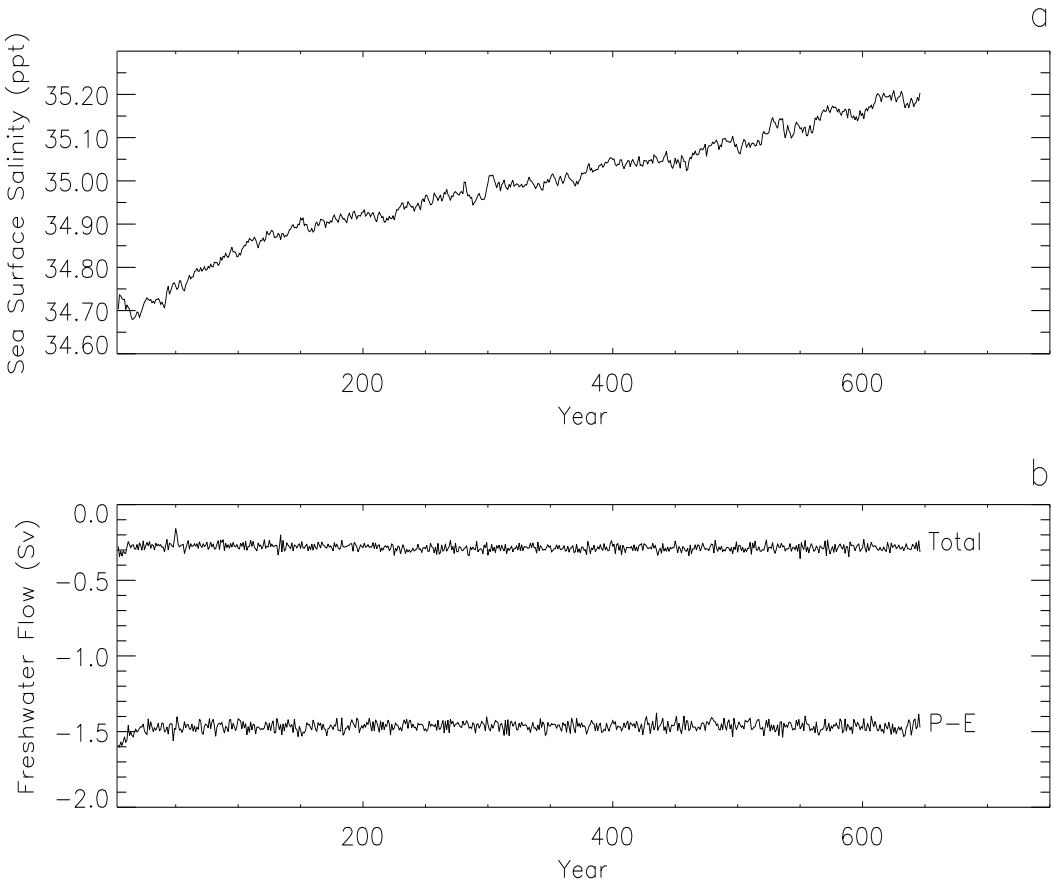

Figure 12: Time series of global and annual average (a) SSS and (b) total and P-E only freshwater flow into the ocean. Freshwater flow is considered positive into the ocean.

a river model) and to conserve quantities like heat and freshwater when exchanged between the atmosphere and ocean models. Fig. 12b shows that river model has some effect in balancing the freshwater flux: without it the net flow of freshwater out of the ocean would be almost five times greater.

Since the trends are small and steady—the heat and freshwater flows are nearly constant—they do not affect the variability within the time periods considered. Other coupled models, including some with flux corrections, have trends in salinity, temperature and other quantities (von Storch *et al.*, 1997; Boville and Gent, 1997). Improving the conservation of freshwater in long integrations of climate models remains a challenge.

Average storage in one part of the cryosphere, the snow cover, is shown in Fig. 13. This time series shows a curious "jump" in total snow volume around Year 230. This increase comes mostly in the form of a permanent snow cover over Siberia. Prior to year 230, snow in Siberia melted completely in the summer. This regional climate shift was a response to the cooling of the Arctic ocean as it reached an equilibrium under the coupled forcing. Once the arctic surface climate allowed for a larger summer sea-ice cover, the climate shifted slightly into this colder regime and remained there for the rest of the integration.

3.2 Annual Means

As with the trends, FOAM's mean quantities are typical of current coupled models, including those with higher resolution.

Due to the large volume and unwieldy format of the atmosphere data sets,

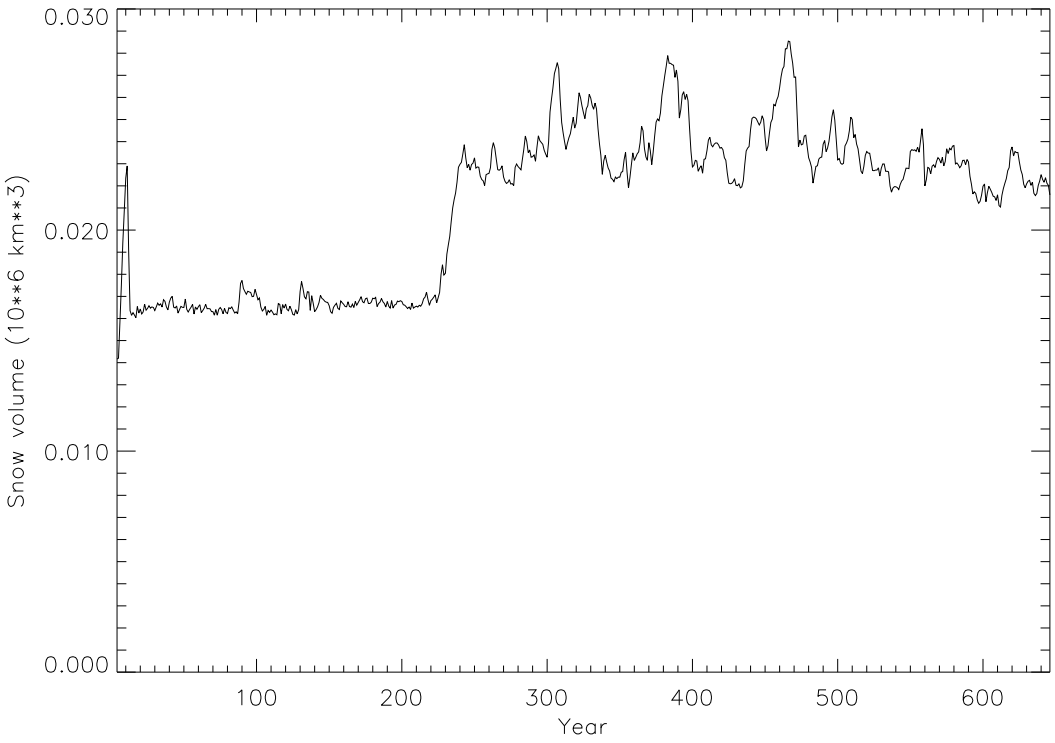

Figure 13: Annual average total snow volume.

annual means for the atmosphere are calculated from the last 40 years of the run as indicated in Fig. 10. Seasonal averages are also calculated on this time period for convenience. Since annual averages of the ocean and atmosphere are already available for the entire run, annual averages for those components' fields are calculated over the 546 year period indicated in Fig. 10.

Table 4 gives globally and annually averaged values of typical properties used to assess a climate model's performance. The first 3 columns are adapted from Table 1 in Hack *et al.* (1997). Sources for the observed values can be found therein. The "CCM2" and "CCM3" columns are from uncoupled runs using climate SSTs and the T42 version of each atmosphere model. "PCCM3" contains values averaged over a 5 year uncoupled run using FOAM's atmosphere and climate SSTs. Overall, CCM3 comes much closer to the observations than CCM2 and FOAM retains those features. The new deep convection formalism increased the high cloud amount between CCM2 and CCM3 (Hack *et al.*, 1997). FOAM, which contains a combination of the CCM2 land model and the new convection routines, produces even more high cloud from vigorous land-based convection. The land model is most likely also the reason the net surface solar radiation in FOAM is nearly the same as in CCM2. Comparison between the PCCM3 and FOAM values shows that coupling to an ocean model does not greatly affect global annual mean quantities in the atmosphere.

Table 4: Global Annual Average Properties.

	Observations	CCM2	CCM3	FOAM	PCCM3
Outgoing Longwave Radiation (W/m^2)	234.8	241.10	236.97	237.00	234.78
Absorbed Solar Radiation (W/m^2)	238.1	245.35	236.88	237.78	236.75
Longwave Cloud Forcing (W/m^2)	29.2	30.76	29.25	28.90	29.80
Shortwave Cloud Forcing (W/m^2)	-48.2	-50.14	-49.54	-40.79	-41.48
Cloud Fraction (Percent)					
Total	52.2 - 62.5	52.86	58.83	63.46	63.93
Low	26.0 - 43.8	30.52	34.75	31.44	31.95
Middle	18.0	22.20	20.84	16.44	17.07
High	14.0	28.89	34.62	43.17	43.96
Latent Heat Flux (W/m^2)	78.0	104.04	89.97	94.49	93.68
Sensible Heat Flux (W/m^2)	24.0	9.32	20.47	20.66	19.93
Precipitation (mm/day)	2.69	3.58	3.09	3.24	3.22
Net Surface Solar Radiation (W/m^2)	168	180.89	171.05	180.32	179.30
Net Surface Longwave Radiation (W/m^2)	66	62.58	60.68	64.42	63.83

Fig. 14 shows the annual average SST produced by FOAM and its difference from the Shea climatology. The error values in SST are typical of other coupled models, particularly the two degree cold error in the West Pacific and the too-warm waters off the coast of South America (Mechoso *et al.*, 1995). The latter is generally believed to be caused by a chronic inability of spectral atmosphere models to produce marine strato-cumulus clouds west of the Andes (Guilyarid and Madec, 1997; Kiehl *et al.*, 1994). Relatively weak pressure systems in the R15 atmosphere result in smaller transports in the western boundary currents and less advection of warm water leading to the negative anomalies seen there. The error in the ACC temperature is believed to be caused by too high values for the diffusion coefficients in the ocean model which were not retuned after converting to the nonlinear equation of state. Some preliminary exploration of the diffusion parameter space in ocean-only runs suggest that the diffusion coefficients can be reduced by 50%, resulting in stronger ACC flow and temperature gradient.

The zonal mean of the annual temperature in the ocean and atmosphere are shown in Fig. 15. The atmosphere biases, notably the too cold polar upper atmosphere, are no different from uncoupled CCM3 (Hack *et al.*, 1997). Vertically well mixed regions in the Southern ocean are visible in Fig. 15 and the downward slope of isotherms towards the northern bottom are the signature of the models North Atlantic deep water formation. A thermocline is present though not as sharply defined as in the real ocean but typical for ocean models of this resolution.

A closer view of the simulated zonal ocean structure in the Pacific along 154W is shown in Fig. 16. The South Equatorial Current (SEC) is stronger and more centrally located than observations (Pickard and Emery, 1990) in response to the

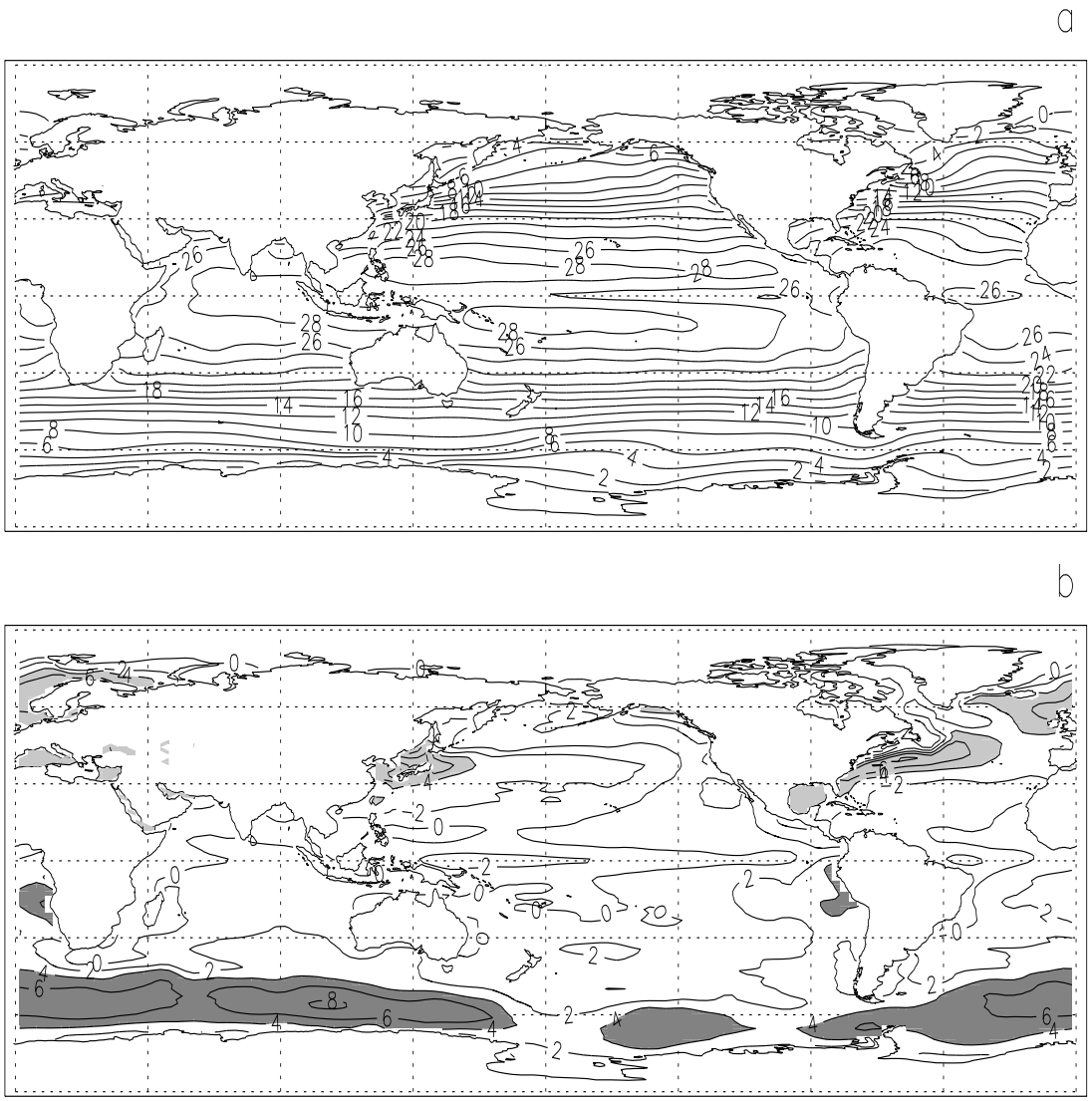

Figure 14: (a) Annual Mean SST from the coupled run. (b) Model SST - Shea Climate SST. Contours are 2°C in both. In (b) values greater than 4° are shaded dark gray while values less than -4° are shaded light gray. Note that in this and subsequent figures, real continental outlines are used to facilitate orientation.

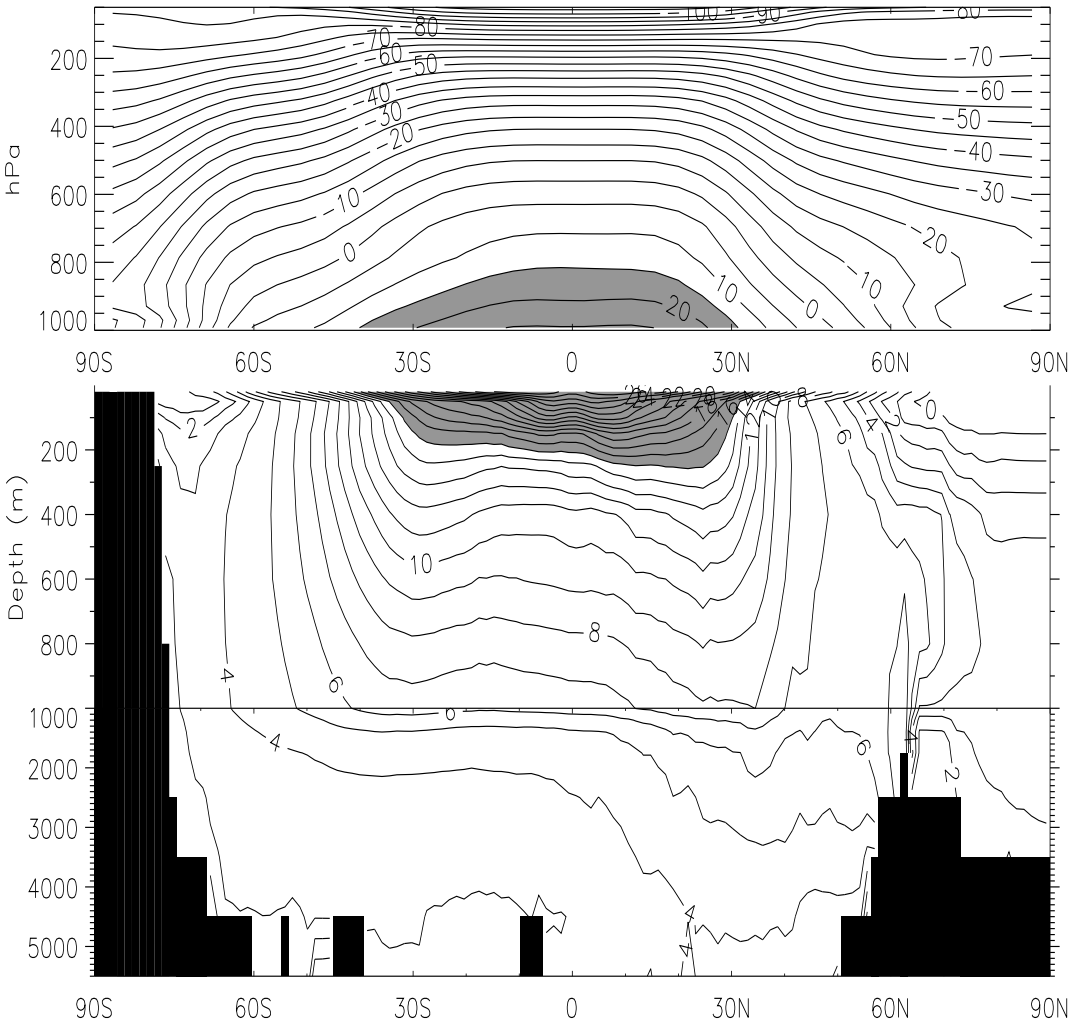

Figure 15: (a) Zonal mean of the annual mean temperature in the atmosphere and potential temperature in the ocean. Contour interval is 5°C in the atmosphere and 1°C in the ocean. Values greater than 15°C are shaded.

strong easterly wind stress on the equator (See Chapter 5). The large counter currents are a response to this strong SEC and to the equatorial upwelling. The South Equatorial Counter Current (SECC) is about twice as strong as observed and contributes to the large tongue of warm water in the South Pacific (Fig. 14). The Equatorial Undercurrent and North Equatorial Counter Current (NECC) are both weaker then observed by half. The center of the undercurrent is at approximately the correct depth (150m) while the NECC is too wide. Similar current structures—strong SEC, other currents weak—have been seen in the CSM coupled model (Danabasoglu, 1997) which has a similar horizontal resolution.

In the annual and zonal averaged zonal wind, Fig. 17, the jet cores are a little too strong in the southern hemisphere when compared to observations and to an uncoupled R15 CCM2 (Williamson *et al.*, 1995). The gain in strength probably comes from the increased Hadley circulation which accompanied the new convection parameterizations (Hack *et al.*, 1997). The latitudinal placement is satisfactory although the northern hemisphere jet has a slight poleward shift.

Returning to horizontal annual averages, the models precipitation field is shown in Fig. 18. The precipitation tends to be located over the warmest waters and over steep orographic features–the latter still a nagging problem for the T42 CCM3 (Hack *et al.*, 1997). Another common feature of coupled models, a split Inter-Tropical Convergence Zone (ITCZ) (Mechoso *et al.*, 1995), is also visible in the precipitation field. The Southern Hemisphere branch of the ITCZ is a response to the warm tongue also located there (Fig. 14). The dry regions over the Sahara and Middle East are well simulated while the Indian monsoon circulation is located too far North and East.

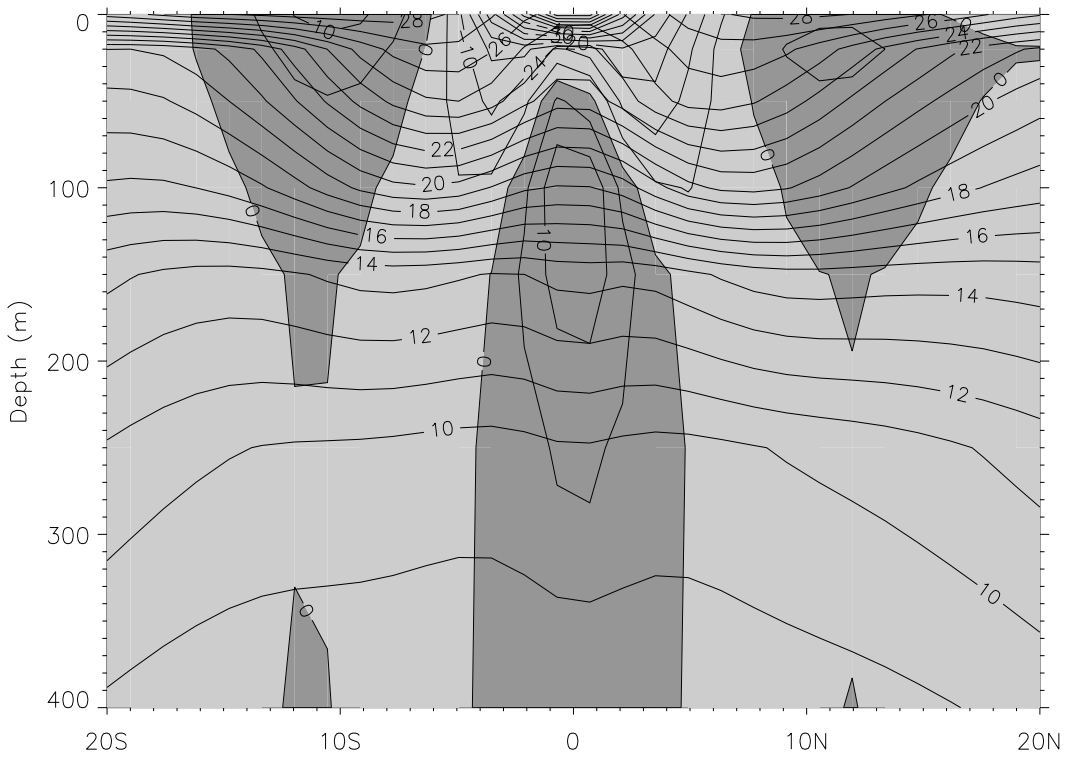

Figure 16: Annual mean temperature and currents along 154°W. Temperature contours are 1°C. Current contours are 5 cm/s. Eastward currents are shaded dark, westward light.

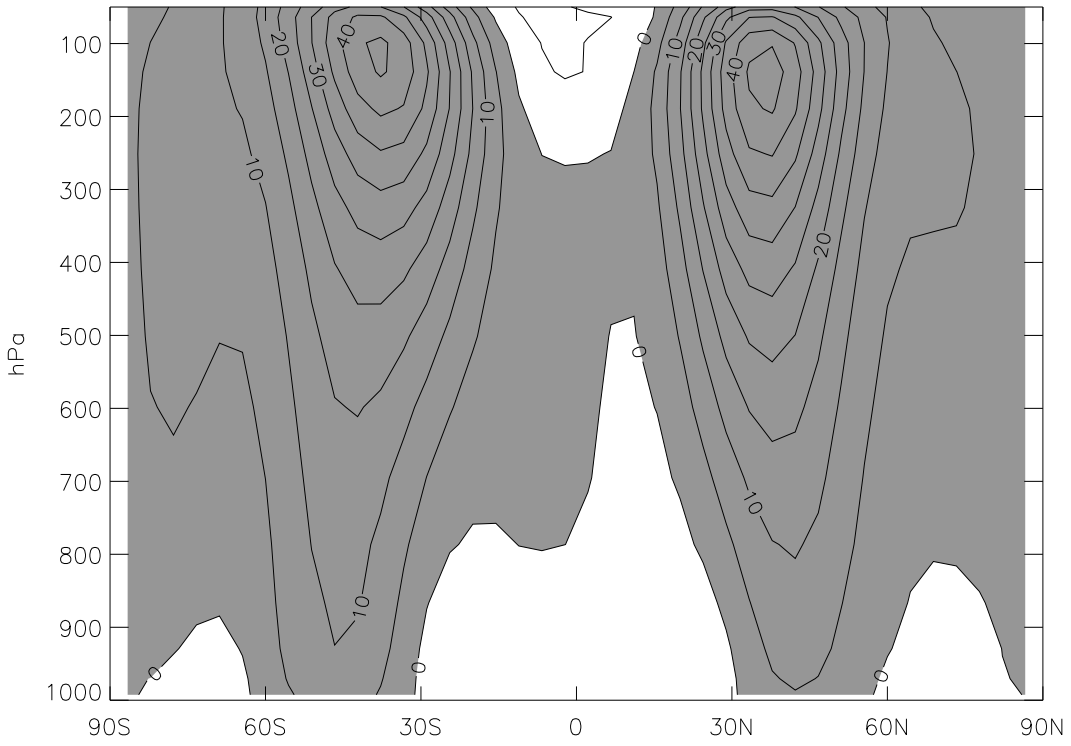

Figure 17: Annual and zonal averaged zonal wind. Contours are in 5 m/s with positive (westward) values shaded.

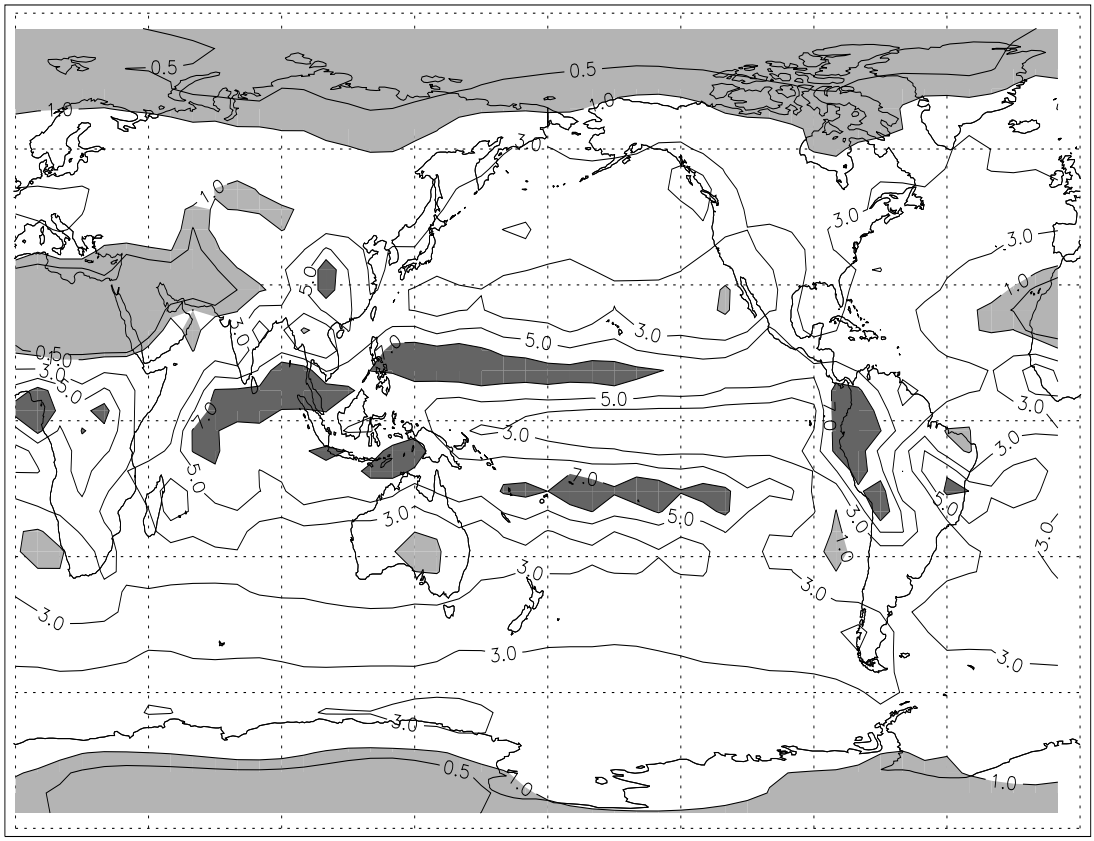

Figure 18: Annual mean precipitation (mm/day) from the coupled model. Contour intervals are 0.5, 1, 3, 5 and 7 mm/day. Values less than 1.0 mm/day are shaded light gray. Values greater than 7 mm/day are shaded dark gray.

The model's simulated annual salinity field and its difference from the Levitus (1982) climatology is shown in Fig. 19. Overall the model does well in reproducing the high salinities in the subtropics and relatively fresh water in the poles. There is a a tongue of relatively low salinity extending through Indonesia and into the Indian ocean as observed. Some features, such as the shifting of the North Pacific salinity maximum towards the coast and positive anomalies in the North Pacific and Indian ocean, have been seen in other models which try to simulate the salinity field without flux adjustments (Guilyarid and Madec, 1997). High salinities off the west coast of North and South America are another consequence of the lack of marine stratus clouds already noted. The salinity minimum in the South Pacific (Fig. 19) is a response to the southern half of the split ITCZ.

Some salinity minima can be seen near major river mouths (Congo, Yellow) where FOAM's river model is simulating large flows in response to the large land-based precipitation. The simulated annual average flow from selected rivers and their observed values (Milliman and Meade, 1983) are given in Table 5. Many river outflows agree well with observations such as the Columbia, Indus, and the combined Ob and Yenesei. The Amazon is underestimated because much of its source precipitation is falling on the west side of the Andes (Fig. 18). Other rivers with sources in the tropics (Nile, Congo) show the effects of the strong precipitation over land. The overestimate of the St. Lawrence is probably caused by the lack of any Great Lakes in the model. The total outflow is overestimated by about 19 percent which can be called a success considering how simple the hydrology model is and that the rivers are sourced by predicted precipitation.

This overview of FOAM's climate concludes with one seasonal cycle. As seen

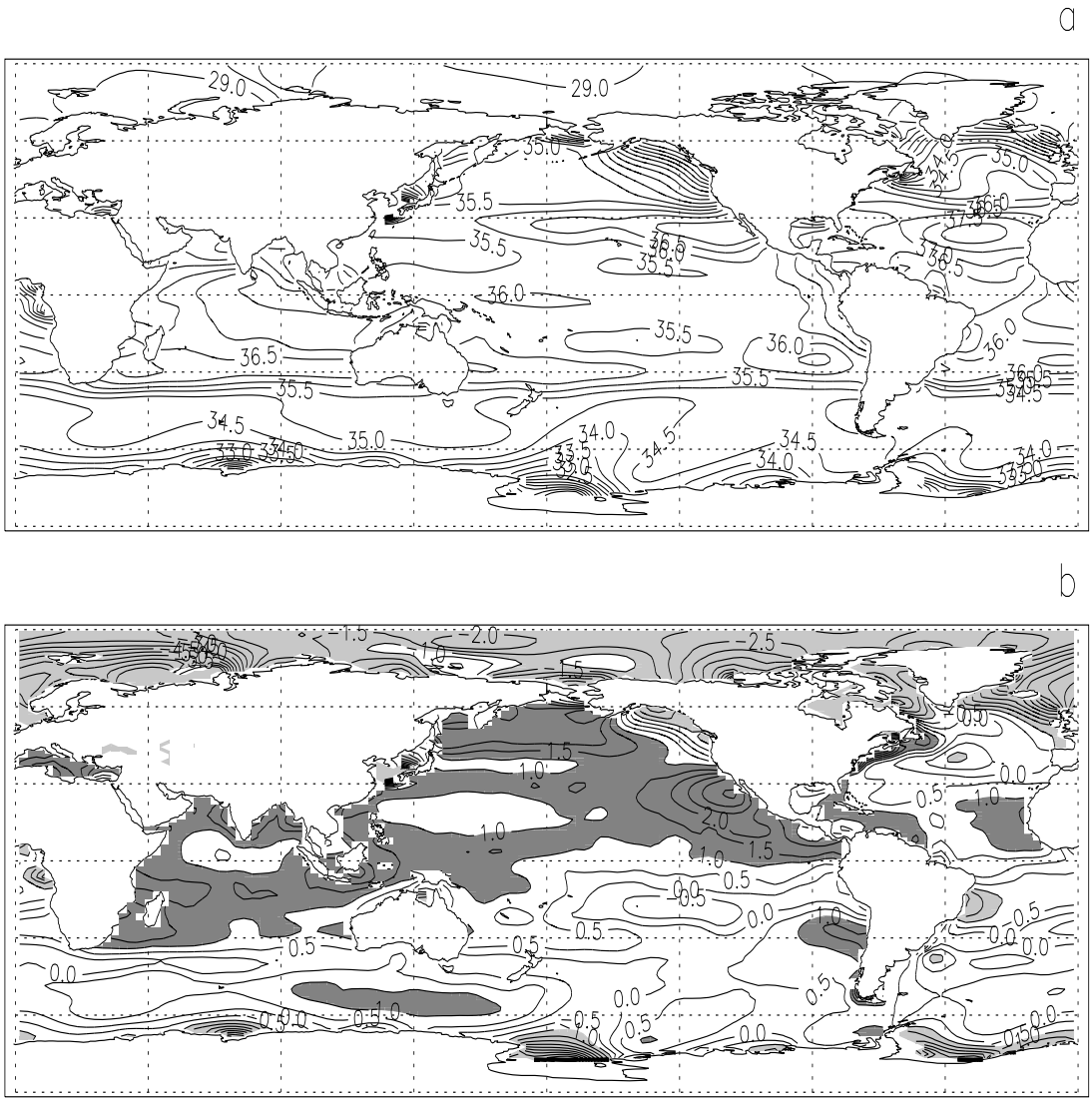

Figure 19: (a) Annual mean sea surface salinity. Contour interval is 0.5 ppt. (b) Model SSS minus Levitus climatology. Values greater than 1.0 ppt are shaded dark gray while values less than -1.0 ppt are shaded light gray.

Table 5: Annual average river outflow (10^3 m^3 s^{-1})

River	FOAM	Observations
Amazon	83	199
Brahmaputra and Ganges	5	17
Columbia	14	13
Congo	79	17
Indus	3	5
Lena	11	17
Mekong	5	8
Mississippi	29	17
Niger	24	2
Nile	28	9
Ob and Yenesei	33	38
Orange	1	2
Orinoco	22	10
Parana	20	41
St. Lawrence	20	10
Yangtze	65	17
Yellow	45	6
Yukon	10	25
Zambezi	12	1
Total	509	428

in Fig. 20, FOAM simulates the phase of the sea ice cycle well compared to observations (Peixoto and Oort, 1992). The Arctic sea ice maximum is too large (19.5 vs. 15) but occurs in late January/early February as observed. The Arctic minimum is too small but occurs at the correct time. Antarctic sea ice also has the correct phase but is consistently underestimated probably because FOAM's ice model contains no sea ice dynamics which are important in the growth of Antarctic sea ice.

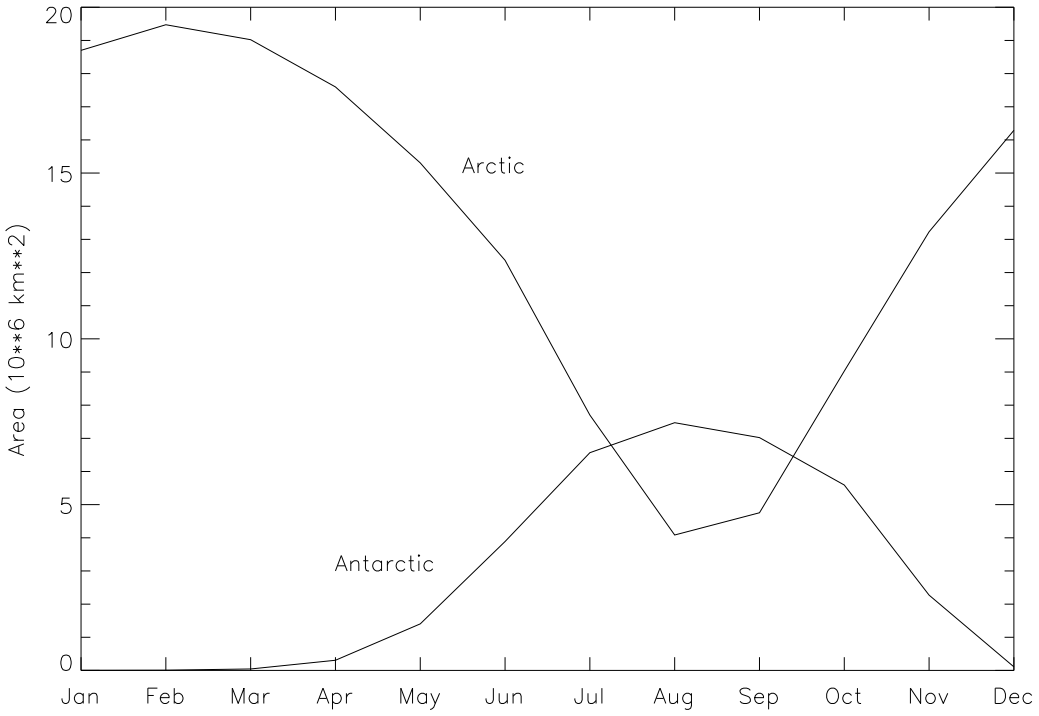

Figure 20: Annual cycle in sea ice cover in 10^6 km^2 for the Arctic and Antarctic calculated from last 40 years of the integration.

In conclusion, FOAM produces a mean climate that compares well with other contemporary climate models and does not suffer greatly when compared to ones

with higher resolution atmospheres. Trends in long integrations such as this one are a problem that FOAM and other climate modeling efforts still have to address. To continue the current integration for many thousands of years would not be useful in the face of the simulated trend in salinity. However the current 600+ year integration can still be used for studies of internal variability which are discussed next.

Chapter 4

Variability in FOAM

The main focus of this work, surveying the range of the internal variability of the atmosphere ocean system, is presented here. The output from the long run described in the previous Chapter was used. Although the main interest is low frequency variability, results are presented for (relatively) higher frequencies such as ENSO as well, so that FOAM's ability to simulate internal variability can be compared against phenomena for which there are more observations and model results.

4.1 Analysis Method

The analysis begins by assuming that the variability in the whole atmosphere-ocean system is well represented by the variability in the sea surface temperature field. Because of its tight coupling with both the atmospheric forcing and the ocean response, SST is a natural choice. The variability in the model ocean-atmosphere system is then characterized through a rotated EOF (Empirical Orthogonal Function) analysis of the global SST anomaly field in each of three separate frequency bands. The frequency bands chosen correspond roughly to the ranges of variability already suggested by other modeling work and observations: a relatively high

frequency band with a cutoff of five years (the interannual variability), a midband consisting of frequencies between five and thirty years (decadal variability) and a low frequency band of all signals thirty years or longer (interdecadal and longer). These frequencies are isolated by applying Finite Impulse Response (FIR) filters with the above cutoff frequencies to the SST anomalies.

The three analyses are referred to as the highpass, bandpass, and lowpass analysis, respectively, in accordance with the filter applied. (Similar lowpass and highpass filters were also used by Delworth (1993) and (1996), respectively. See Oppenheim and Schafer (1975) for a general discussion of FIR filter techniques). The highpass analysis is applied to monthly anomalies while the bandpass and lowpass analyses are applied to annual SST anomalies. Prior to the application of each filter, linear trends are removed by fitting a straight line to the time series at each spatial point and subtracting. After filtering, each point is weighted by the cosine of latitude to account for the area represented by each grid point. (The weighting is removed for plotting.) Then for each of the three sets of filtered SST time series, a VARIMAX rotated (Harman, 1967; Horel, 1981) EOF analysis is performed.

The analysis technique is straightforward. What is unique to this study is the size of the data set analyzed both in space and time and the number of degrees of freedom of the source model. (e.g. Delworth (1996) examined lowpass filtered data from the simpler GFDL coupled model.) By analyzing the entire global SST data set no assumptions are made about where the variability might be by limiting the domain of analysis. The result is a general survey and cataloging of the most prominent locations of atmosphere-ocean variability sorted by prominence (as

contained in the explained variance) and period (by doing separate analyses for three different frequency bands).

The following sections present results from each of the three EOF analyses beginning with the highpass. In the discussion, HPEOF1 refers to the first EOF of the highpass filtered data, BPEOF1 is the first EOF from the bandpass filtered data and so forth. All EOFs shown below have been rotated unless otherwise noted. In selected cases, the physics behind the variability patterns are examined more closely although a complete description of the physics behind all the variability found in the model is beyond the scope of this thesis.

4.2 Interannual Variability

To determine the most prominent sources of variability with periods of less than 5 years, we begin with the 6552 monthly averages of SST from Year 100 to Year 646 (Fig. 10). Year 100 was chosen as being sufficiently far removed from the transient activity associated with models adjustment after the initial coupling (See Section 3.1 and Fig. 11a). The mean seasonal cycle is defined over the same period and then removed from each corresponding month to form the anomaly field.

Ten EOFs were found which together explain 29% of the variance. The first 5, which explained 19% of the variance, are discussed below.

The dominant source of variability over the globe on interannual time scales is, unsurprisingly, ENSO. HPEOF1, Fig. 21 is the models ENSO signal. It is properly located in the East Pacific although the center is located to far west. The strong variability in the West Pacific, seen in Fig. 22, is a problem common to

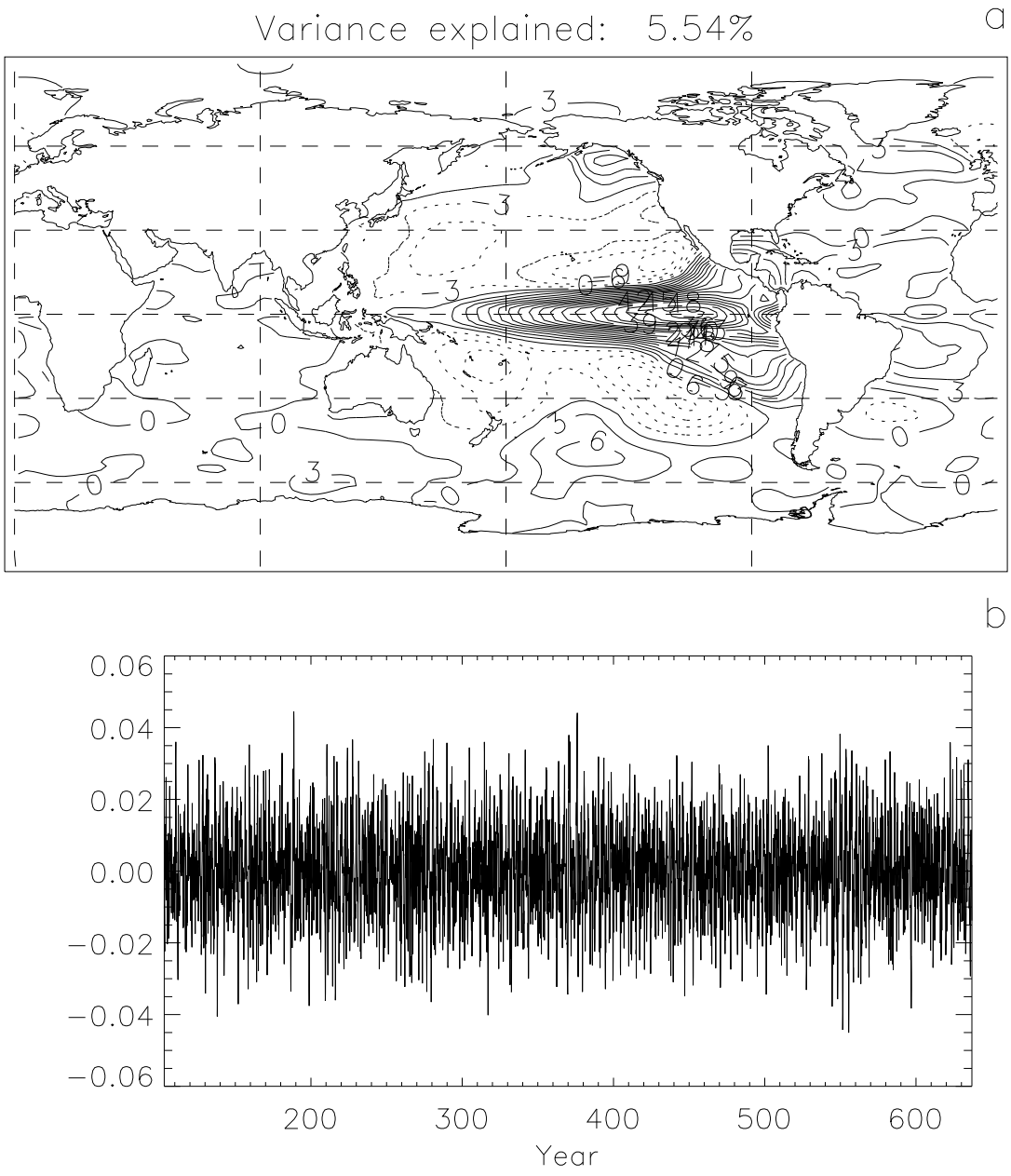

Figure 21: First EOF (a) and time series (b) of highpass filtered monthly average SST anomalies.

other coupled models including ones with higher resolution atmospheres such as CSM (Neelin *et al.*, 1992; Meehl and Arblaster, 1997). These models also have in common the "skinny" cold tongue which penetrates far to the west and the split ITCZ. All these features are most likely related.

HPEOF1 represents the variability in the NINO3 region (between 5°N-5°S and 150°W-90°) as can be seen by comparing HPEOF1's time series with the models NINO3 time series subject to the same highpass filter. A portion of each is shown in Fig. 23. These two time series have a correlation of 0.92. That correlation could probably be even higher except the westward displacement of ENSO means the NINO3 region is not as representative of ENSO variability in the coupled model. The strength and frequency of the NINO3 anomalies are again typical for coupled models, 1-1.5°C and 3-5 years, but somewhat better than models with similar atmospheric resolution (Neelin *et al.*, 1992). This particular portion of the time series shows a transition from a period of weak ENSO variability to strong variability at about Year 624.

HPEOF3 (3.04%) (Fig. 24) is most likely not an independent mode of variability but is instead the Indian ocean response to ENSO. The signal is most prominent in the vicinity of the highly variable northern gyre. The northern gyre in the Indian Ocean reverses direction in response to the forcing of the Monsoon winds. Statistical evidence for a relation between interannual variability in the Indian monsoon and ENSO is as old as the study of ENSO but a causal explanation is still lacking (Hastenrath, 1986).

In all, ENSO related signals account for 10.3% of the global SST variability on interannual timescales. In a similar EOF analysis of observed SST, confined to

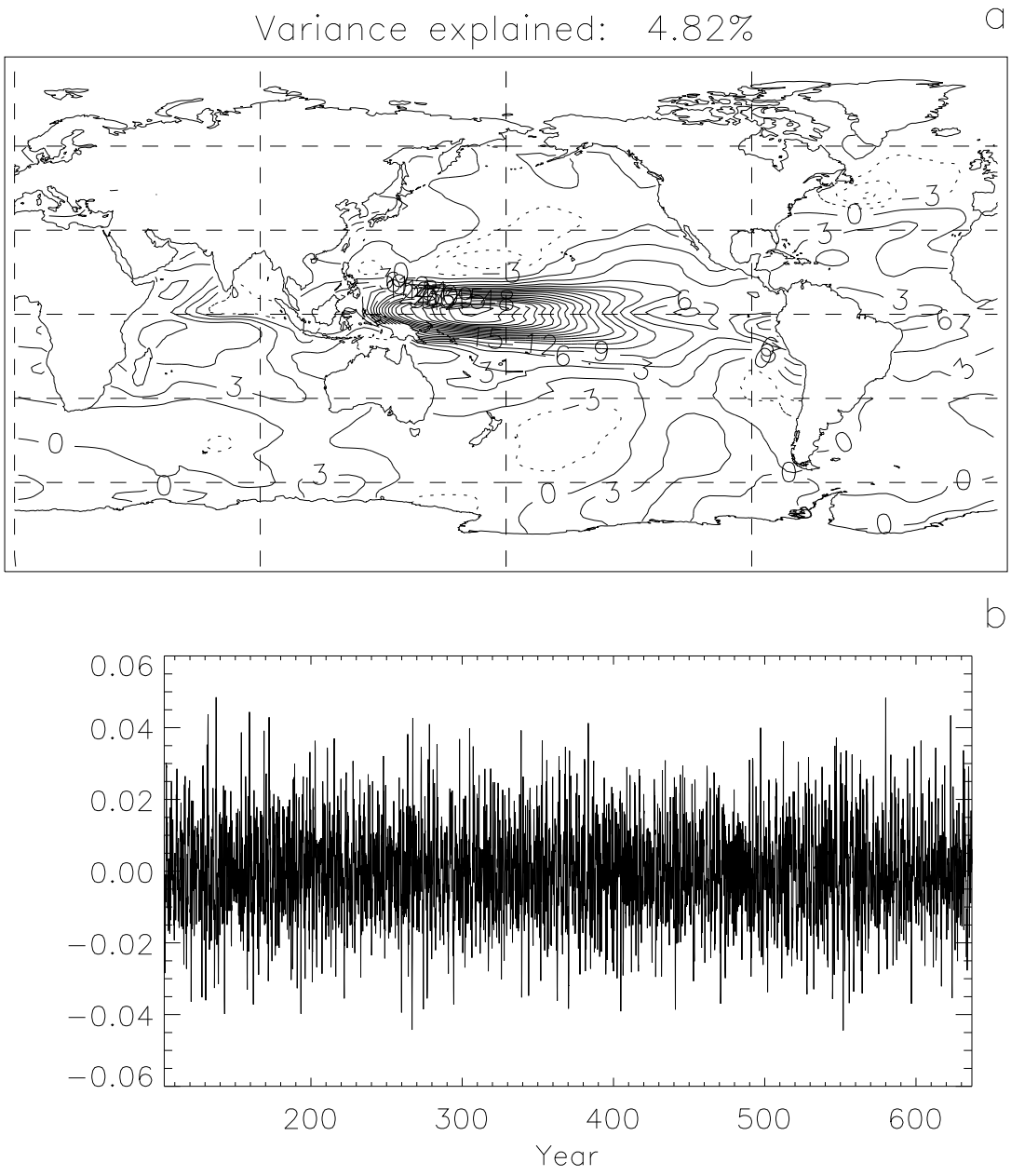

Figure 22: Second EOF (a) and time series (b) of highpass filtered monthly average SST anomalies.

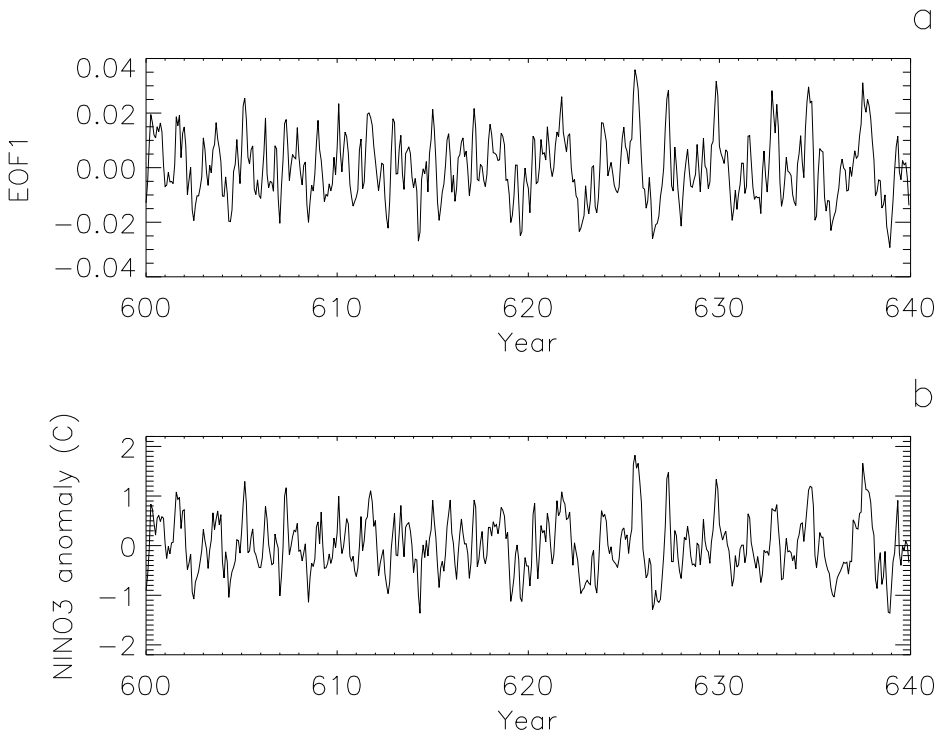

Figure 23: Coincident time series for (a) HPEOF1 and (b) NINO3 temperature.

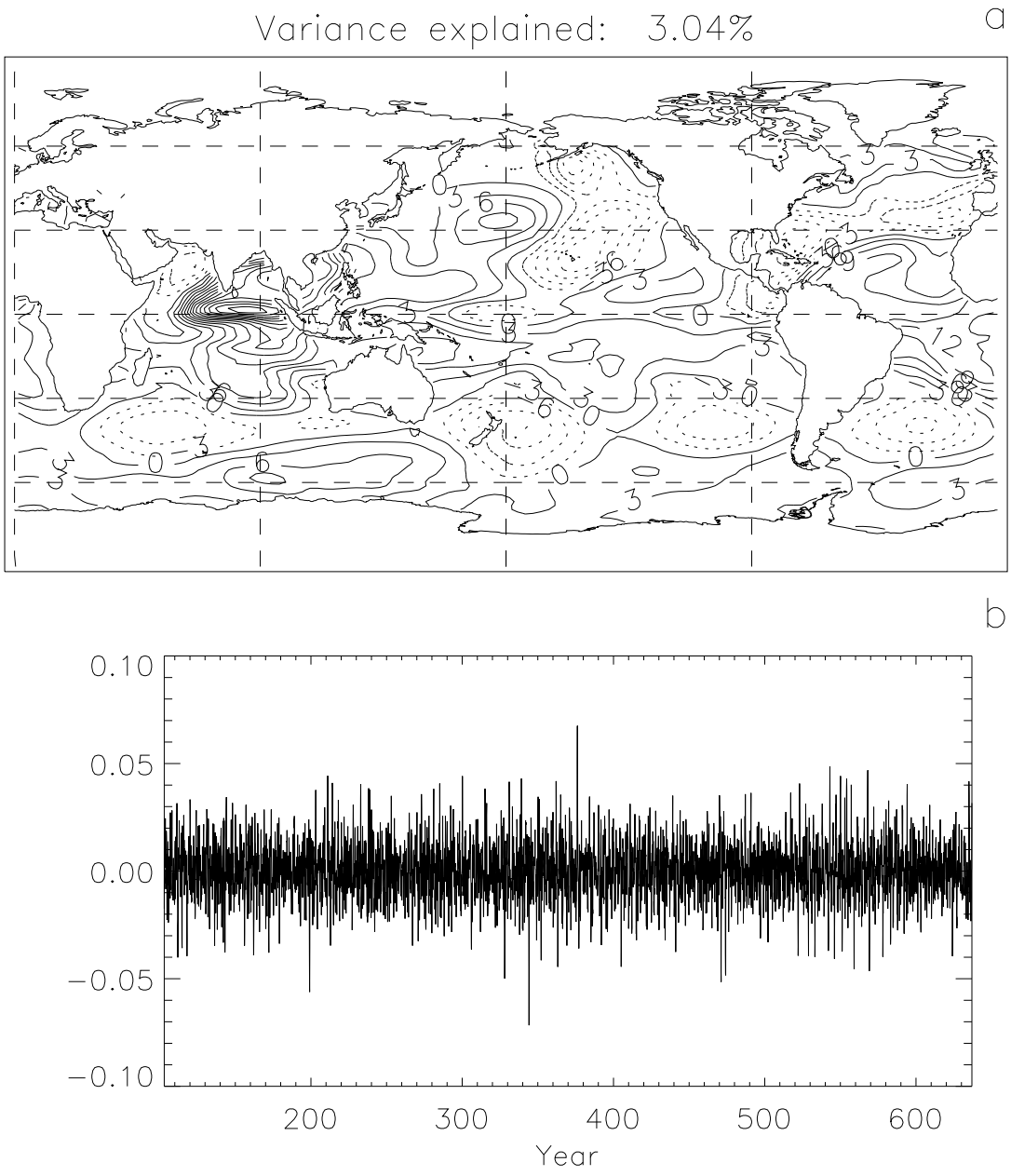

Figure 24: Third EOF (a) and time series (b) of highpass filtered monthly average SST anomalies.

the tropical Pacific, ENSO explains 68% of the variance (Zebiak and Cane, 1991). Kawamura (1994) performed a rotated EOF analysis on 34 years of SST from 30°S to 55°N and found the ENSO mode, also the first mode, accounted for 8.3% of the variance. The differences are mostly due to the different domains of analysis but also by the character of the model ENSO.

The next largest source of variability are in the gyres of the northern oceans. HPEOF4(2.97%) and HPEOF5(2.83%) (Fig 25 and Fig. 26) describe the interannual SST variability associated with the main gyre circulations of the North Atlantic and North Pacific respectively. These are most likely caused by variability in the ocean gyres. The North Pacific oscillation shown in HPEOF5 is explored further in the bandpass analysis where it is more prominent.

The second EOF found by Kawamura (1994) was a combination of Indian and North Pacific modes that explained 4.9% of the variance. This compares well with the 5.86% total for HPEOF5 and HPEOF3. HPEOF4 is interesting because it shows the influence of multidecadal variability on the interannual variability. The amplitude of the associated time series decreases steadily from Year 150 to about Year 240 (Fig. 25b). Year 240 coincides with the sudden increase in annual average snow cover over Siberia (Fig. 13). This trend was caused by the gradual cooling of the Arctic ocean as the Arctic ocean-atmosphere system reached an equilibrium. A separate change begins after Year 430. There is a 50 year modulation of the amplitude associated with a 50 year thermohaline oscillation which did not begin until that year. This oscillation is discussed in Section 4.4. HPEOF4 strongly resembles the third EOF found by Kawamura (1994) which explained 3.6% of the variance.

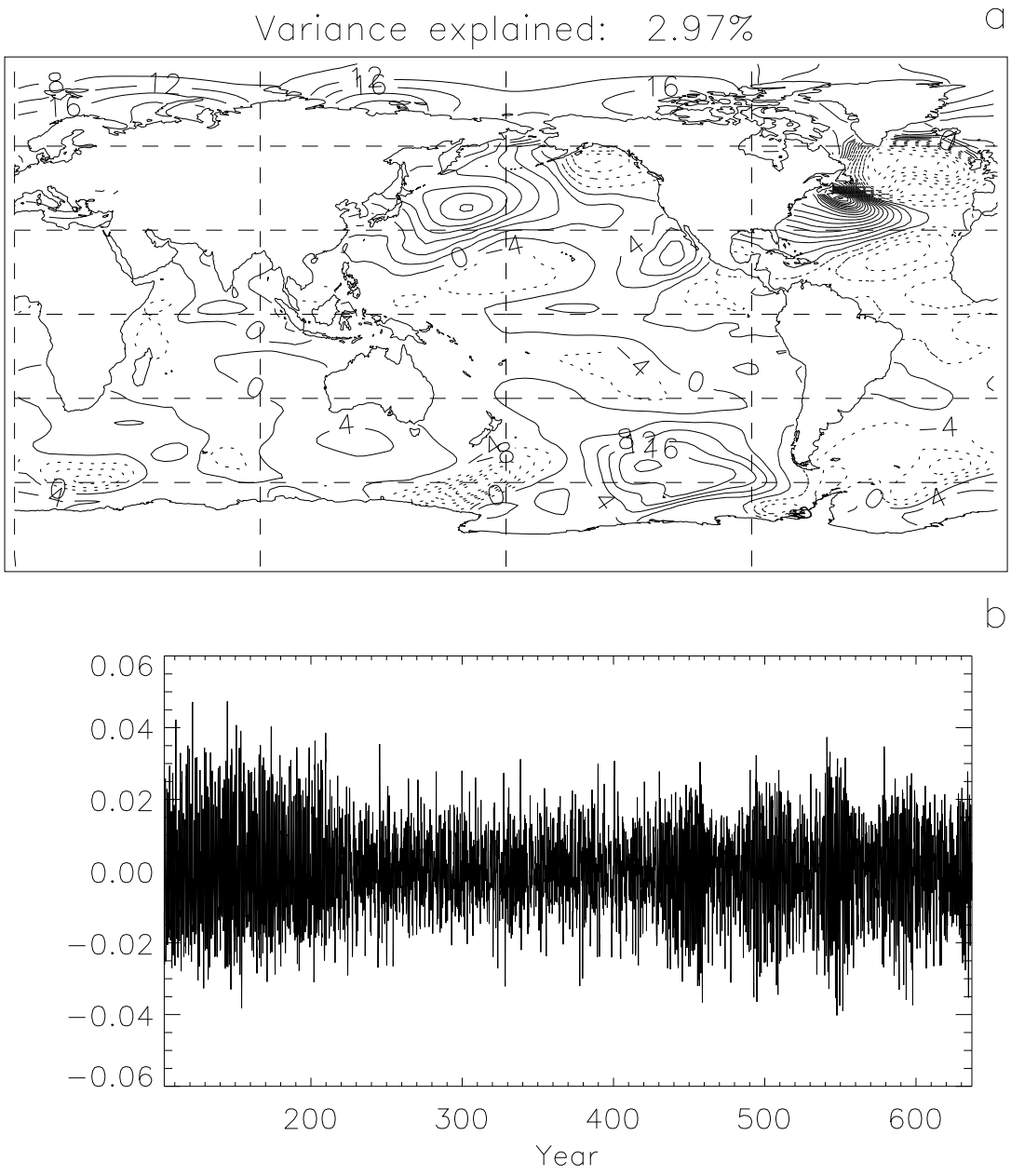

Figure 25: Fourth EOF (a) and time series (b) of highpass filtered monthly average SST anomalies.

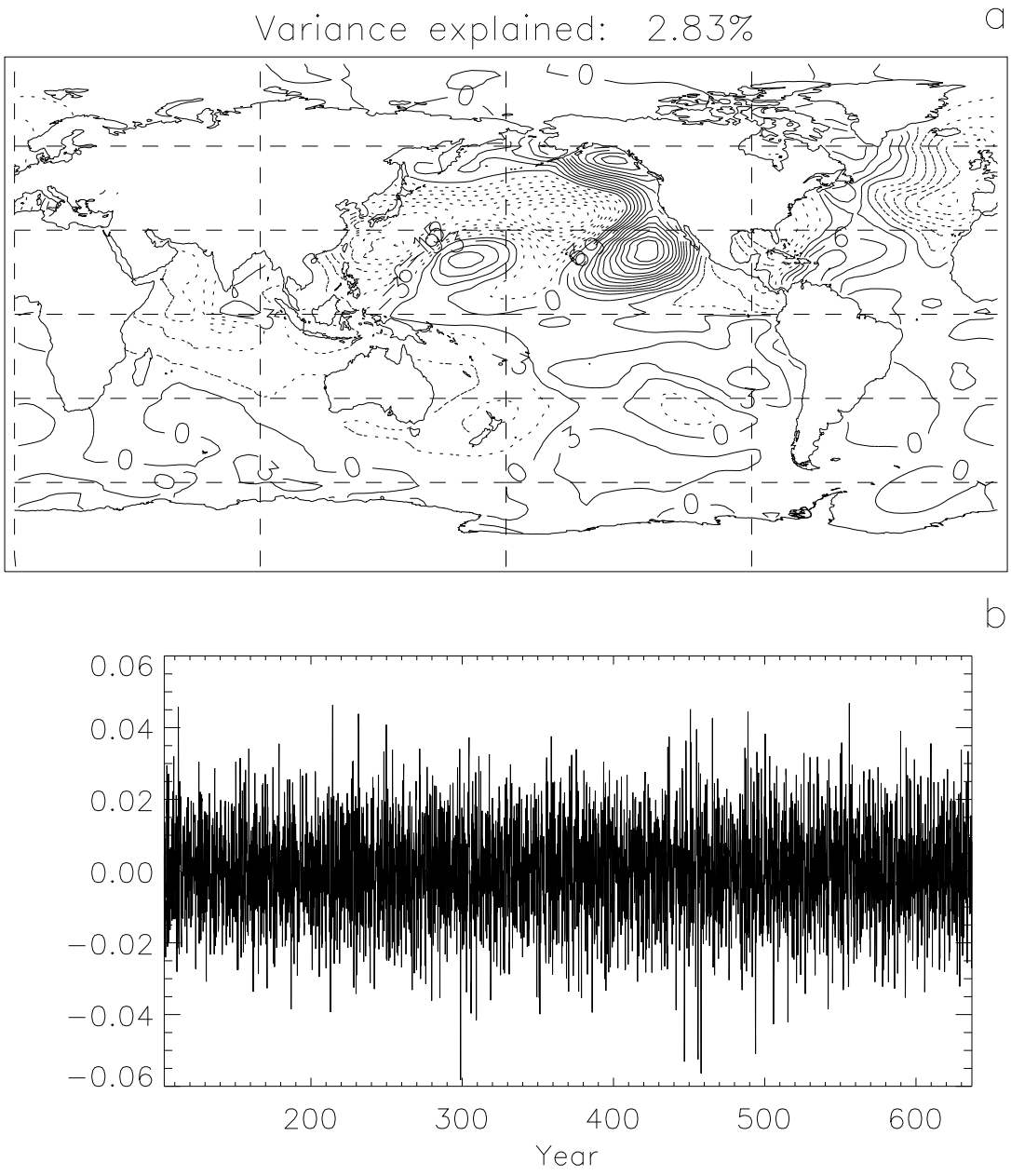

Figure 26: Fifth EOF (a) and time series (b) of highpass filtered monthly average SST anomalies.

4.3 Decadal Variability

To assess the model's decadal variability, the analysis begins with annual averages of SST constructed from each of the 547 sets of 12 monthly history files from Year 100 to Year 646. (Fig. 10). This period corresponds to that used in the interannual variability analysis discussed above. The bandpass filter was applied and ten EOFs were found which together account for 49% of the variance. The first 5 (34%) were rotated and are discussed here.

Nearly 15% of the decadal variability is associated with variability in the tropics as seen in BPEOF1 (Fig. 27). It resembles an ENSO signal: strongest positive anomalies in the Eastern Pacific and weaker positive anomalies in the Indian and Atlantic ocean with negative anomalies in the North Pacific and North Atlantic. Because the cutoff frequency was five years, some of the lower frequency ENSO activity is probably included in this pattern. But there is also decadal scale variability, with periods of about 10-15 years, as seen in the associated time series of BPEOF1 and in the spectrum of that time series (Fig. 28). Simple coupled models (without a full atmospheric GCM) used to simulate the tropical Pacific have exhibited decadal variability in long integrations (Zebiak and Cane, 1991; Latif, 1996). There is also some observational evidence for decadal variability in the tropics. Predictive models initialized with observed data indicate ENSO was less predictable in the 1970's compared to the 1980's, a feature associated with changes in the seasonal phase locking of ENSO (Balmaseda *et al.*, 1995). Variability not associated with ENSO, such as an upward trend in SST in the West Pacific over the past twenty years, has also been detected (Gutzler, 1996). However it is

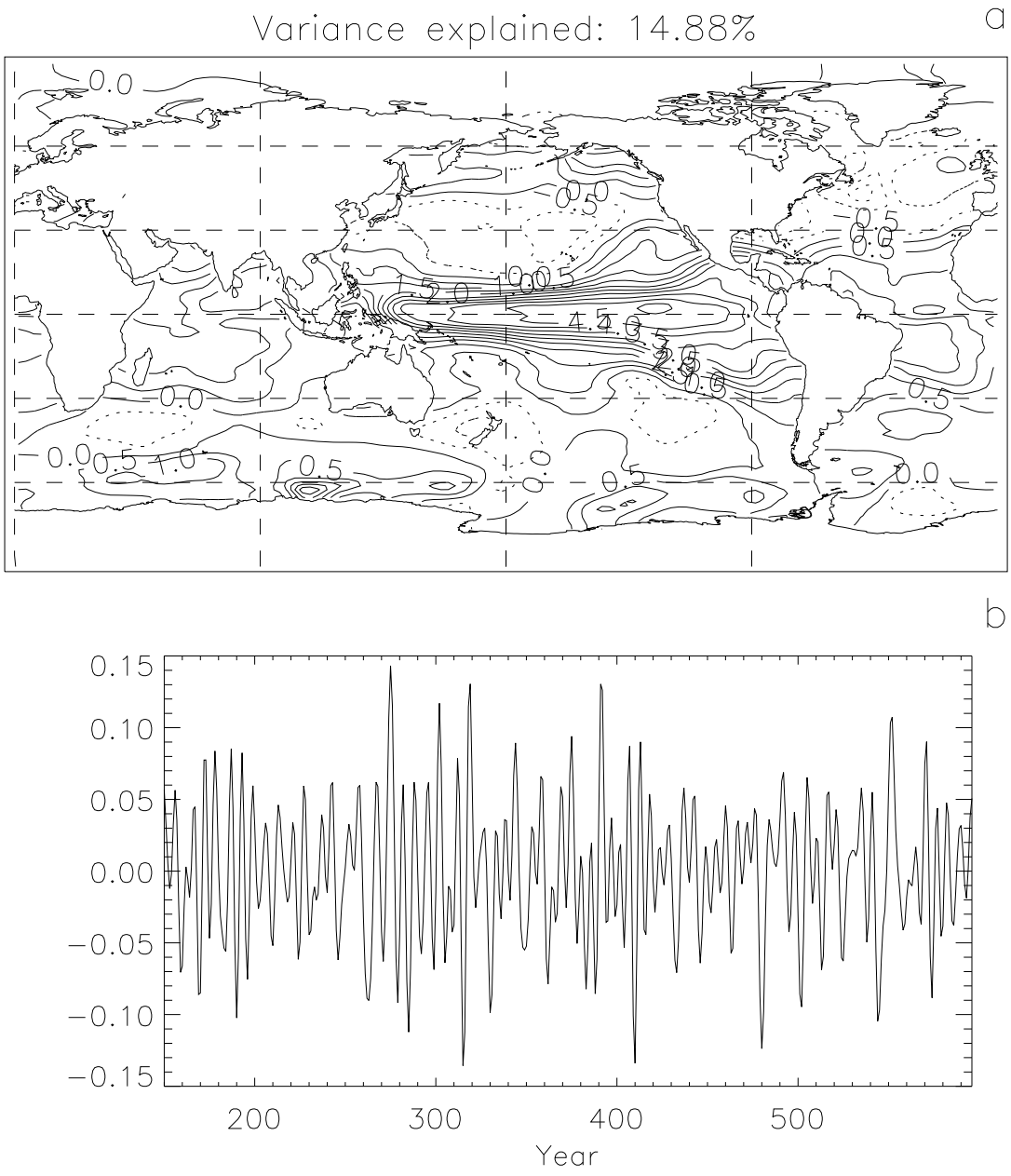

Figure 27: First EOF (a) and time series (b) of bandpass filtered annual average SST anomalies.

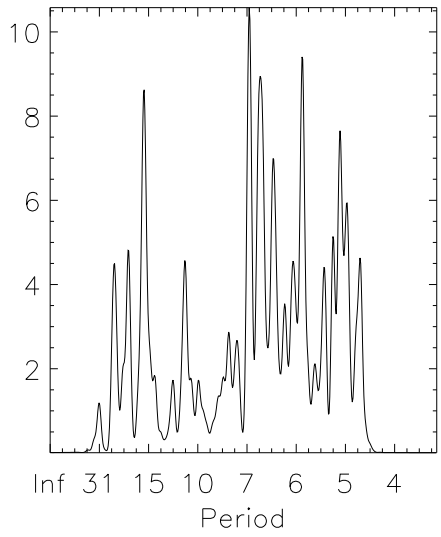

Figure 28: Spectrum of the associated time series for BPEOF1 (Fig. 27). Period is in years.

unclear how much of the observed variability is related to anthropogenic warming, an effect not included in this model.

Latif *et al.* (1997) have performed a POP analysis (an objective technique similar to more traditional EOF analysis) on 42 years of observed SST in the region between 30°S-60°N and found, after the dominant ENSO mode, a tropical Pacific decadal mode with a period of 13 years which explains 10% of the SST variance, results similar to those of BPEOF1. The same authors cite support for a decadal scale tropical variability in coral records. Unlike BPEOF1, their decadal mode has little amplitude in the East Pacific but instead resembles a "horseshoe" with maxima extending from the eastern subtropics to the West Pacific. As mentioned above, these differences may be caused by too much of the normal ENSO mode being captured by the bandpass EOF analysis. The positive contours extending

into the subtropics on the eastern end of BPEOF1 could be the ends of the horseshoe. The relationships between tropical and extratropical decadal variability in the Pacific are discussed further in Section 4.3.1.

The next largest source of variability on decadal time scales is in the Antarctic. (BPEOF2, Fig. 29) The location of the maximum variability coincides with the point on the Antarctic coast which contains the warmest and saltiest water (See Figs. 14 and 19). This mode is very similar to a 20-year oscillation seen in the HOPE ocean-only model which had its strongest signal at nearly the same point and was attributed to a westward traveling density anomaly (see Drijfhout *et al.* (1996) for details). An additional pattern of Antarctic decadal variability is seen in BPEOF5 (Fig. 30). The axis of this dipole pattern corresponds to a tongue of cold temperature and low salinity emanating from the Ross Sea (See Figs. 14 and 19 again). It may also be related to the propagation mechanism discussed by Drijfhout *et al.* (1996). There are no other coupled model results available for comparison and few observations. A report of westward propagation of sea ice extent anomalies was attributed to advection by the westward Antarctic Coastal Current (Osborn, 1997).

The variability in the North Atlantic seen in BPEOF3 (Fig. 31)accounts for nearly 5% of the interdecadal variability in global SST. A similar pattern of North Atlantic decadal variability is found in the coupled models of Latif *et al.* (1996) (with a period of 17 years) and Zorita and Frankignoul (1997) (who find two modes with 10 and 20 year periods) but not in the GFDL coupled model (Delworth, 1996). BPEOF3 also resembles decadal variability in the North Atlantic reported in observations by Deser and Blackmon (1993) with a period of about 12 years.

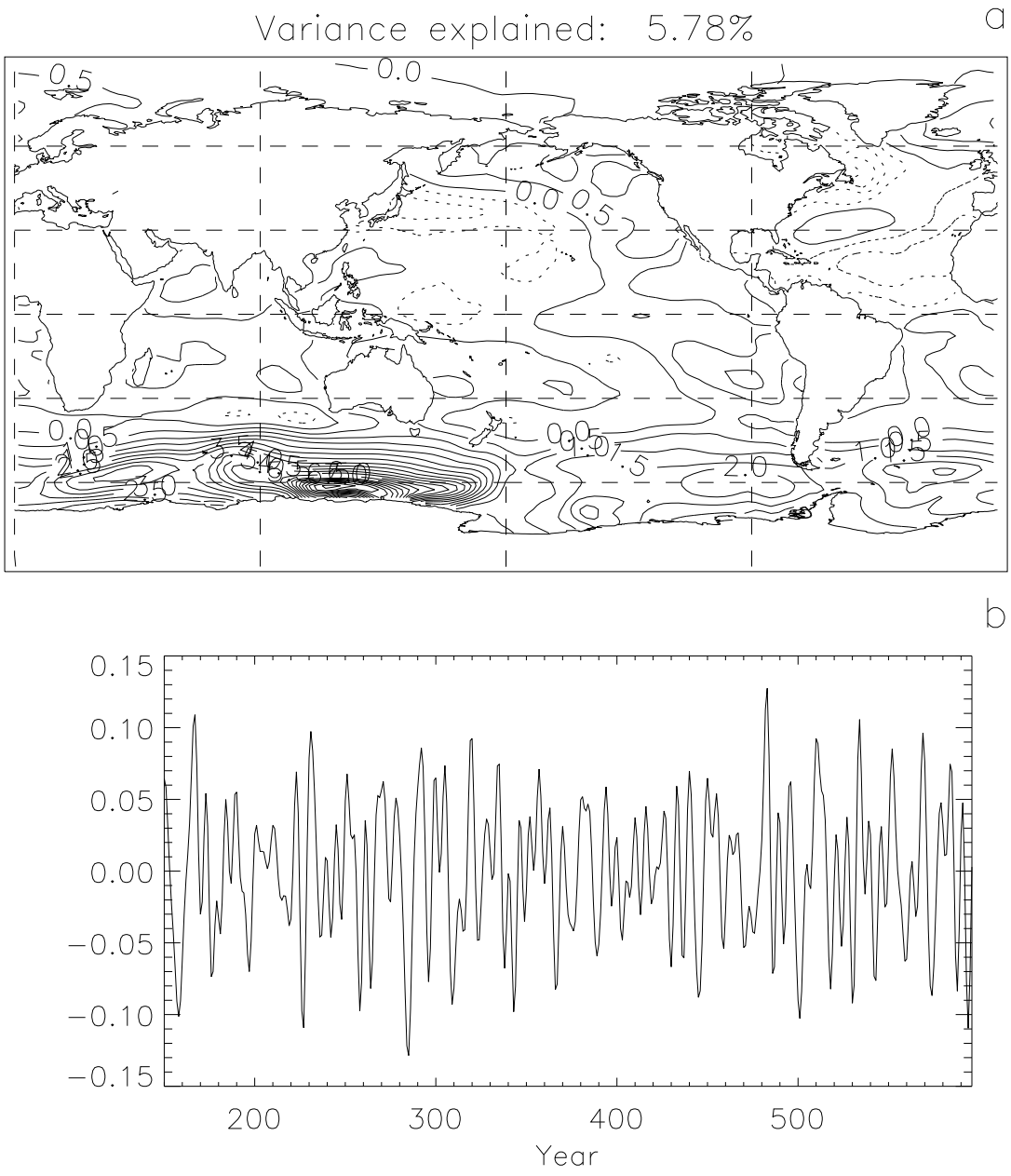

Figure 29: Second EOF (a) and time series (b) of bandpass filtered annual average SST anomalies.

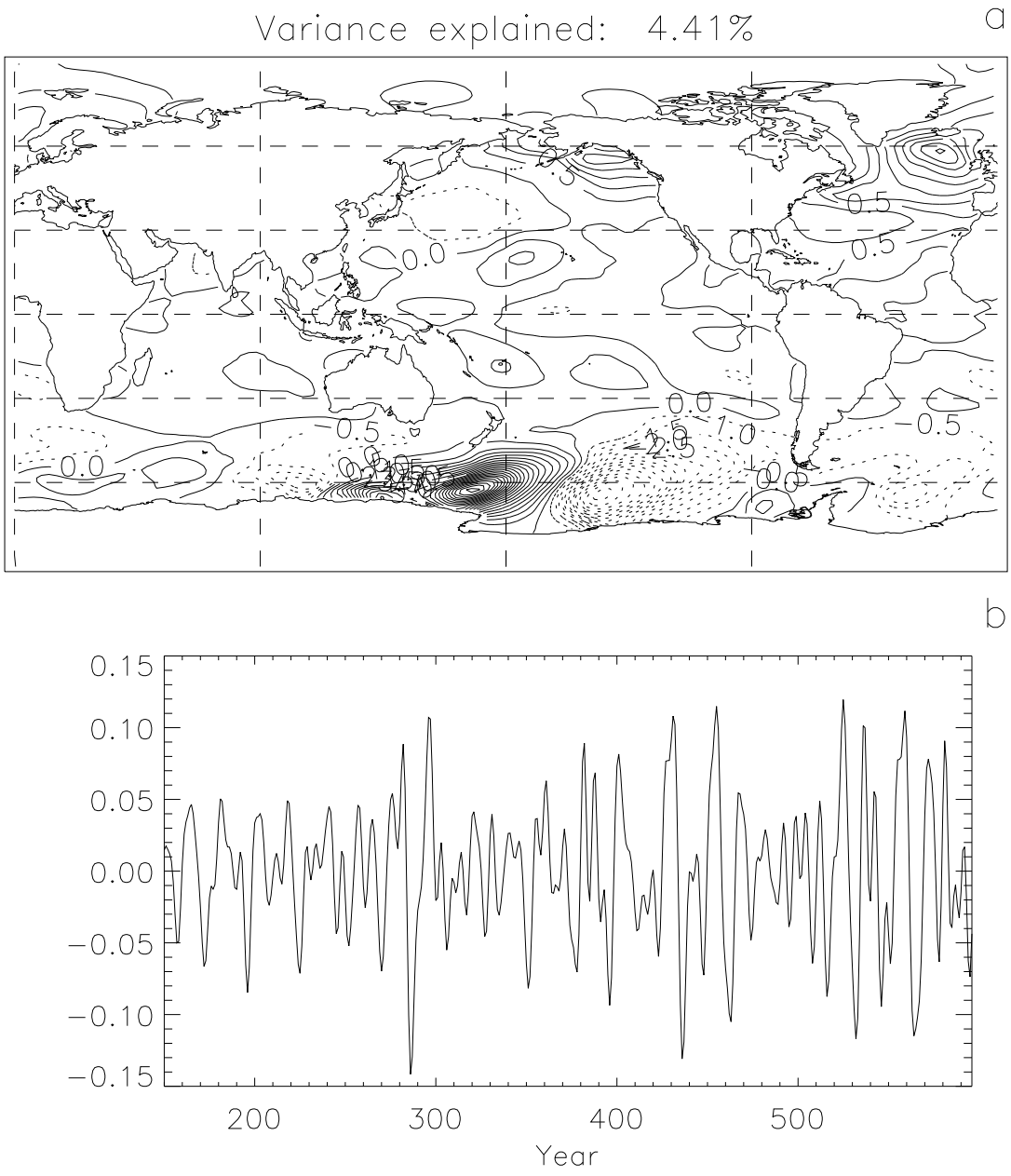

Figure 30: Fifth EOF (a) and time series (b) of bandpass filtered annual average SST anomalies.

The mechanism for this variability is thought to be a coupled interaction between the wind and ocean gyres (Latif, ibid.) as described below for the North Pacific but there is also the possibility that these modes are just the ocean's response to the stochastic forcing by the atmosphere (Frankignoul *et al.*, 1997).

Before concluding the bandpass analysis with a discussion of the North Pacific variability, note that very little decadal variability was found in the tropical Atlantic except that associated with the tropical Pacific variability (BPEOF1). In particular, the proposed decadal dipole mode which straddles the equator in the Atlantic (Chang *et al.*, 1997) is not found in the first ten EOFs of global SST. The absence of this pattern may indicate a deficiency in the model simulation, however there is still some debate about whether or not this mode really exists as a distinct phenomenon (see Latif (1996c) and references therein).

4.3.1 North Pacific decadal variability

The decadal variability in the North Pacific, BPEOF4 (Fig. 32), explains 4.41% of the global SST variability. As mentioned in Chapter 1.3, decadal variability in the North Pacific was one of the first internal modes of low frequency found by a coupled model; the ECHO coupled model of Latif *et al.* (1994). Because of its prominence in current research on low-frequency variability of the climate, this mode is examined more closely in this section.

First, to gain more information about the behavior of the North Pacific variability, a complex EOF analysis (Anderson and Rosen, 1983; Horel, 1984) was conducted on the bandpass filtered annual SST anomalies. The first 3 complex

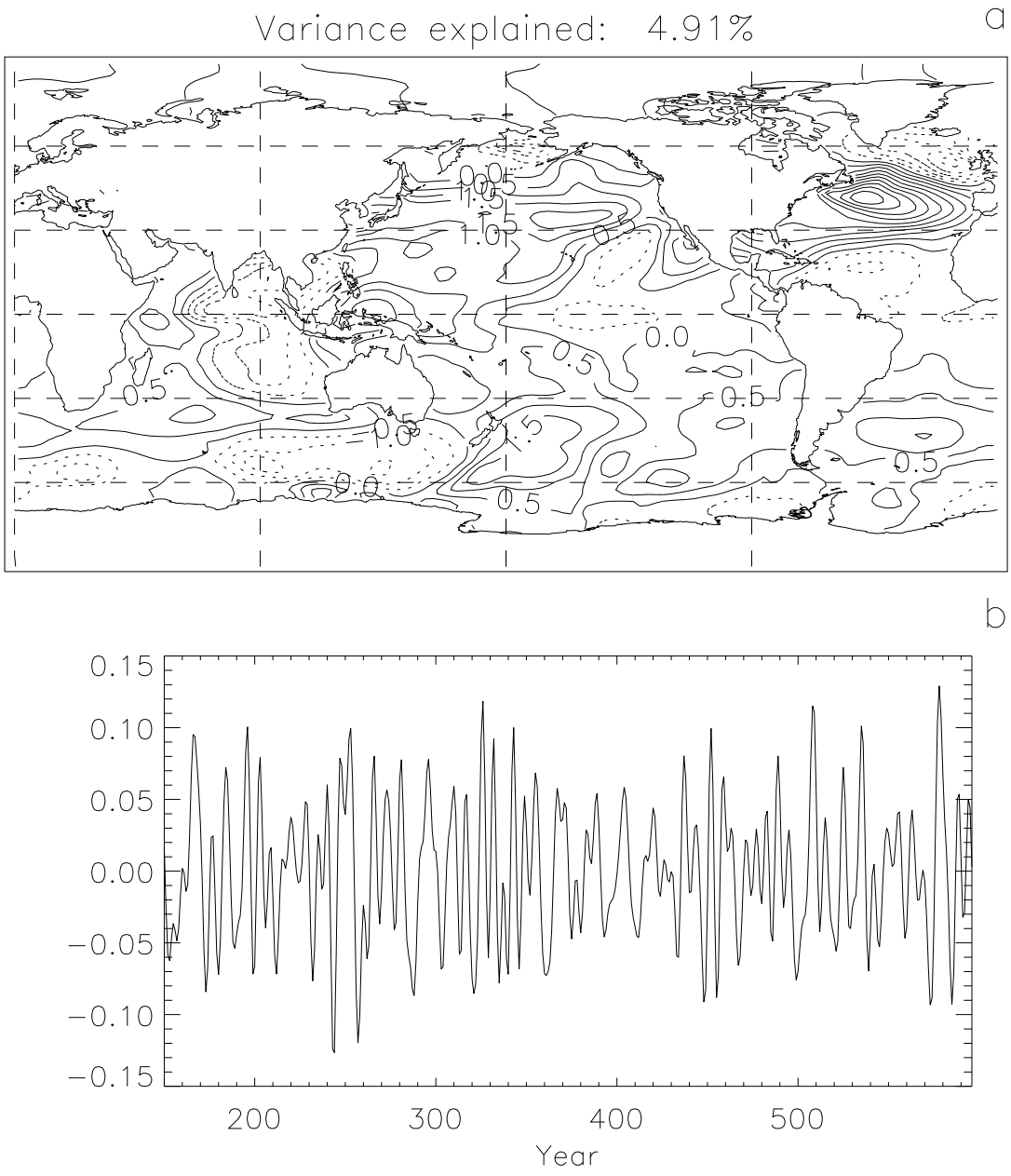

Figure 31: Third EOF (a) and time series (b) of bandpass filtered annual average SST anomalies.

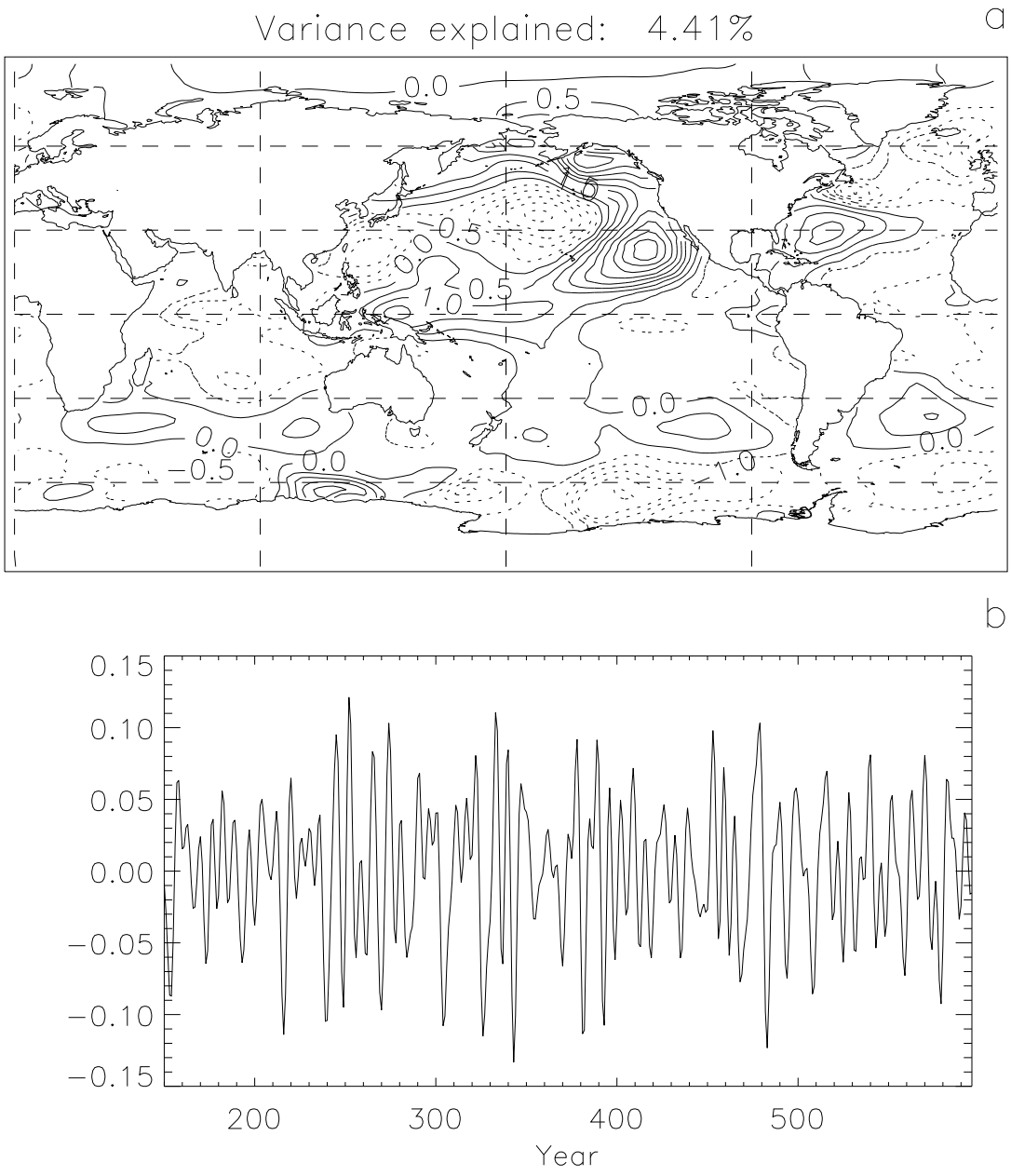

Figure 32: Fourth EOF (a) and time series (b) of bandpass filtered annual average SST anomalies.

EOFs corresponded to BPEOF1, BPEOF2 and BPEOF 5 respectively. The fourth complex EOF, BPCEOF4, contained the North Pacific mode and explained 4.95% of the variance. As for the EOF analysis, the domain was the entire globe. For clarity, the amplitude and phase of the BPCEOF4 is shown in Fig. 33 for the North Pacific region only. The arrows show the relative phase between the regions of maximum variability and indicate that this is a standing and not a propagating mode.

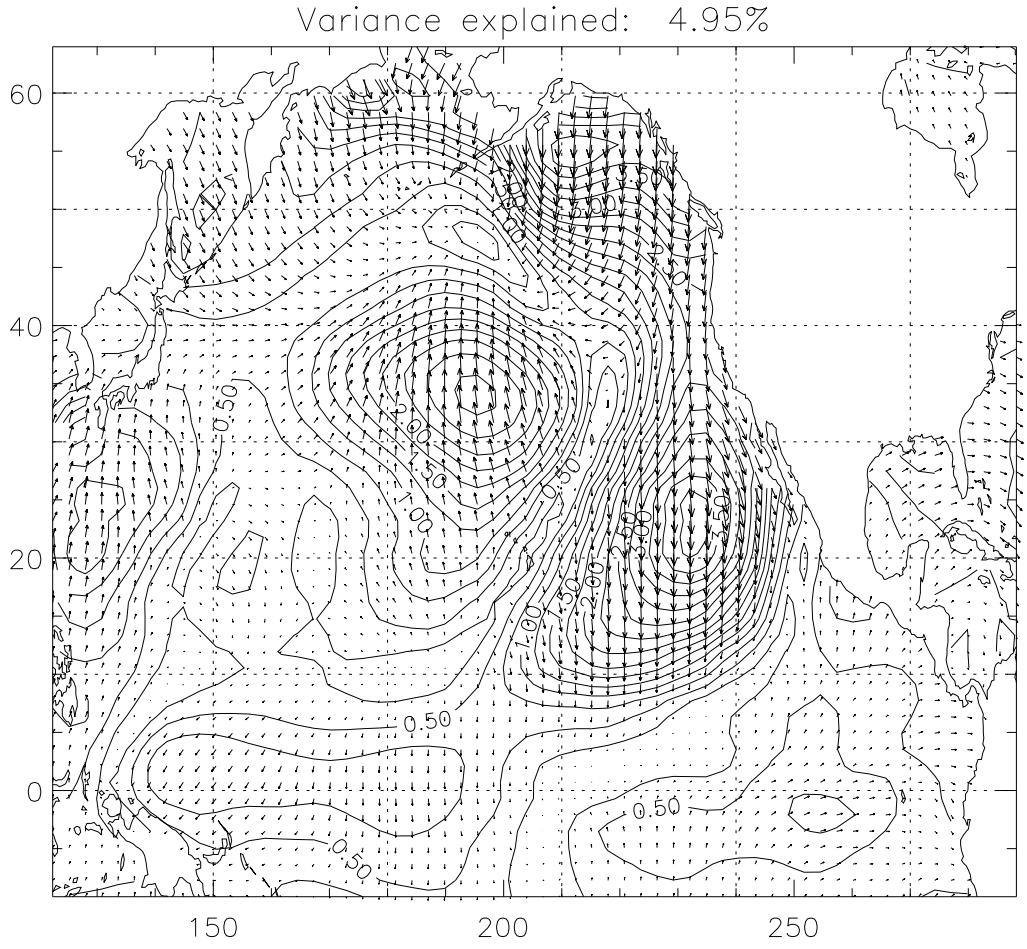

Figure 33: Fourth Complex EOF of bandpass filtered annual average SST anomalies. Arrows indicate magnitude and relative phase.

Using the phase information from the North Pacific CEOF of SST, a composite of this North Pacific oscillation can be constructed for all the model fields. Fig. 34 shows conditions when the SST anomaly in the central Pacific is large and positive. There is a corresponding anticyclonic wind stress anomaly. The contour pattern

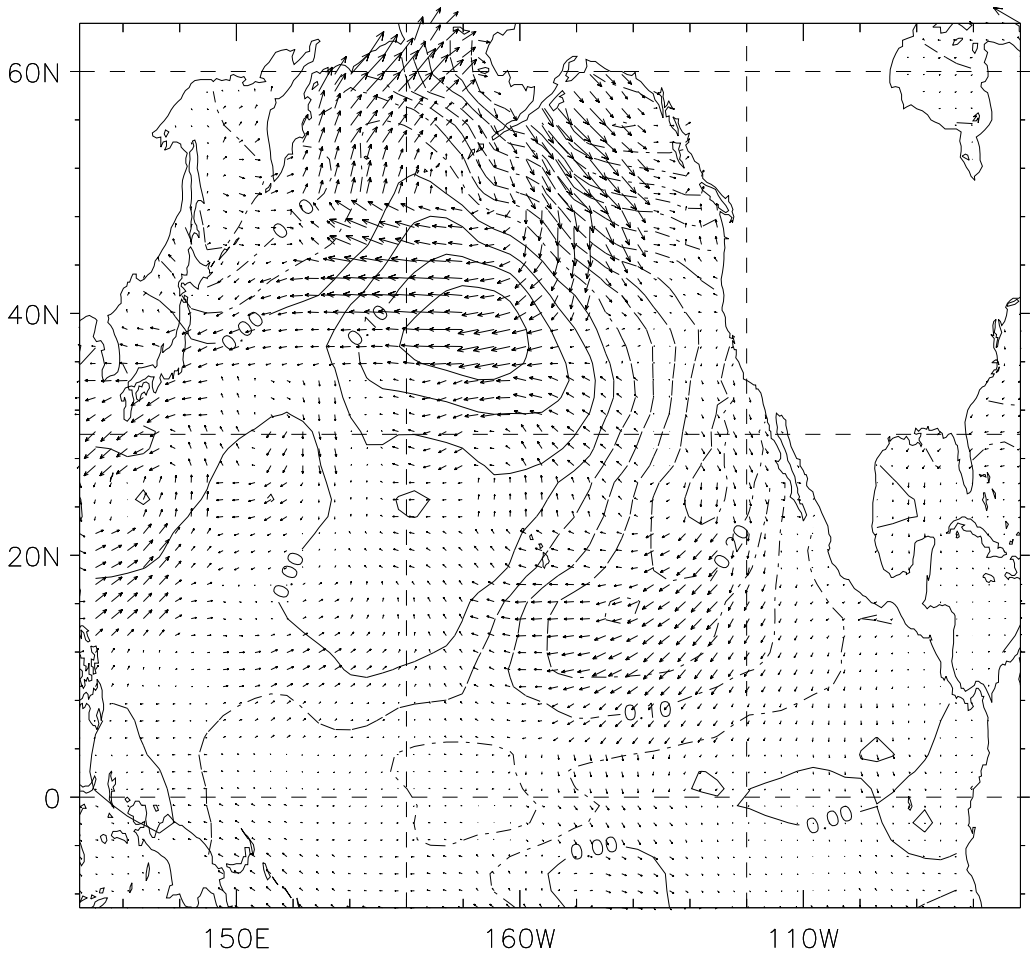

Figure 34: The SST anomaly and wind stress anomaly when the North Pacific oscillation is at a maximum. Constructed from the North Pacific CEOF. Temperature contours are .05°C and the reference wind stress vector in the upper right is .01 N/m^2.

in BPEOF4 and Fig. 34 strongly resembles the SST change associated with an observed shift in the North Pacific climate which occurred during the winter of

1976-77 (Miller *et al.*, 1994). LB96 have suggested that this shift was one incidence of a 20 year oscillation in the North Pacific which they found in the ECHO coupled model. BPEOF4 and the first EOF of North Pacific SST from ECHO are very similar. Evidence for a 20 year oscillation in the Pacific is summarized by Trenberth and Hurrell (1994) and further evidence is presented by Latif (*ibid*). In the composite oscillation, the temperature difference between the cold and warm phases (not shown) is about half of the observed difference (See Miller *et al.* (1994) Fig. 6).

LB96 propose the following mechanism for North Pacific variability. Variable wind stress in the mid Pacific generates planetary waves which propagate westward and enhance the western boundary currents (as described in theoretical work e.g. Gill (1982)). The stronger boundary currents (in this case the Kuroshio and its extension) advect a warm SST anomaly into the Pacific yielding a situation similar to Fig. 34. The warm anomaly reduces the meridional SST gradient across the North Pacific which causes a poleward shift of the Aleutian low. The resulting reduction in wind stress, also seen in Fig. 34, causes the gyre to slowly spin down and the reduced advection of warm water allows the meridional SST gradient to build again. This is a coupled mode with the time scale controlled by the spinup time of the gyre.

This explanation contrasts with that offered by Trenberth and Hurrell (1994) and Graham (1994) who argue that the oscillation is controlled by teleconnections through the atmosphere from low frequency ENSO variability. But LB96 were able to reproduce the atmospheric response to the SST anomalies in an atmosphere-only model where the tropical SST variability was near zero. A North Pacific

mode with a similar mechanism to that of Latif and Barnett was found in the coupled model of Robertson (1996) which contains no ENSO-type variability. The oscillation maximum shown in Fig. 34 contains an anticyclonic wind stress anomaly associated with a positive SST anomaly, as in LB96, while the SST anomaly in the tropics is near zero. Thus the North Pacific oscillation in BPEOF4 is most likely of the LB96 type.

Observational support for the LB96 mechanism is mounting. An LB96-type oscillation has recently been seen in 30 years of observations of upper ocean temperature (Zhang and Levitus, 1997). Nakamure *et al.* (1997) found that the cooling around the subarctic front associated with the North Pacific climate shift of 76-77 could not be explained by tropical influences.

Although the decadal variability in the North Pacific may be caused mostly by processes local to the North Pacific, an interaction between tropical and mid-latitude decadal variability can not be ruled out especially since both forms of variability involve the subtropics (Compare BPEOF1 and BPEOF4). BPEOF4 shows a weak connection between the eastern subtropics and the western tropical Pacific. Latif *et al.* (1997) suggest such linkages indicate a possible role for subduction processes (Liu *et al.*, 1994) in interdecadal variability, a theory also advanced by Gu and Philander (1997). The same observational analysis by Nakamure *et al.* (1997) shows a strong connections between tropical and subtropical decadal variability in the Pacific. Deser *et al.* (1996) have also seen the subduction of a temperature anomaly along isopycnals associated with the cooling after 76-77. The generation/interaction of decadal variability between the tropical and north Pacific requires further study.

4.4 Interdecadal Variability

Like the decadal variability discussed in the previous section, assessment of the interdecadal variability begins with annual averages of SST and anomalies formed from them. However the first attempt to make an EOF analysis of of the Year 100- Year 646 variability revealed a trend which persisted after removing linear trends. So the range of study for the low frequency was reset to Year 300-646 (Fig 10). The analysis then proceeds as before but with the mean calculated from years 300-646. The detrended SST anomaly fields were filtered with a lowpass FIR filter to remove any signals with a period of less than 30 years and 10 EOFs were derived which account for 92% of the variance. The first five (78.5%) were rotated.

LPEOF1 and its associated time series is shown if Fig. 35. Clearly this is a significant signal, accounting for more than 50% of the variance. The maximum variance (at 50°N, 34°W) is located over a center of deep water formation in the model and its period can be seen by inspection of Fig. 35b to be about 50 years. The peaks in the time series correspond to positive SST anomalies. Here one sees the benefit of including the entire SST field in the analysis: the domain was not restricted to the North Atlantic and yet the North Atlantic is shown to have the most significant low frequency variability. Focusing attention on this region may then be justified. First the other LPEOF patterns are reviewed.

LPEOFs 2-4 (Figs. 36, 37, and 38 respectively) are located over Antarctic deep water formation regions. The seas that contain the most of the variability, the Weddell and Ross, are known to be deep water production regions in the ocean (Warren, 1981) but the locations of deep water formation in FOAM are

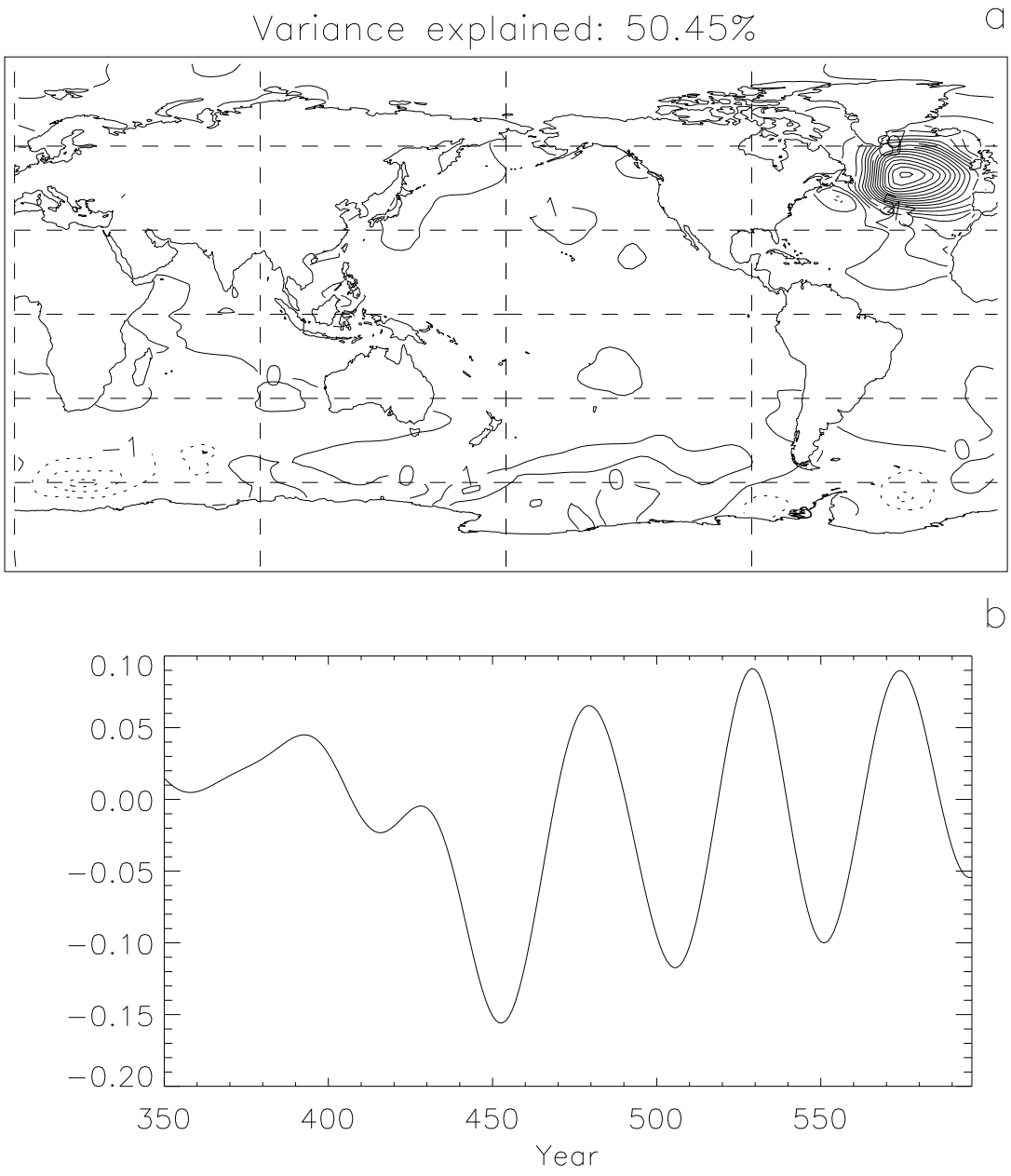

Figure 35: First EOF (a) and time series (b) of lowpass filtered annual average SST anomalies.

generally located too far east and offshore.

Figs. 35- 38 are encouraging because they suggest the model is capable of generating deep water in locations analogous to those in the real ocean despite the lack of such mechanisms as sea ice advection and shelf flow and the ad hoc nature of the sea ice model. Instead of forming near the coast, Antarctic deep water in FOAM is undoubtedly produced by convective overturning. The associated time series suggest that the periods are irregular and that some are longer than the integration length available. The coupled models surveyed in Section 1.3 have little to say about variability in the Antarctic. The shortest variability longer than thirty years found in ocean only models is the 300-350 year oscillation discussed by Drijfhout *et al.* (1996) and Pierce *et al.* (1995). The integration considered here is not long enough to address those phenomena but there is evidence in Figs 35- 38 that FOAM contains variability on multi-century time scales.

The fifth rotated EOF is shown in Fig. 39. This is a second North Atlantic mode that is ascribed as the associated variability of the model Gulf Stream with the signal in LPEOF1. The amplitude appears to vary while the period is similar to that of LPEOF1.

The remaining 5 EOFs (not shown) explain a total of 13.7% of the variance and are concentrated in either the North Atlantic or Antarctica. None of the ten EOFs contained any significant variability in the tropics.

The variability in SST seen in LPEOF1 and LPEOF5 resemble observations of interdecadal variations reported by Kushnir (1994). Kushnir derived two patterns of interdecadal variability in the North Atlantic based on observed temperatures collected before and after World War II. LPEOF1 resembles the pre-WWII pattern

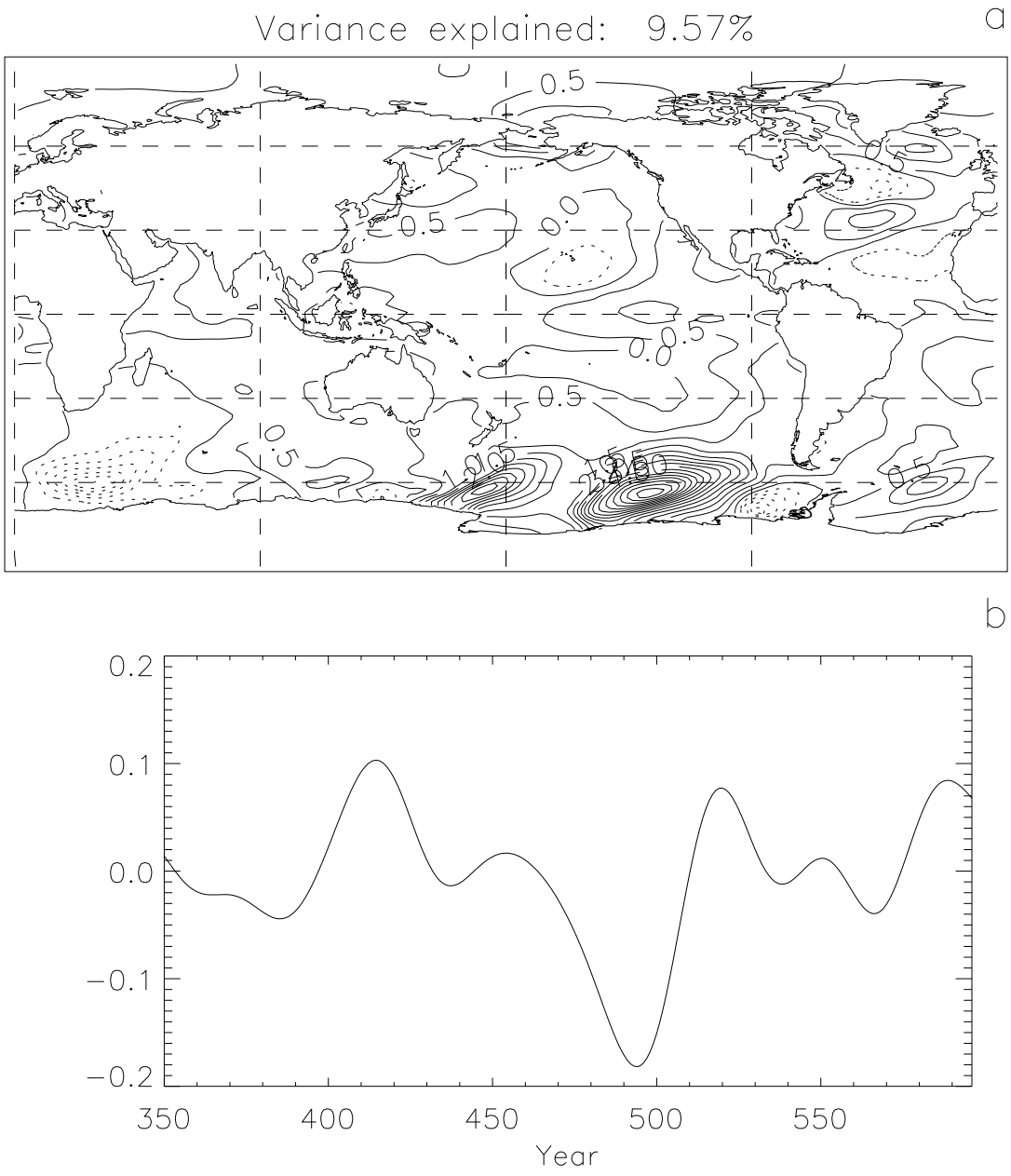

Figure 36: Second EOF (a) and time series (b) of lowpass filtered annual average SST anomalies.

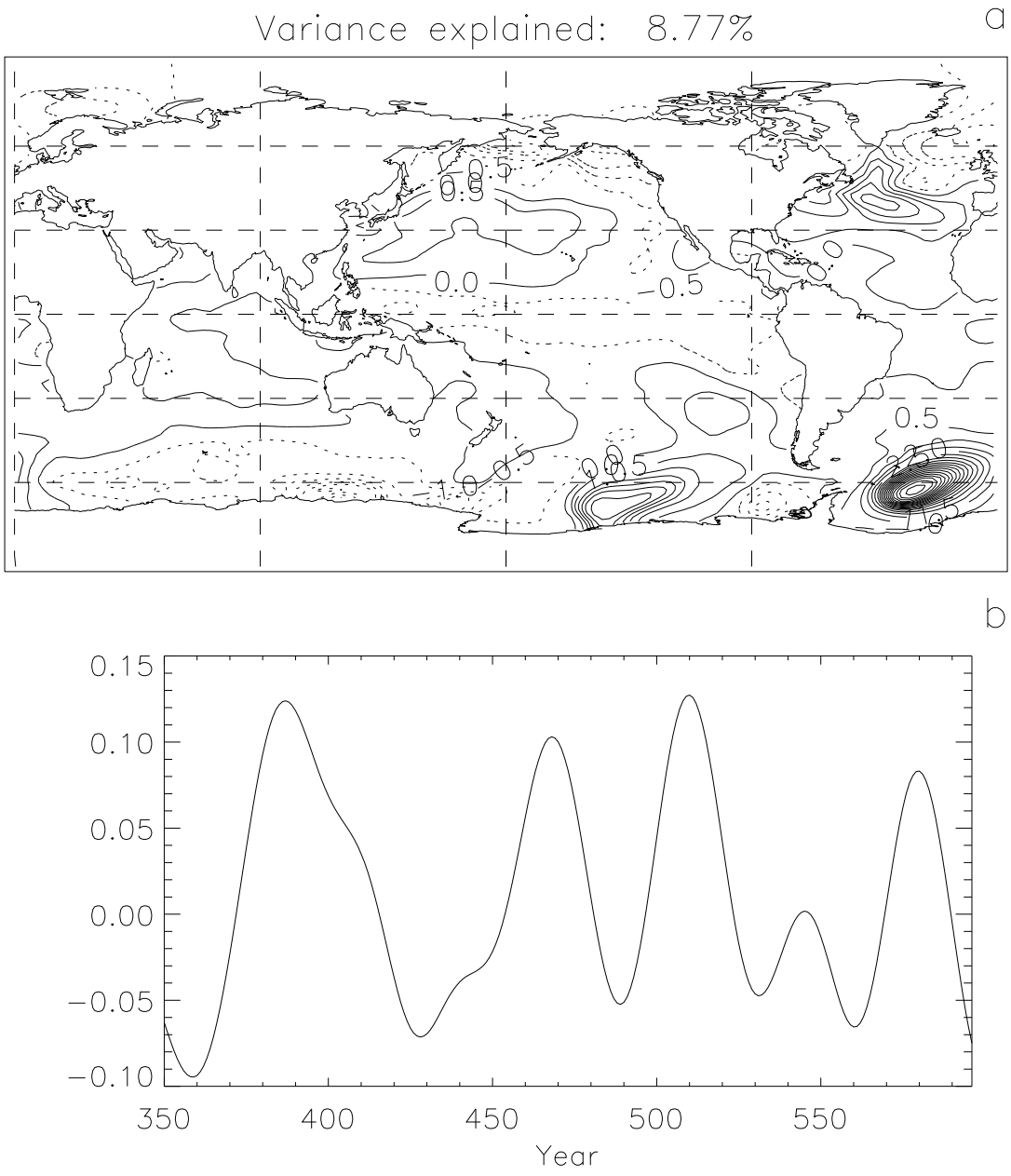

Figure 37: Third EOF (a) and time series (b) of lowpass filtered annual average SST anomalies.

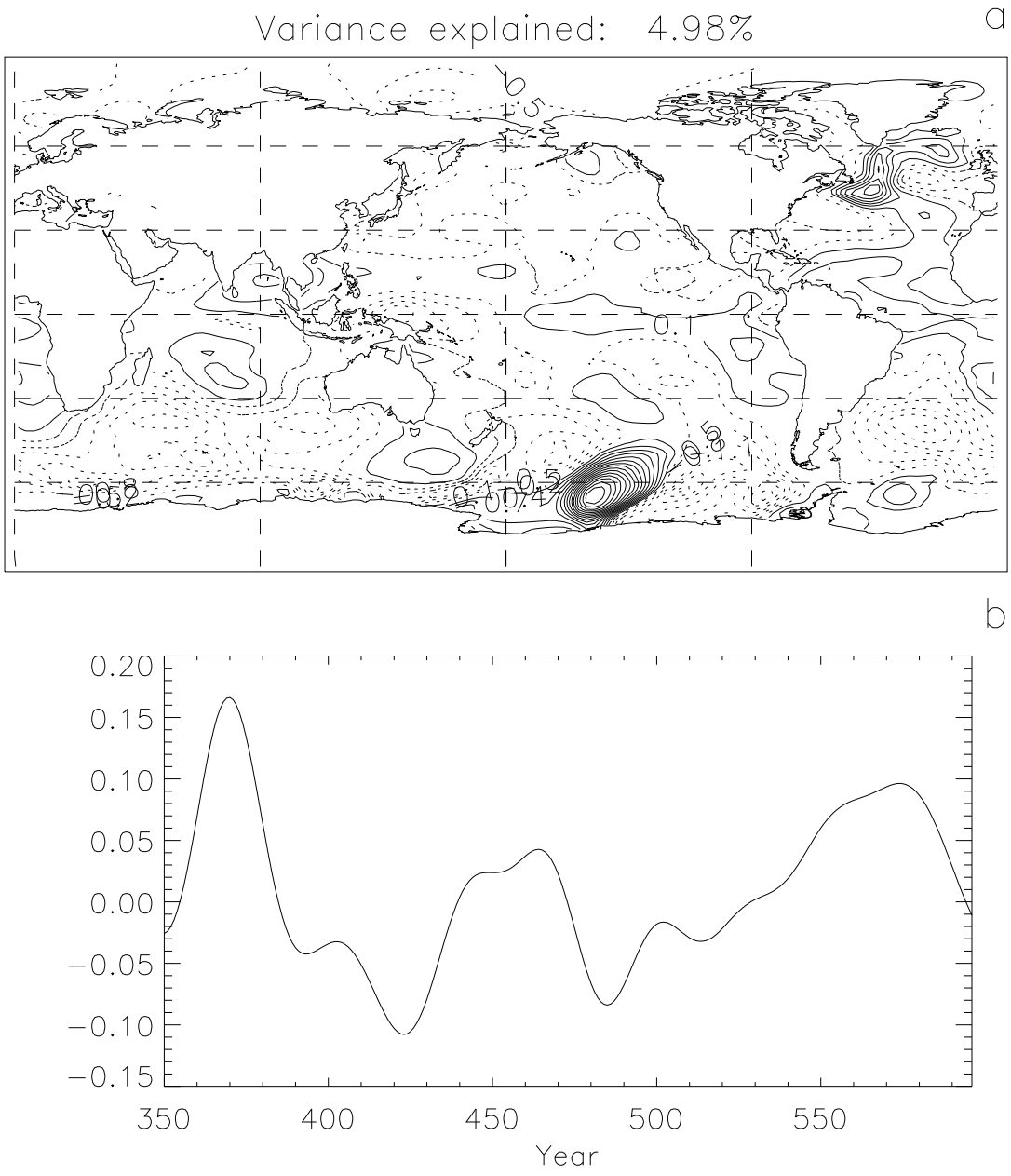

Figure 38: Fourth EOF (a) and time series (b) of lowpass filtered annual average SST anomalies.

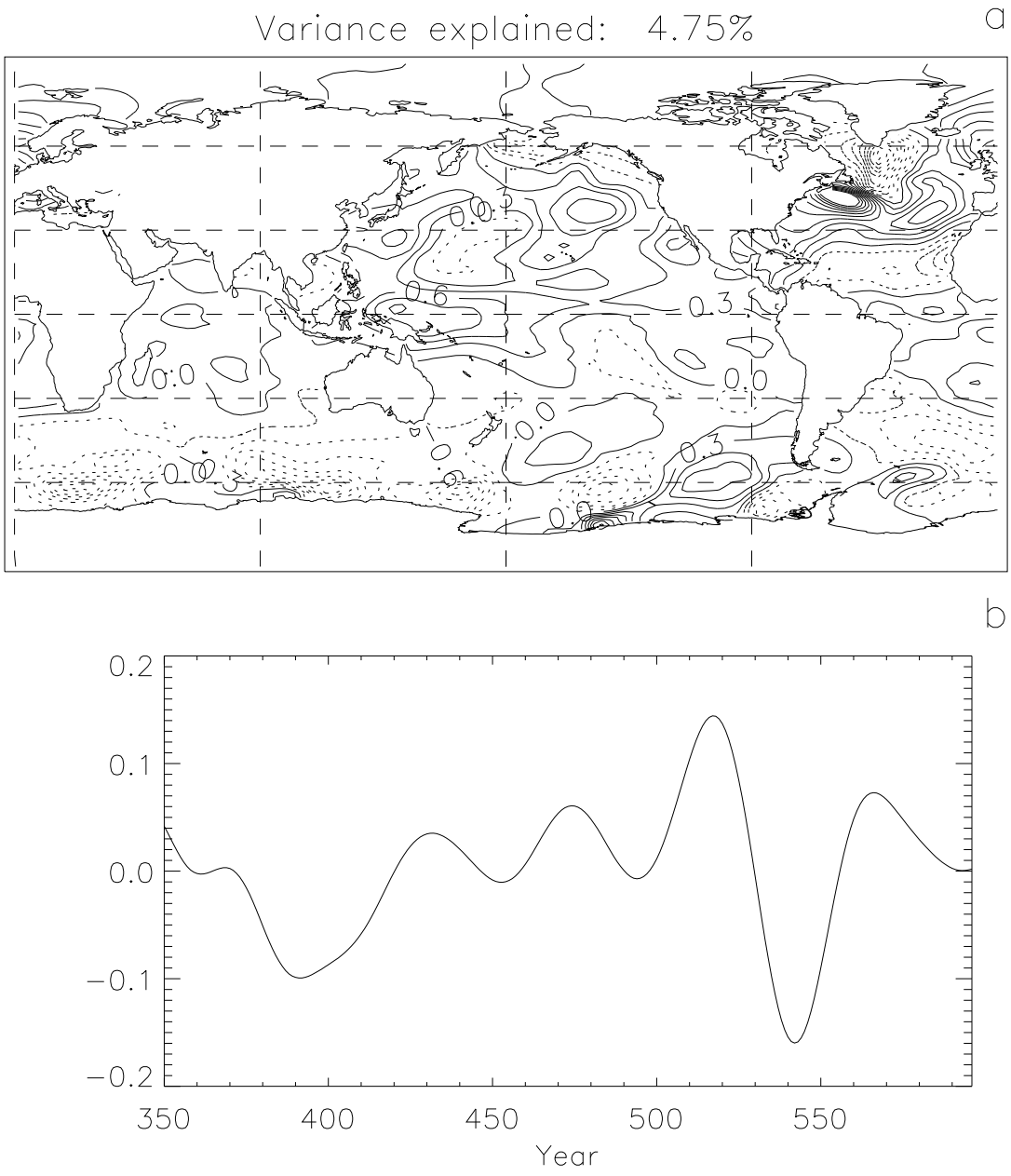

Figure 39: Fifth EOF (a) and time series (b) of lowpass filtered annual average SST anomalies.

with a large anomaly over the entire North Atlantic while LPEOF5 resembles the post-WWII data.

4.4.1 A North Atlantic Thermohaline Oscillator

As in Section 4.3, one of the EOF modes is selected for a closer physical study. The obvious choice is LPEOF1.

As mentioned above, the pattern of LPEOF1 is roughly centered over a region of low vertical stratification created by convective mixing. This is the downward branch of the model's thermohaline circulation. This region, which occurs at about 45-50°N, can be seen in a vertical cross section of the North Atlantic along 34°W shown in Fig. 40. The vertical profile indicates that the model's NADW has a temperature of about 8.5°C and a salinity of 36 psu (practical salinity units). The density profile (not shown) confirms that water at this location is the most dense in the region during the Northern Hemisphere winter. The model NADW is about 5 degrees warmer and 1 psu saltier than true NADW but are at appropriate values considering the location of the sinking.

The reason FOAM makes deep water where it does can be seen in the average North Atlantic circulation shown in Fig. 41. The first feature to note is the path of the North Atlantic Drift which does not penetrate far enough north. The second feature is a strong subpolar gyre caused by an Icelandic low which is on average simulated too far south by the R15 PCCM3. (A similar deficiency in the simulation of the Icelandic low was found for both T42 and R15 versions of CCM2 (Hurrel *et al.*, 1993).) The combination of a weak subtropical gyre and strong subpolar

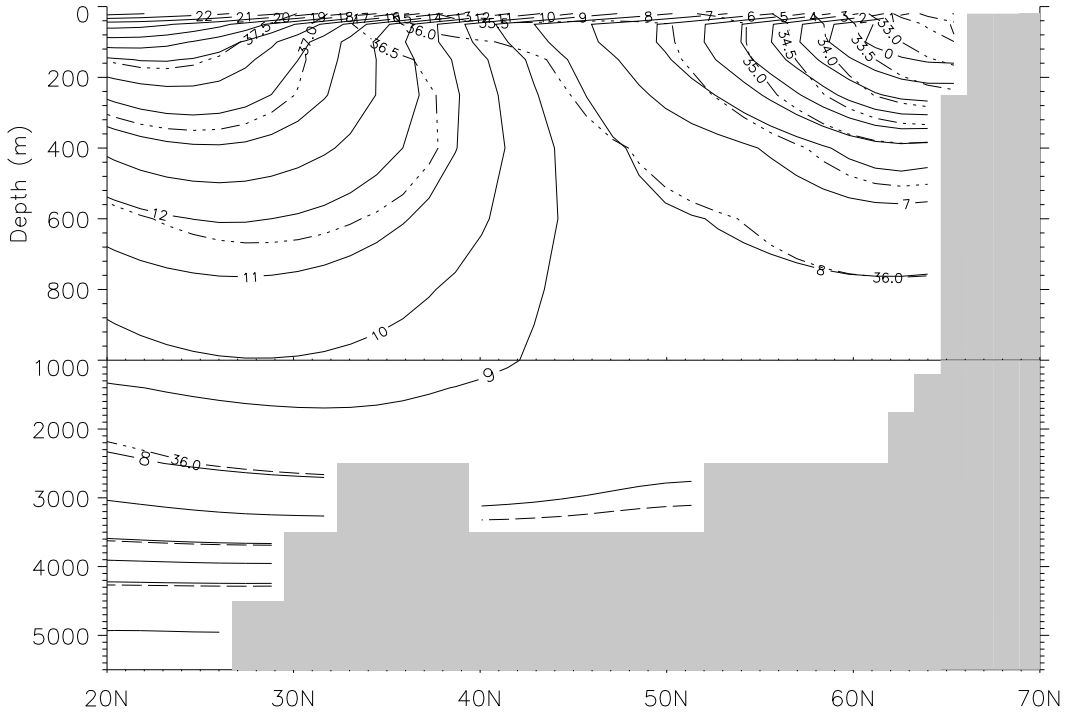

Figure 40: Zonal cross section along 34°W of annual mean temperature and salinity. Temperature contours (solid line) are 1°C and salinity contours (dot-dashed line) are 0.5 psu. Note that there are two scales for the depth axis.

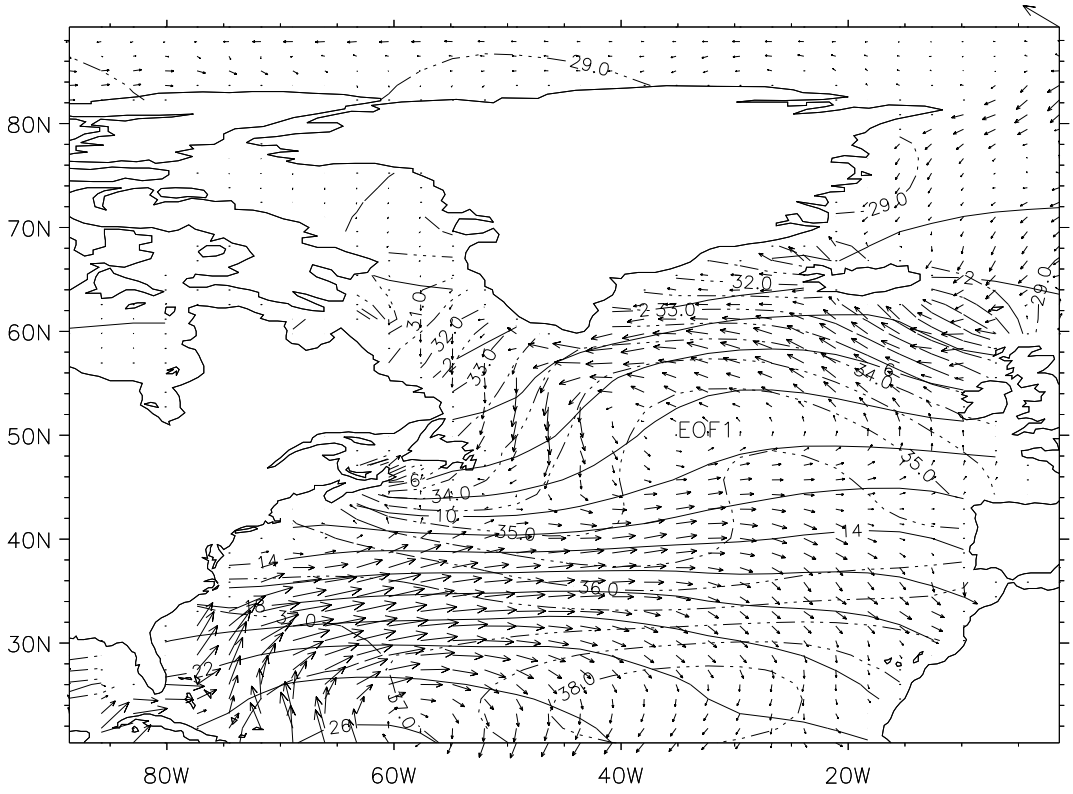

Figure 41: Simulated annual mean SST, SSS and currents in the North Atlantic. Currents are shown for one level below the surface to avoid Ekman drift. "EOF" indicates the position of the maximum in variance shown in Fig. 35. Temperature contours (solid line) are 2°C and salinity contours (dot-dashed line) are 0.5 psu. The scale vector in the upper right corner represents a current of 5 cm/sec.

gyre prevents the North Atlantic Drift from delivering high salinity water to the coldest regions of the North Atlantic. (This can also be seen in SSS differences in Fig. 19). Normally, NADW is produced when high salinity water is advected into the high North Atlantic where it cools faster than it freshens and becomes dense enough to sink. In FOAM, the waters around Greenland and in the Labrador Sea remain relatively fresh and thus do not convect to depth. (A trapped pool of cold fresh water off the Southeast tip of Greenland is visible in the upper right corner of Fig. 40.)

Having established that LPEOF1 is associated the the production of model NADW, the forcing behind this oscillation is considered. The first possibility considered was that this oscillation is forced by heat and freshwater fluxes. To help determine this, an EOF analysis on precipitation and heat flux into the ocean was performed in a manner similar to the SST analysis presented above (find annual anomalies, filter, etc.). The sea surface salinity field was also subject to an EOF analysis to gain more understanding about the role of salinity. For each field, the largest explained variance was concentrated in the North Atlantic (not shown). The associated time series for each of these North Atlantic EOFs are shown in Fig. 42. The time series in Fig. 42 have some apparent correlation with the oscillation seen in Fig. 35b. These relations are elucidated by calculating the cross correlation function for each time series against that of the LPEOF1. The correlation functions are shown in Fig. 43. The correlation of salinity and temperature show that positive salinity anomalies occur nearly simultaneously with positive temperature anomalies in the region. Fig 43 strongly suggests that the response of the atmosphere is to damp the anomalies throughout the course of an

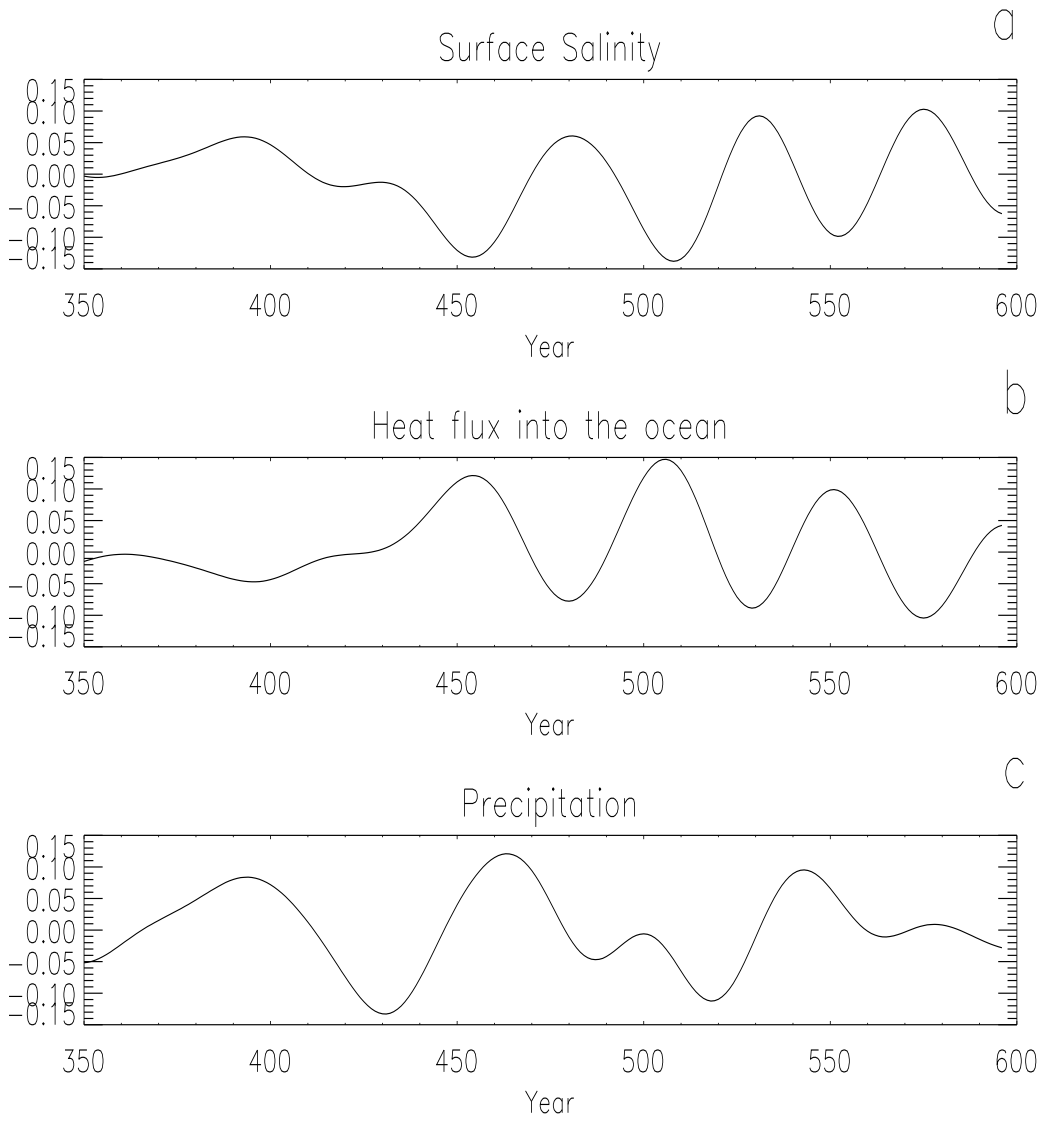

Figure 42: The associated time series for the "North Atlantic" EOF of (a) Sea Surface Salinity (b) Heat flux into the ocean and (c) Precipitation.

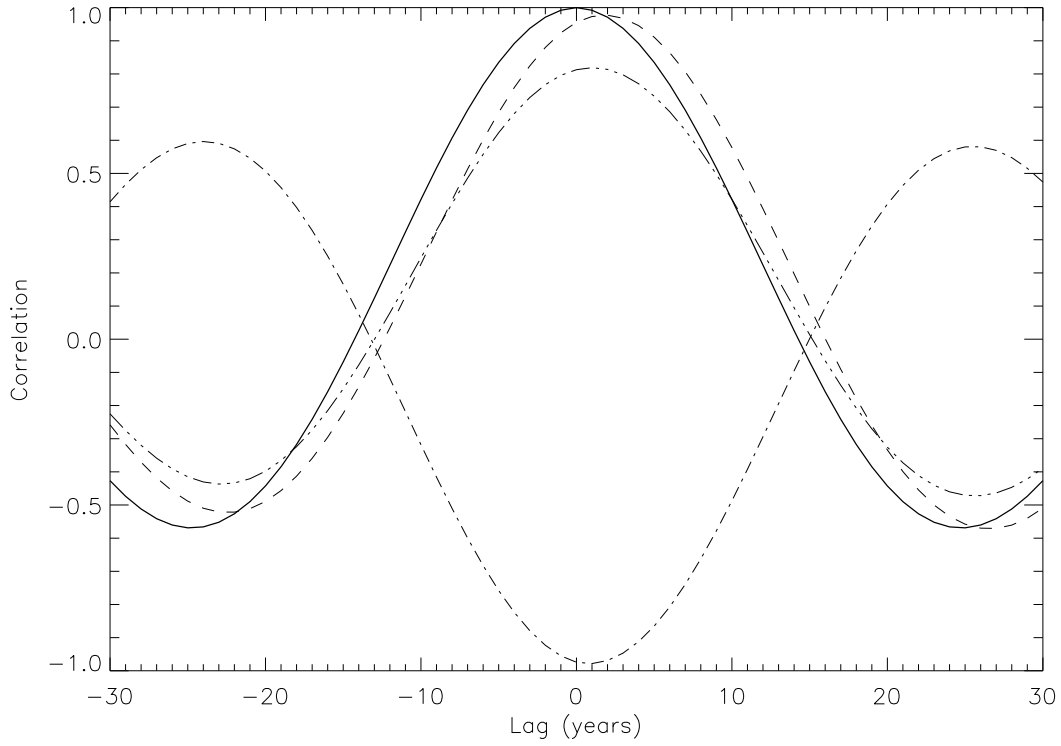

Figure 43: Cross correlation function for time series of LPEOF1 correlated with itself (solid line) and the corresponding EOF time series of salinity (dashed line), heat flux into the ocean (dot-dash) and precipitation (3 dots-dash) shown in Fig. 42.

oscillation. The appearance of positive temperature and salinity is associated with an increase in precipitation and a decrease in heat flux into the ocean.

This result suggests that this oscillation is not being forced by the surface fluxes of heat and freshwater. In order to gain more information about the ocean's influence on the surface anomalies a THC index is formed by calculating the zonally integrated meridional transport at each depth and latitude in the North Atlantic and taking the maximum. The anomalies for the THC index and the lowpass filtered time series are shown in Fig. 44a. The filtered time series can also be correlated with the time series of LPEOF1 and this is shown if Fig 45. The maximum in THC leads the SST maximum by about 12 years. This suggests an interaction between temperature anomalies and the thermohaline circulation. But the picture is still far from clear so a three dimensional composite oscillation was constructed from the 3 realizations visible in Fig 35b. This composite was formed using the 4 extreme points in each oscillation (the peaks, the valleys and the midpoints). The resulting sequence (not shown) revealed an associated temperature anomaly at a depth of around 400m. A time series of 400 m North Atlantic temperature (averaged for the area between 45°N and 60°) is shown in Fig 44b and its correlation with the surface SST anomaly is shown in Fig. 45. The subsurface anomalies lead the surface anomalies by about 17 years and indicate a possible role for northward heat transport. The heat transport above 600 m at 35°N is shown in Fig. 44c and its correlation with the SST time series is also shown in Fig. 45. The maxima in heat transport and temperature at 400 m are nearly in phase and slightly lead the increase in THC and they all occur prior to the maximum in SST.

From the composite cycle and the cross correlations shown above a possible

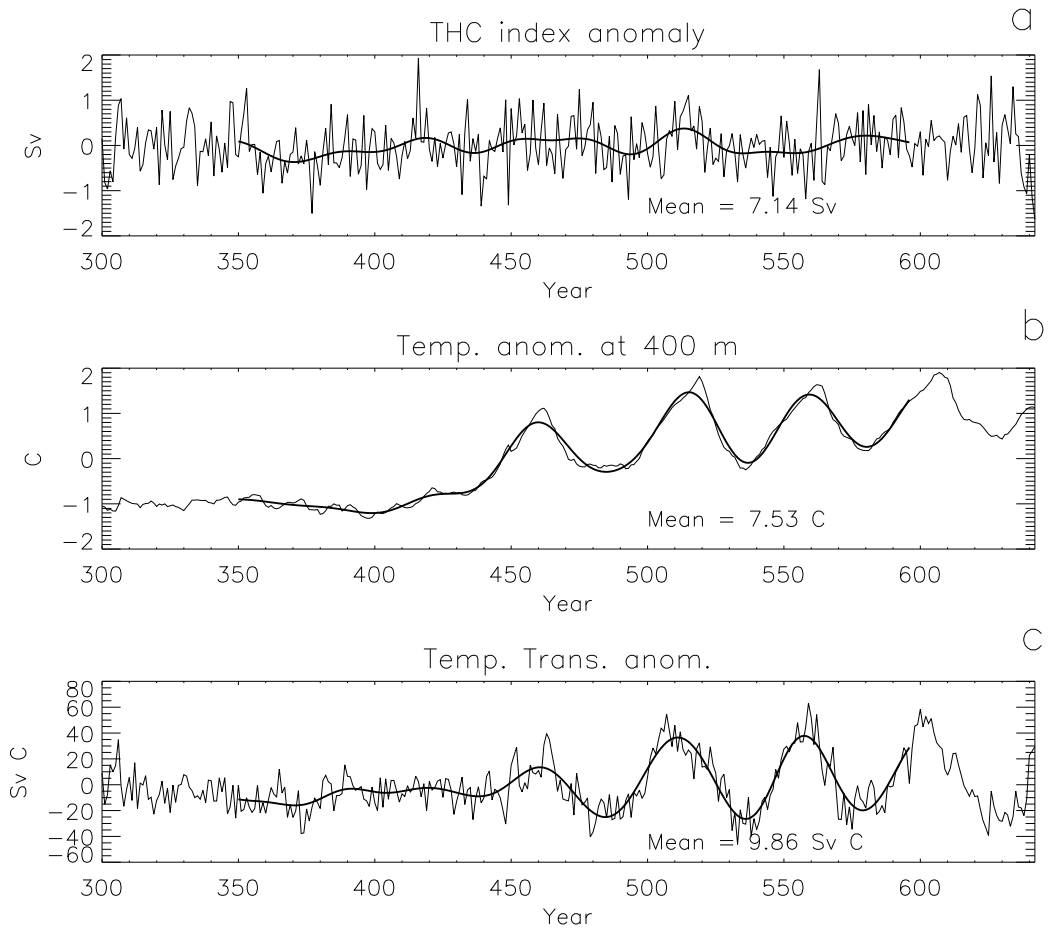

Figure 44: The time series (thin line) and lowpass filtered time series (thick line) of anomalies of (a) THC index, (b) temperature transport at 35 N in the North Atlantic above 600 and (c) temperature at 400 m in the North Atlantic. The means for each quantity are also indicated.

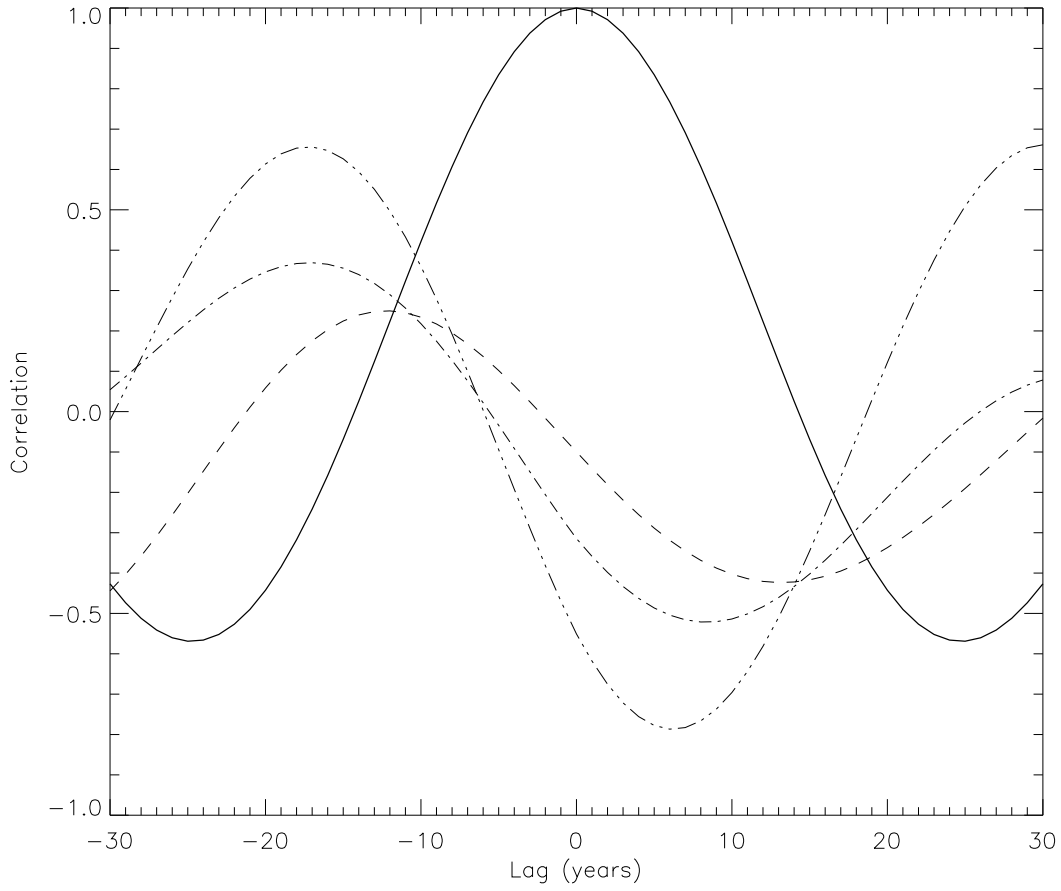

Figure 45: Cross correlation function for time series of LPEOF1 correlated with itself (solid line) and the filtered time series of THC index (dashed line), temperature at 400 m (dot-dash) and temperature transport at 35N (3 dots-dash) shown in Fig. 44.

sequence for this oscillation can be constructed. As the positive SST anomaly builds it decreases the density of the surface waters and the THC subsides. As a result of decreased THC, the North Atlantic drift dips southward taking the associated storm tracks with it. This lessens the Icelandic low and the subpolar gyre. With a lessening of the subpolar gyre, the warm and salty tongue on its east side visible in Fig. 41 subsides and a fresh and cold anomaly replaces the warm anomaly. As the THC reaches a minimum, relatively warm and salty water continues to penetrate at depth beneath the fresh and cold surface pool. The sinking region is then destabilized by warming at depth and becomes vertically well mixed again. As the THC increases, the North Atlantic Drift is nudged northward and warmer water, more precipitation and a stronger Icelandic Low return to the region and the cycle begins again.

This proposed sequence, although still speculative, at least fits all the facts at hand. Although the midlatitude storm tracks and their relation to the SST gradient are needed to explain high correlations between SSS and precipitation, this is predominantly an ocean-only mode of thermohaline oscillation. The oscillation results from an interplay between the North Atlantic Drift, the THC, and the subpolar gyre. The absence of this oscillation prior to Year 430 suggests that its existence is sensitive to the structure of the North Atlantic salinity, temperature and current fields which were further from an equilibrium. The 400 year period without any oscillation can be viewed as a measure of the model North Atlantic's thermodynamic equilibration time.

The spectra of model-generated SST at selected points in the North Atlantic are shown if Fig. 46. (The spectra were calculated using the unfiltered monthly

anomalies.) These spectra are similar in shape to those shown if Fig. 2 of D93 and resemble red noise. The point at 59°N and 19° W is close to a location for which there is an observed spectrum shown in D93's Fig. 2. 49°N and 34°W is a point near the center of LPEOF1 and shows more power at lower frequencies than the observation point or a point far from the center of variability (31°N 66°W).

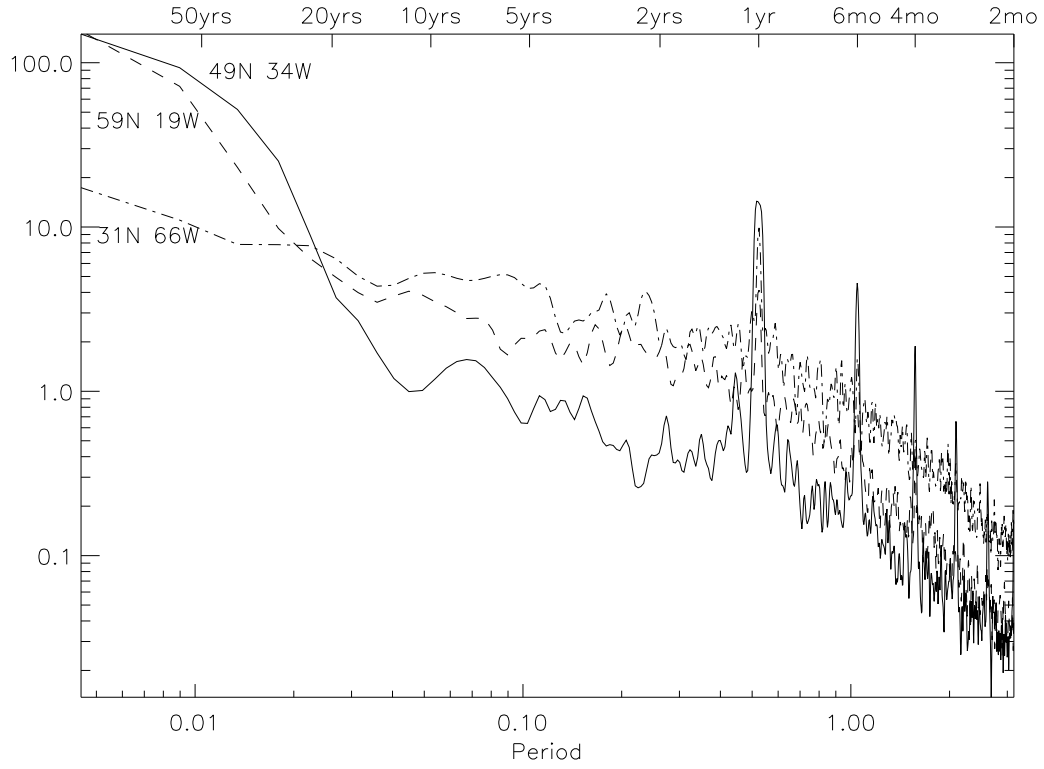

Figure 46: Spectra of sea-surface temperature in the North Atlantic for locations corresponding to the center of LPEOF1 (solid line), a point far from the center of LPEOF1 (dot-dash line) and a point close to one for which an observed spectrum is available (dashed line).

An oscillation in the North Atlantic with approximately 50 year time scale has been seen in both the GFDL (Delworth *et al.*, 1993) and the CSM (Capotondi and Holland, 1997) coupled model and in some ocean only models (Capotondi and

Holland, 1997; Greatbatch and Zhang, 1995). In all cases the oscillation was related to variability in the thermohaline circulation and the advection of temperature and salinity by the gyres. Stocker and Mysak (1992) note that a 50 year period is seen in many paleoclimate records around the North Atlantic. The details of FOAM's oscillation are slightly different from D93 and the thermohaline oscillator in FOAM undoubtedly depends greatly on the location of the deep water formation region. Most probably the details would be different if sinking were occurring further north. But the persistent discovery of 50-year oscillations in other models suggest that FOAM would continue to have variability of this type as long as the sinking region is in the vicinity of high latitude gyres.

Chapter 5

Coupled experiments with atmospheric parameterizations

One of the most frustrating obstacles encountered during the development of FOAM was the consistently poor simulation of the tropical Pacific ocean–both the mean and interannual variability. This deficiency was present in the earliest versions of the model but was neglected in favor of more pressing concerns such as increasing the throughput and the parallel efficiency. Since FOAM's goal is simulation of low frequency climate variability, it might be argued that correct simulation of the tropical Pacific climate is a low priority. But the results discussed in Chapter 4 suggest that ENSO variability is related in a nontrivial way to lower frequency variability. Furthermore, since simulation of internal climate variability is a goal of FOAM, the model should be able to simulate the most basic and well understood internal variability signal, El Nino. Finally, since much coupled model development was spurred by El Nino research, correct simulation of the tropical Pacific has developed into a kind of litmus test for overall model fidelity (Neelin *et al.*, 1992). FOAM had to produce a satisfactory tropical Pacific simulation if its low frequency results were to gain any credence. Eventually efforts were undertaken to improve FOAM's simulated tropical Pacific.

Not wanting to alter the internals of the atmosphere model, initial attempts tried to work with CCM2 to improve the tropical Pacific. The first attempt was to switch the atmospheric resolution from the T21 resolution initially used in development to R15. R15 did not improve the tropical Pacific but did provide stronger Southern Hemisphere winds and so was retained. Another attempt involved adjusting the land mask in the western tropical Pacific where large numbers of small islands yield some freedom in picking the most representative land/ocean mask at the surface resolution. Islands were added and subtracted at various places in the western tropical Pacific in an attempt to use CCM2's land-precipitation bias to coax the main area of tropical Pacific precipitation further east toward the observed position. The resulting new circulation would hopefully yield a better coupled simulation but such was not the case. Again using the coarseness of the resolution as justification, the ocean bottom topography was adjusted to try to manipulate the ocean currents into producing a better Pacific simulation. These efforts were also unsuccessful. New values for the coefficients in the ocean's vertical mixing scheme were also tried, values closer to observations by Peters *et al.* (1988). This resulted in a slight warming of the warm pool but otherwise did not redress the problem.

One attempt was made to change the formalism of PCCM2 by implementing the new cloud drop nucleus parameterization described by Kiehl (1994). In this scheme, the size of the nucleus depends on whether a point is over land or ocean. Although there was a slight reduction in the magnitude of the precipitation (as also seen by Kiehl (1994)), the Pacific simulation did not improve. (This parameterization is now part of the CCM3 physics.)

Shortly after CCM3 was released, its new physics parameterizations were added to PCCM2. A dramatic improvement was immediately apparent in coupled integrations with the new physics in the atmosphere model. Seeing that the Pacific mean climate was now in a reasonable state, the integration was continued until the data set analyzed in the previous chapter was produced. This section describes a series of numerical experiments which attempt to isolate which of the CCM3 changes is most responsible for improving the simulation of the Pacific.

To illustrate a typical case of CCM2 and CCM3 tropical Pacific temperatures, two additional 30 year coupled integrations, each beginning with the same initial conditions in both the ocean and the atmosphere, were performed. One integration used the CCM2 version of FOAM and the other CCM3. Ocean and coupler components were identical. The simulated annual SST field in the topical pacific for year ten of each integration is illustrated in Fig. 47. Several differences are apparent. In general, CCM2 temperatures are more uniform in the North-South direction across the entire tropical Pacific. Both simulations have the long, narrow cold tongue which penetrates too far to the west but the CCM2 simulation is about a degree colder. The cold water off the west coast of South America is warmer and more uniform in CCM2. This is probably associated with reduced upwelling due to the onshore windstress in CCM2 also seen in Fig. 47. The CCM2 simulation contains strong wind stress in the annual average on the equator across the entire Pacific with the strongest stress occurring over the west Pacific warm pool. The stress is much weaker in this area in CCM3. Finally, the CCM2 simulation contains a strong onshore windstress off the west coast of Central America which is absent in CCM3 (and in the climatology).

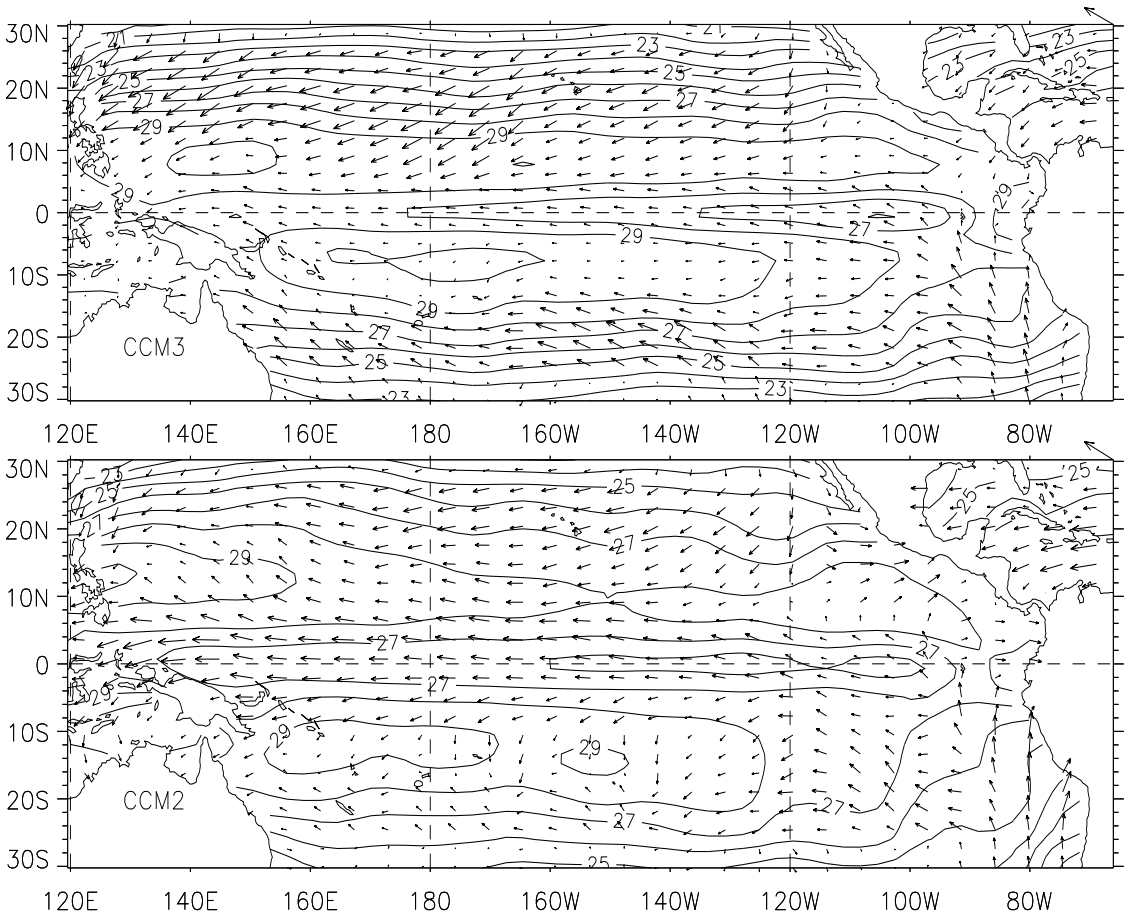

Figure 47: Simulated SST and wind stress in the tropical pacific for FOAM using A) CCM3 and B) CCM2 atmospheres. The reference vector in the upper right corner of each panel represents 0.12 N/m^2.

CCM3 also has more variability than CCM2 as can be seen from a time series of NINO3 region temperature anomalies shown in Fig. 48. The range of the NINO3

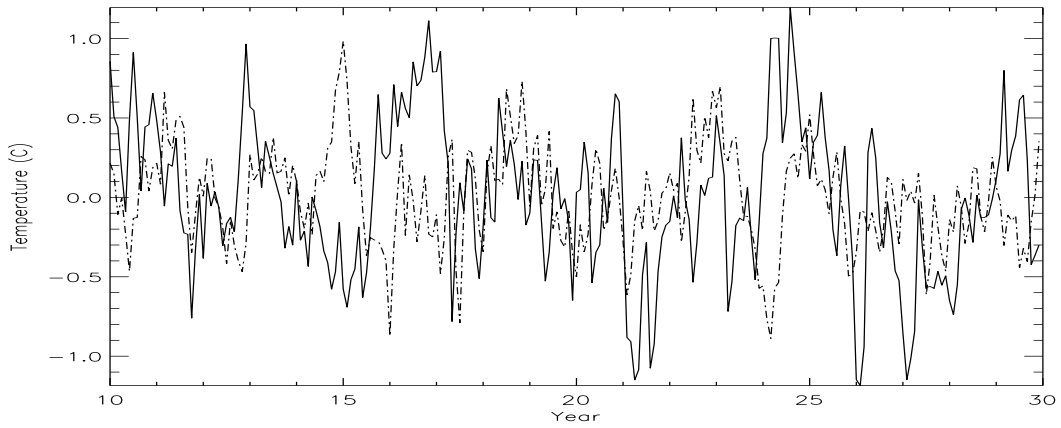

Figure 48: Seasonal cycle of simulated NINO3 temperature anomalies for FOAM using CCM2 and CCM3.

anomalies is nearly twice as large in CCM3 compared to CCM2.

Using FOAM, a series of numerical experiments were conducted to see if just one group of parameterizations was responsible for the improved Pacific climate. The new parameterizations CCM3 and were described in Section 2.1.2. Kiehl *et al.* (1996) divided the new CCM3 changes into three main groups: the radiation, the hydrologic cycle and the land surface. As mentioned, PCCM3 does not include the new land surface model of CCM3 so the remaining changes were divided up into four groups summarized in Table 6. These groupings were motivated both by physical considerations and by the structure of the code (they were located in separate parts of the calling tree.) The radiation and cloud diagnostics are treated as one group because of strong coupling between clouds and radiation. The hydrologic cycle changes were separated vertically into three parts: the surface, the boundary layer and the rest of the atmosphere. To perform each experiment, a

version of FOAM was created which had the PCCM2 code plus one of the groups of changes in Table 6. The ocean and coupler components were identical in each experiment. A 10 year coupled integration was conducted for each case using the

Table 6: Parameterization groupings for CCM2 experiments

CCM3 Parameterizations added	Experiment
All radiation changes including addition of aerosol and trace gas effects as well as changes to cloud diagnostics	CCM2RAD
New deep convection parameterization and new stratiform evaporation parameterization	CCM2CON
New boundary layer height formula	CCM2BL
New ocean flux formulae	CCM2FLX

same initial conditions as for the CCM2 and CCM3 examples described above. Experience has shown that a 10 year integration is sufficient for determining what path the tropical Pacific simulation is going to take.

The annual average from the last year of each experiment (Figs. 49 and 50) can be compared with those in Fig. 47. Examination of Figs. 49 and 50 shows that the CCM2CON experiment captures most of the features seen in the PCCM3 simulation. The temperature of the cold tongue, and nearly all the tropical Pacific, is raised by a degree to nearly match the PCCM3 case. The wind stress over the west Pacific is reduced and the strong onshore winds off the coast of Central America are eliminated in CCM2CON as in PCCM3. The other 3 cases show little difference from PCCM2: the wind stress on the equator still reaches a maximum

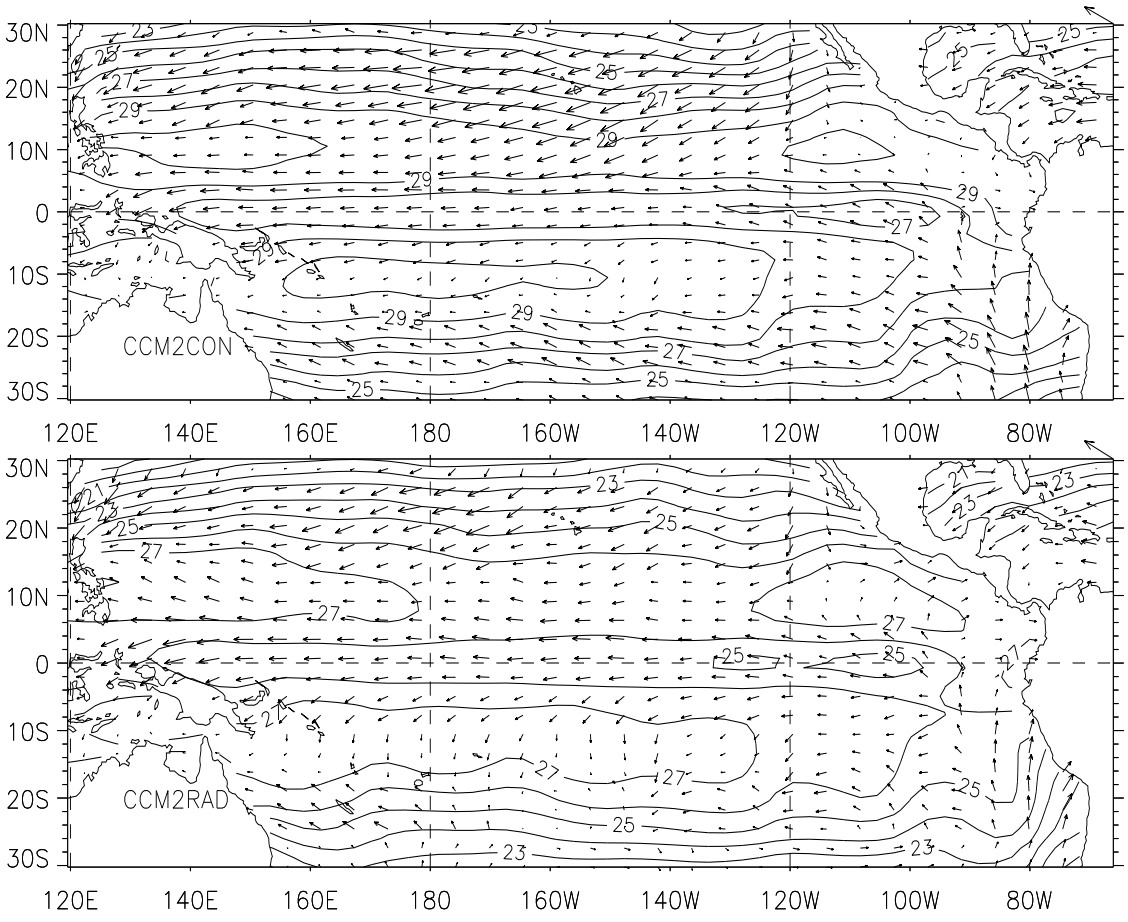

Figure 49: Simulated SST and wind stress in the tropical Pacific for cases CCM2CON and CCM2RAD. The reference vector in upper right is as in Fig. 47.

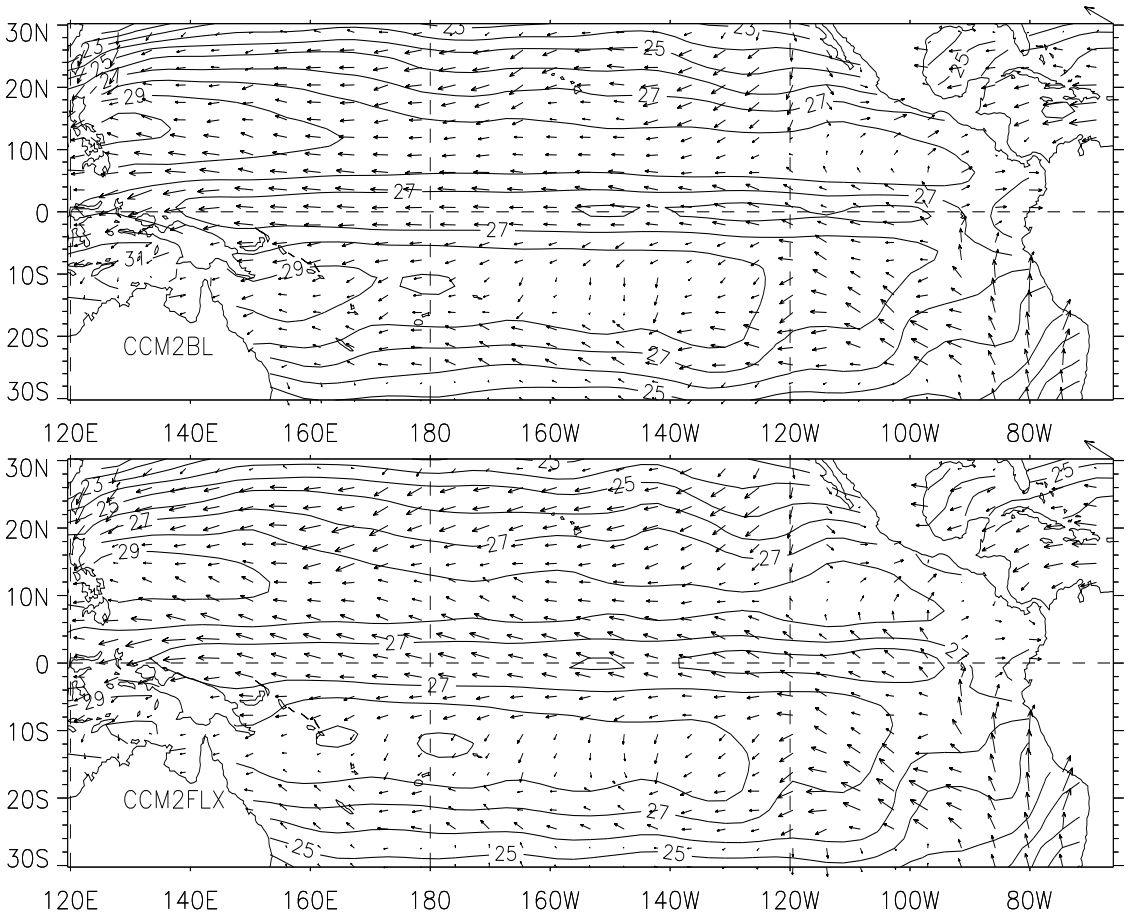

Figure 50: Simulated SST and wind stress in the tropical Pacific for cases CCM2BL and CCM2FLX. The reference vector in the upper right is as in Fig. 47.

in the West Pacific around 130E and the onshore winds near Central America are still present. The SST's in the other cases are also little changed from PCCM2. Note however that the CCM2RAD case seems to lower the SST by a degree over the entire Pacific compared to PCCM2.

Further evidence for CCM2CON being the most important group of changes is provided by comparing time series of temperatures in the NINO3 region shown in Fig. 51. Only CCM2CON captures most of the mean and the seasonal variability in this simulated by the full PCCM3 atmosphere.

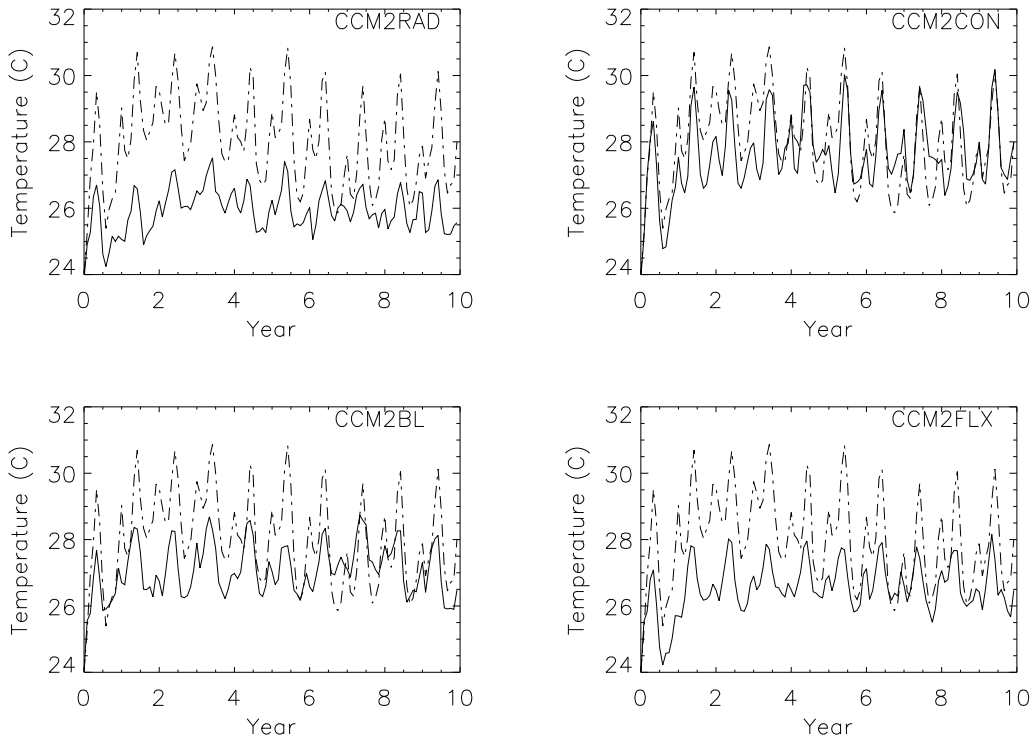

Figure 51: Time series of temperature in the NINO3 region for each case. The PCCM3 case is shown for reference (dot-dash line) in each figure.

To begin to understand how the CCM2CON group of changes is improving the

simulation, the total precipitation field from each run is examined. Fig. 52 shows that the CCM2CON group of new parameterizations smoothes the precipitation field and reduces the amount of precipitation over land. The "land-locking" of precipitation was a known problem in CCM2 (Hack, 1994; Hack *et al.*, 1994). Although still present somewhat in CCM2CON, the various maxima are not as strong. In particular the precipitation maximum over Indonesia is greatly reduced.

The change in strength and concentration of the precipitation centers has a corresponding effect on the model's Walker circulation as shown if Fig. 53. The strong

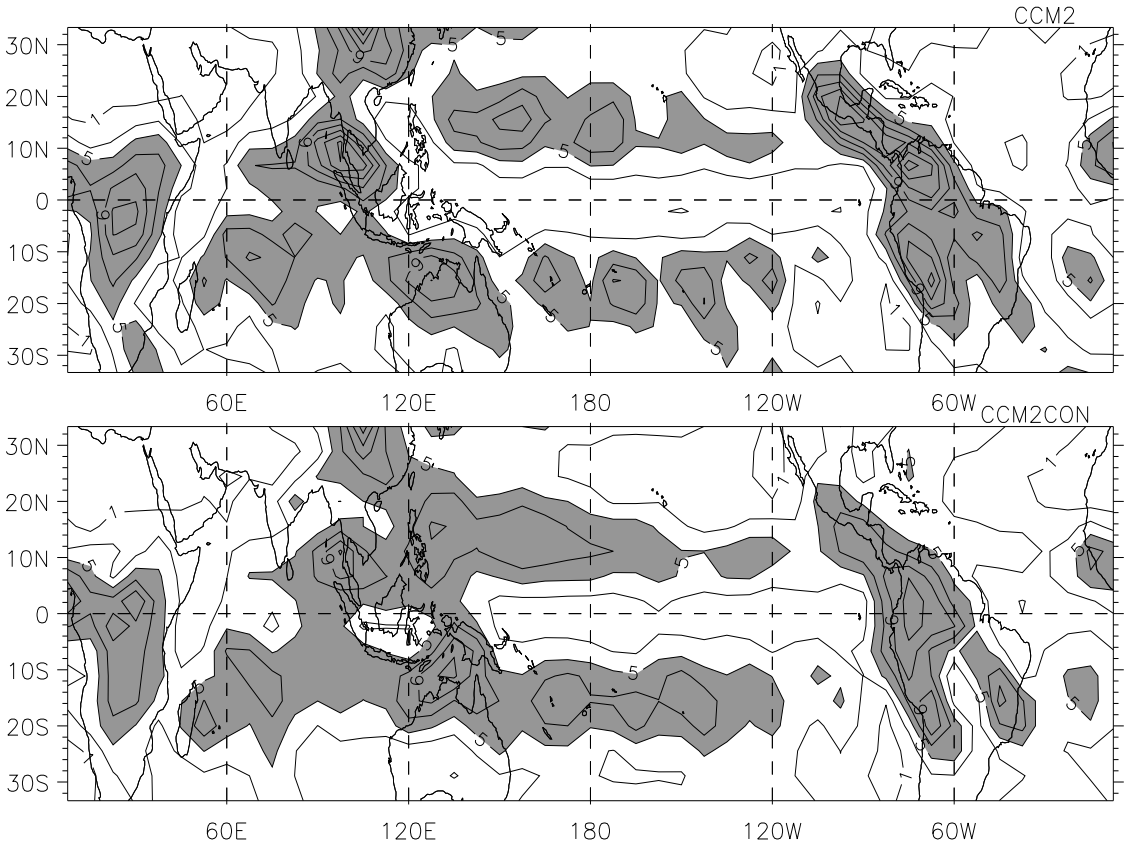

Figure 52: Annual average precipitation for CCM2 and CCM2CON cases. Contours are drawn at intervals of 2 mm day^{-1}. Values greater than 5 mm day^{-1} are shaded.

center of upward motion associated with the Indonesian precipitation maximum in CCM2 is greatly reduced in CCM2CON. Overall, the strength of the Walker

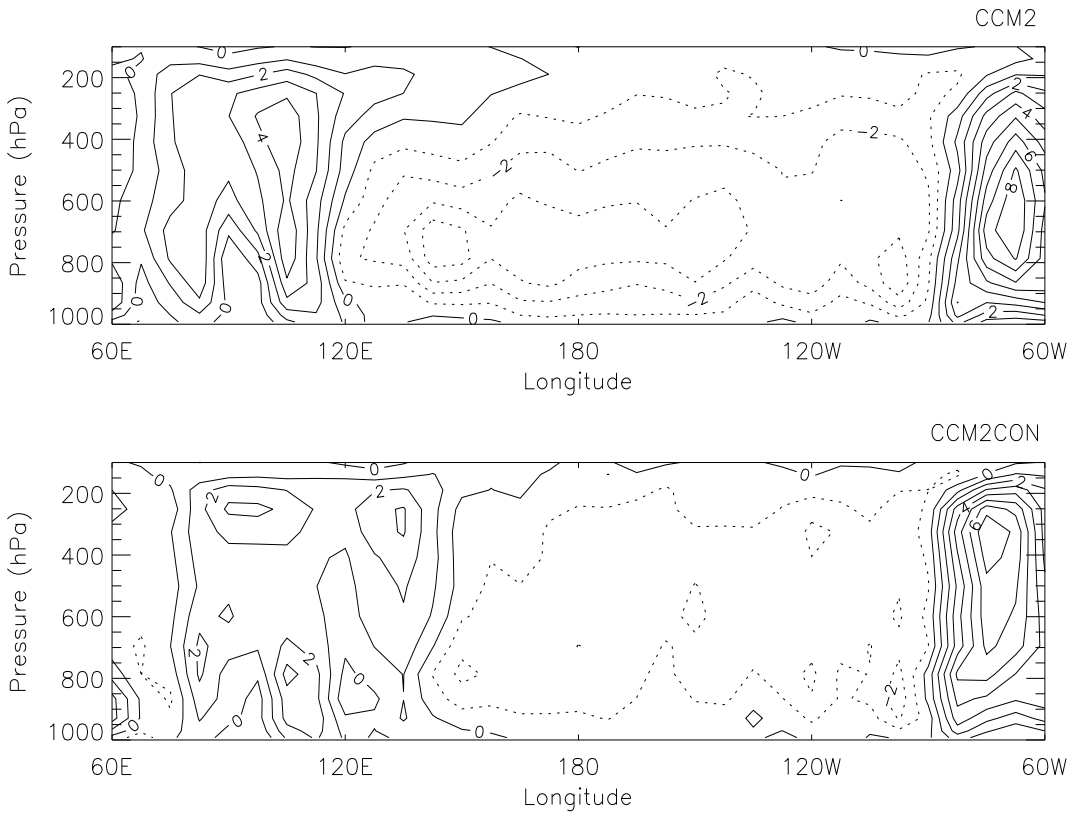

Figure 53: Vertical velocity in the atmosphere averaged from 5S to 5N for CCM2 and CCM2CON cases. Contours are $-\omega$ in units of 1 Pa s^{-1}.

Circulation over the Pacific is reduced. The strong wind stress over the western Pacific in CCM2 (Fig. 47) is simply the surface part of the model's Walker Circulation. Thus the smoothing and reduction of the precipitation maximum weakens the Walker circulation and reduces the wind stress over the West Pacific.

The reduction in easterly wind stress is responsible for most of the SST increase in CCM2CON. Fig 54 shows the difference (CCM2CON - CCM2) in ocean vertical temperature profile for the two cases. The reduction in wind stress has caused a

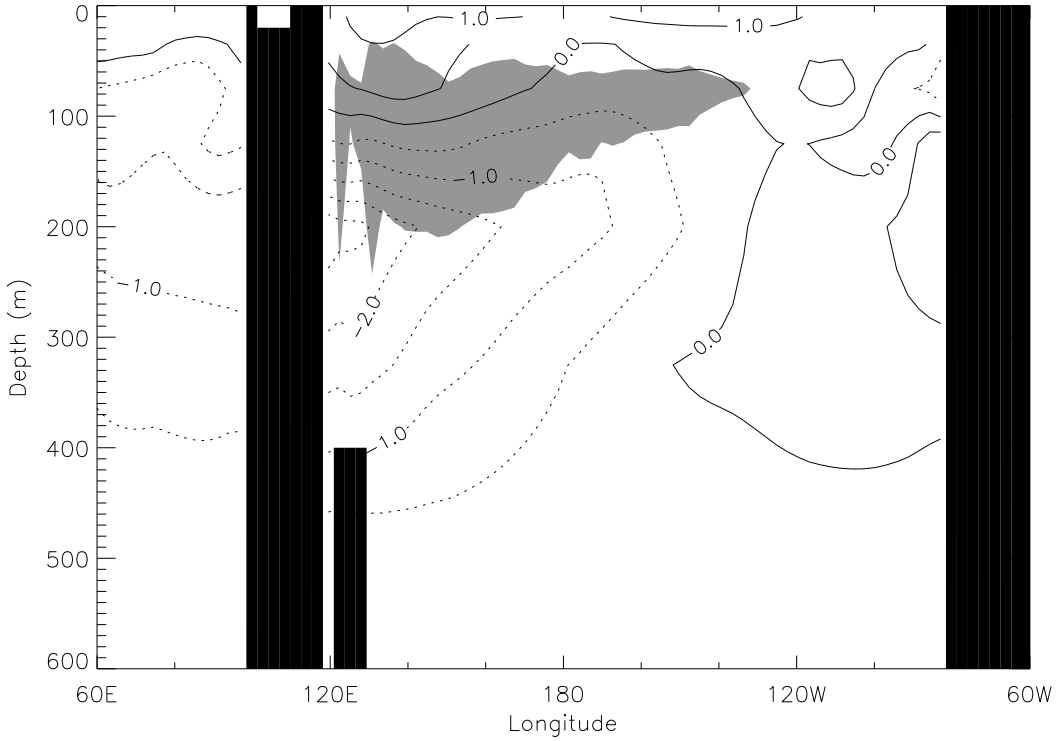

Figure 54: Ocean temperature differences between CCM2CON and CCM2 along the equator. Contour interval is $0.5°C$. Also shown is the region where upward vertical velocity decreased by at least 1 m day^{-1} (shaded).

decrease in the amount of upwelling (shaded region of Fig. 54) between the warm pool and the cooler subsurface waters. The result is that the surface is warmer and the subsurface cooler in CCM2CON. The resulting increase in SST and decrease in easterly equatorial wind stress can be seen in Fig. 55. An additional temperature increase comes from a reduction in latent heat loss by evaporation under areas of deep convection. A similar reduction in latent heat loss by the ocean has also been seen in CCM3 simulations with fixed SSTs and is also attributed to the new deep convection parameterizations (Hack *et al.*, 1997).

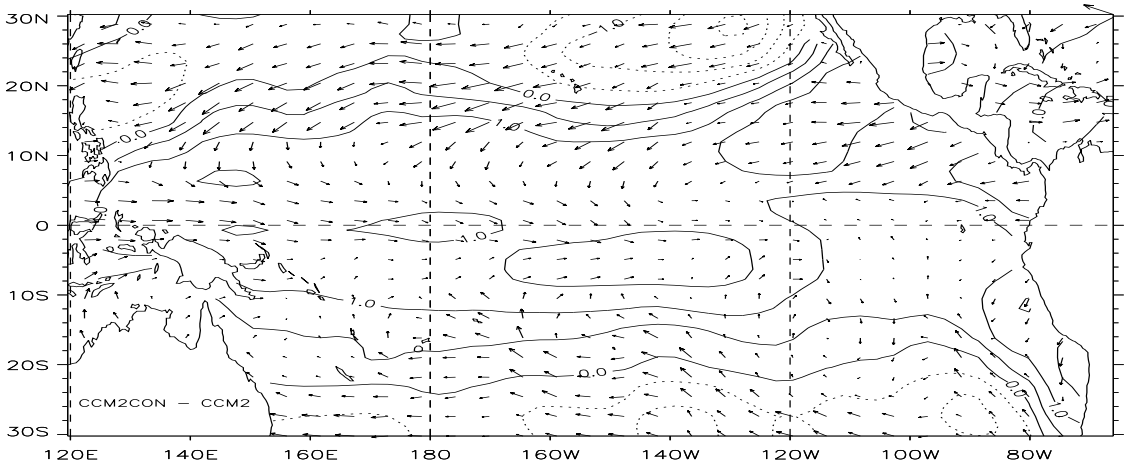

Figure 55: SST and wind stress differences between CCM2CON and CCM2. Contour interval is $0.5°C$. The reference vector in the upper right corner is $0.06 Nm^{-2}$.

The increase in seasonal variability in the NINO3 region in CCM2CON is also caused by the smoother, less intense convection. In the CCM2 case, the split ITCZ is more pronounced in the sense that the tropical precipitation is nearly always on either side of the equator in any monthly average. In CCM2CON, although the annual average still shows a split ITCZ, the seasonal cycle (not shown) does contain times (May - July) when there is significant precipitation directly over the

equator. The corresponding reduction in westward wind stress allows the seasonal warming of waters in the NINO3 region to occur. In the PCCM2 case, there are always strong monsoonal winds with a substantial westward component blowing across the equator to one or the other convective region. This maintains equatorial upwelling year-round leading to a persistent cold tongue with little seasonal variability. By suppressing the seasonal cycle of SST in the Pacific, the PCCM2 case also suppresses ENSO variability.

As the name implies, CCM2CON contains all of the changes to the way the model handles moist convection. The major change is the introduction of a new parameterization for deep convection which will be discussed further below. An additional change, the introduction of a scheme for evaporation of stratiform precipitation, is credited with helping to maintain the thermodynamic structure in the lower troposphere (Hack *et al.*, 1997) but is not believed to play a role here. Another change in CCM2CON is the elimination of the interaction between the atmospheric boundary layer and the original convection scheme. This was identified by Hack (1994) as a possible cause of the large precipitation values over land. To see if this alone would solve the simulations problems, an additional coupled experiment was performed where the only change was to eliminate this interaction. Although the precipitation did decrease slightly over land, the mean Pacific climate remained poor.

The original convection scheme of PCCM2 is a simple mass flux (SMF) scheme similar to that of Arakawa and Schubert (1974). The scheme employs a 3 level cloud model to stabilize a moist statically unstable column in the atmosphere via convective transport of heat and moisture and by the condensation and fallout of

precipitation. The 3 level model starts at the bottom of the column and is applied repeatedly up the atmospheric column until the column is stabilized. Details can be found in Hack (1994). In contrast the "deep" convection formalism of Zhang and McFarlane (1995) considers the convective stability of the entire atmospheric column at once and allows for the transport of heat and water vapor directly from the bottom of the troposphere to the top. Zhang (1994) found results similar to those presented here: namely that the precipitation is reduced and somewhat smoothed, accompanied by a reduction in wind stress and latent heat flux although his basis of comparison was a simulation using moist adiabatic adjustment. Zhang's explanation for the change is that the deep convection increases the moist static stability of the tropical troposphere through a more efficient transport of moist static energy from the bottom to the top of the atmosphere. The net result is a relative drying of the lower troposphere and heating in the middle and upper troposphere. The increased stability of the troposphere decreases the low-level convergence and thus decreases the precipitation. Hack *et al.* (1997) reports the same effect (low level drying and upper level heating) in comparison of T42 CCM3 and CCM2 simulations using fixed SST's and ascribes it to the new deep convection. This pattern can also be seen in the difference between the PCCM2 and CCM2CON humidity and temperature fields (not shown).

The deep convection scheme does not replace the original formalism, however. The new deep convection scheme is now called first in the model's calling sequence. Whereas before the SMF scheme handled all forms of convection, it now only adjusts those columns not already stabilized by deep convection. Thus the tendency for the SMF scheme to produce small intense precipitation regions is eliminated

by reducing the moist static instability with the deep convection first.

Finally it is important to note that the poor PCCM2 Pacific simulation is a coupled response to the SMF scheme. If PCCM2 is run with fixed SST's, the precipitation, although large, remains over the warm pool and the West Pacific wind stress maximum is no longer present. In the coupled simulation the strong precipitation maximum over Indonesia sets up a strong Walker circulation whose lower branch creates more upwelling on the equator which rapidly extends the cold tongue into the West Pacific. Since convection is suppressed over the cold equatorial water, the moist static energy has nowhere to expend itself but in the same land-locked precipitation centers and off-equatorial pools of warm water. This keeps the PCCM2 tropical Pacific simulation in an unrealistic state. The weaker Walker circulation of the deep convection scheme allows the normal seasonal cycle in the tropical Pacific to manifest itself despite the presence of a long, narrow cold tongue.

Chapter 6

Conclusions

The low frequency variability of the atmosphere-ocean system was surveyed by a rotated EOF analysis of over 500 years of monthly SST fields output from a new medium-resolution coupled ocean atmosphere model. A new model was deemed necessary because current models either do not have a long enough time series or have too many restrictions on the possible degrees of freedom in the simulated climate. The new coupled model, FOAM, has a mean climate that compares well with similar models and even with higher resolution ones. FOAM is one of the first coupled models to contain several types of proposed variability. FOAM simulates 50-year scale thermohaline oscillators as seen by D93 and Capotondi and Holland (1997), decadal variability in the midlatitudes and tropics, and ENSO variability all in the same model.

FOAM's success in reproducing many of the proposed forms of variability makes the resulting assessment more tenable. The patterns and explained variance of the EOFS compare well with similar analysis using observational data (Kawamura, 1994) and with other coupled model results (LB96).

The survey of the SST variability generated by the model reveals a general pattern in the atmosphere ocean system. The location and explained variance of each of the 15 EOFs discussed here is shown in Fig. 56. The largest interannual

variability occurs in the tropics, the largest decadal variability in the tropics and extratropics, and the largest interdecadal variability is found in the mid to high latitudes.

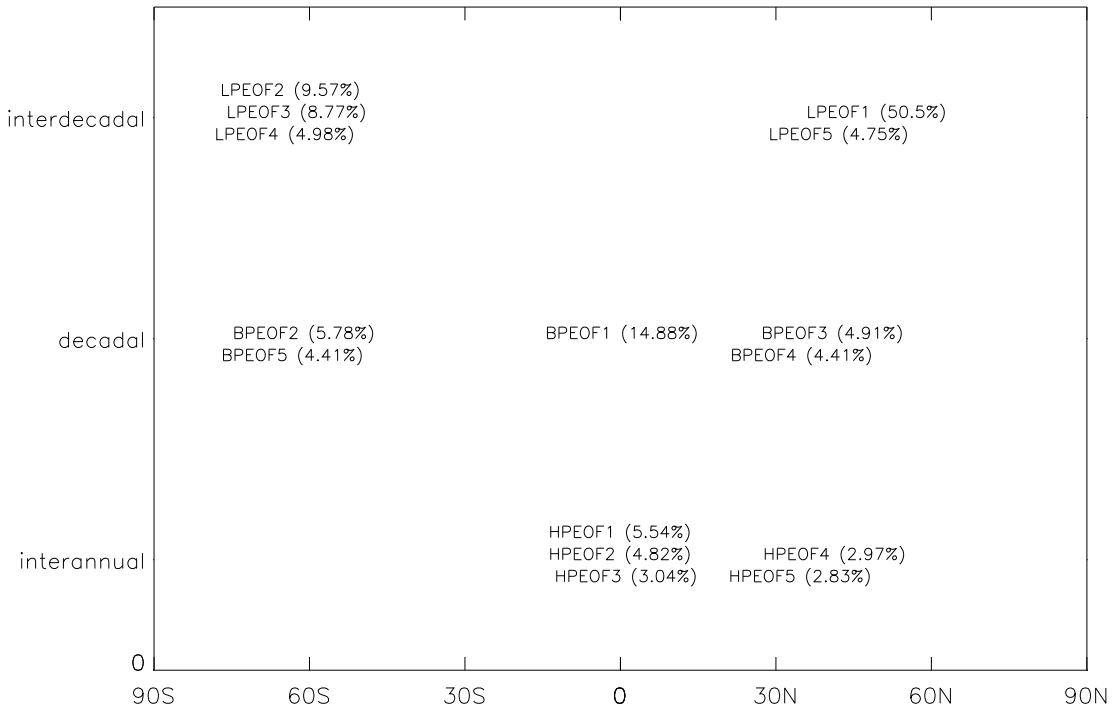

Figure 56: The 15 EOFs found arranged by center of action and frequency band.

The analysis shows that the most prominent source of variability in the global ocean-atmosphere system is ENSO. For low frequency variability, the most prominent source is an interdecadal thermohaline oscillator in the North Atlantic. This is followed by the mid-latitude gyre modes and ENSO related modes.

The analysis suggests that the Antarctic may be an important source of decadal variability in the atmosphere ocean system but the poor quality of data available in this region will make this difficult to confirm for some time. Little interdecadal

variability was found in the tropics except in the lowest order EOFs and almost no strong variability in the Southern Hemisphere midlatitudes at any frequency.

In addition to the survey of low frequency variability, the model was employed in a coupled study of atmospheric parameterizations. The parameterization of deep convection was found to have a profound effect on the models' simulation of the tropical Pacific. This underscores the importance of subgrid scale processes in simulating the climate.

Future work will involve improvements to the model mostly in the form of a new sea-ice model. Some parameters of the atmosphere and ocean models could probably be retuned for the coupled system. The leaks in the models hydrologic cycle must also be found and repaired. Subsequently a second, longer run could be performed to compare with the first, to perform more detailed analysis of the mechanisms behind the oscillations, and to explore even lower frequencies of variability.

Bibliography

Acker, T. L., L. E. Buja, J. M. Rosinski, and J. E. Truesdale, 1996: User's Guide to NCAR CCM3. NCAR Tech. Note NCAR/TN-421+IA, Natl. Cent. for Atmos. Res., Boulder, Co.

Anderson, J. R., and R. D. Rosen, 1983: The latitude-height structure of 40-50 day variations in the atmospheric angular momentum. *J. Atmos. Sci.,* **40**, 1584–1591.

Arakawa, A., 1988: Finite-difference methods in climate modeling. in *Physically Based Modelling and Simulation of Climate and Climatic Change*, Schlesinger, Ed., Kluwer Academic. pp. 79–168.

Arakawa, A., and W. H. Schubert, 1974: Interaction of cumulus cloud ensemble with the large-scale environment. *J. Atmos. Sci.,* **31**, 674–701.

Balmaseda, M. A., M. K. Davey, and D. L. T. Anderson, 1995: Decadal and seasonal dependence of ENSO prediction skill. *J. Climate,* **8**, 2705–2715.

Barnet, T. P., M. Chu, R. Wilde, and U. Mikolajewicz, 1994: Low frequency variability induced by stochastic forcing of various colors. in *Proceedings of the National Research Council Workshop on Decade to Century Timescales of Climate Variability*, Irvine, CA, Sep. 21-25. pp. 1–12.

Bjerknes, J., 1964: Atlantic air-sea interaction. *Adv. in Geophys.,* **10**, 1–82.

Bonan, G. B., 1996: A land surface model (LSM version 1.0) for ecological, hydrological, and atmospheric studies: technical description and user's guide.

NCAR Tech. Note NCAR/TN-417+STR, Natl. Cent. for Atmos. Res., Boulder, Co.

Boville, B. A., and P. R. Gent, 1997: The NCAR climate system model, version one. *submitted to J. Climate,*.

Briegleb, B. P., 1992: Delta-Eddington approximation for solar radiation in the NCAR Community Climate Model. *J. Geophys. Res.,* **97**, 7603–7612.

Briegleb, B. P., P. Minnis, V. Ramanathan, and E. Harrison, 1986: Comparison of regional clear-sky albedos inferred from satellite observations and model computations. *J. Clim. Appl. Meteorol.,* **25**, 214–226.

Broecker, W. S., D. M. Peteet, and D. Rind, 1985: Does the ocean-atmosphere system have more than one stable mode of operation? *Nature,* **315**, 21–26.

Bryan, F., 1986: High-latitude salinity effects and interhemispheric thermohaline circulations. *Nature,* **323**, 301–304.

Bryan, K., 1969: A numerical method for the study of the circulation of the World Ocean. *J. Comp. Phys.,* **4**, 347–376.

Bryan, K., and M. D. Cox, 1972: An approximate equation of state for numerical models of ocean circulation. *J. Phys. Oceanogr.,* **2**, 510–514.

Budyko, M. I., 1956: *Heat Balance of the Earth's Surface*. Leningrad: Gidrometeozidat.

Capotondi, A., and W. R. Holland, 1997: Thermohaline circulation variability in the CSM coupled integration and its influence on the North Atlantic model climate. *submitted to J. Climate,*.

Chang, P., L. Ji, and H. Li, 1997: A decadal climate variation in the tropical Atlantic Ocean from thermodynamic air-sea interactions. *Nature,* **385**, 516–518.

Chen, F., and M. Ghil, 1995: Interdecadal variability of the thermohaline circulation and high-latitude surface fluxes. *J. Phys. Oceanogr.,* **25**, 2547–2568.

Cox, M. D., 1984: A Primitive Equation three-dimensional model of the ocean. GFDL Ocean Group Tech. Rep. 1, GFDL, Princeton, NJ.

Cubasch, U., K. Hasselmann, H. Hock, E. Maier-Reimer, U. Mikolajewicz, B. D. Santer, and R. Sausen, 1992: Time-dependent greenhouse warming computations with a coupled ocean-atmosphere model. *Clim. Dyn.,* **8**, 55–69.

Danabasoglu, G., 1997: On the wind driven circulation of the uncoupled and coupled NCAR climate system ocean model. *submitted to J. Climate,*.

Delworth, T. L., 1996: North Atlantic interannual variability in a coupled ocean-atmosphere model. *J. Climate,* **9**, 2356–2375.

Delworth, T. L., S. Manabe, and R. J. Stouffer, 1993: Interdecadal variations of the thermohaline circulation in a coupled ocean-atmosphere model. *J. Climate,* **6**, 1993–2011.

Delworth, T. L., S. Manabe, and R. J. Stouffer, 1997: Multidecadal climate variability in the Greenland Sea and surrounding regions: a coupled model simulation. *Geophys. Res. Lett.,* **24**, 257–260.

Deser, C., M. A. Alexander, and M. S. Timlin, 1996: Upper-ocean thermal variations in the North Pacific during 1970-1991. *J. Climate,* **9**, 1840–1855.

Deser, C., and M. L. Blackmon, 1993: Surface climate variations over the North Atlantic ocean during winter: 1900-1989. *J. Climate,* **6**, 1743–1753.

Dickinson, R. E., A. Henderson-Sellers, and P. J. Kennedy, 1993: Biosphere-Atmosphere Transfer Scheme (BATS) version 1e as coupled to the NCAR Community Climate Model. NCAR Tech. Note NCAR TN-387 +STR, Natl. Cent. for Atmos. Res., Boulder, Co.

Drake, J., I. Foster, J. Michalakes, B. Toonen, and P. Worley, 1995: Design and performance of a scalable parallel community climate model. *Parallel Computing,* **21**(10), 1571–1591.

Drijfhout, S., C. Heinze, M. Latif, and E. Maier-Reimer, 1996: Mean circulation and internal variability in an ocean primitive equation model. *J. Phys. Oceanogr.,* **26**, 559–580.

Frankignoul, C., P. Muller, and E. Zorita, 1997: A simple model of the decadal response of the ocean to stochastic wind forcing. *J. Phys. Oceanogr.,* **27**, 1533–1546.

Frey, H., M. Latif, and T. Stockdale, 1997: The coupled GCM ECHO-2. Part I: The Tropical Pacific. *Mon. Wea. Rev.,* **125**, 703–720.

Gill, A., 1982: *Atmosphere-Ocean Dynamics.* Dordrecht: Academic Press.

Gordon, H. B., and S. P. O'Farrell, 1997: Transient climate change in the CSIRO coupled model with dynamics sea ice. *Mon. Wea. Rev.,* **125**, 875–907.

Graham, N. E., 1994: Decadal-scale climate variability in the tropical and North Pacific during the 1970s and 1980s: observations and model results. *Clim.*

Dyn., **10**, 135–162.

Greatbatch, R. J., and K. A. Peterson, 1996: Interdecadal variability and oceanic thermohaline adjustment. *J. Geophys. Res.,* **101**, 20467–20482.

Greatbatch, R. J., and S. Zhang, 1995: An interdecadal oscillation in an idealized ocean basin forced by constant heat flux. *J. Climate,* **8**, 81–91.

Griffies, S. M., and E. Tziperman, 1995: A linear thermohaline oscillator driven by stochastic atmospheric forcing. *J. Climate,* **8**, 2440–2453.

Gropp, W., E. Lusk, and A. Skjellum, 1994: *Using MPI: Portable Parallel Programming with the Message-Passing Interface*. Cambridge: MIT Press.

Gu, D., and S. G. H. Philander, 1997: Internal climate fluctuations that depend on exchanges between the tropics and the extratropics. *Science,* **275**, 805–807.

Guilyarid, E., and G. Madec, 1997: Performance of the OPA/ARPEGE-T21 global ocean-atmosphere coupled model. *Clim. Dyn.,* **13**, 149–165.

Gutzler, D. S., 1996: Low-frequency ocean-atmosphere variability across the tropical western Pacific. *J. Atmos. Sci.,* **53**, 2773–2785.

Hack, J. J., 1994: Parameterization of moist convection in the National Center for Atmospheric Research community climate model (CCM2). *J. Geophys. Res.,* **99**, 5551–5568.

Hack, J. J., B. A. Boville, B. P. Briegleb, J. T. Kiehl, P. J. Rasch, and D. L. Williamson, 1993: Description of the NCAR Community Climate Model (CCM2). NCAR Tech. Note NCAR/TN-382+STR, Natl. Cent. for Atmos.

Res., Boulder, Co.

Hack, J. J., B. A. Boville, J. T. Kiehl, P. J. Rasch, and D. L. Williamson, 1994: Climate statistics from the National Center for Atmospheric Research community climate model CCM2. *J. Geophys. Res.,* **99**(D10), 20,785–20,813.

Hack, J. J., J. T. Kiehl, and J. W. Hurrell, 1997: The hydrologic and thermodynamic charactersics of the NCAR CCM3. *submitted to J. Climate,.*

Haney, R. L., 1971: Surface thermal boundary condition for ocean circulation models. *J. Phys. Oceanogr.,* **1**, 241–248.

Harman, H. H., 1967: *Modern Factor Analysis*. Chicago: University of Chicago Press.

Hastenrath, S., 1986: *Climate and Circulation of the Tropics*. Dordrecht: D. Reidel Publishing Company.

Hellerman, S., and M. Rosenstein, 1983: Normal monthly windstress over the World Ocean with error estimates. *J. Phys. Oceanogr.,* **13**, 1093–1104.

Holtslag, A. A. M., and A. C. M. Beljaars, 1989: Suface flux parameterization schemes: Developments and experiences at KNMI. In *Parameterization of fluxes over land surface, October 24–26,1988*, ECWMF Workshop Proceedings, Reading UK. ECMWF.

Holtslag, A. A. M., E. I. F. de Bruijn, and H. L. Pan, 1990: A high resolution air mass transformation model for short-range weather forecasting. *Mon. Wea. Rev.,* **118**, 1561–1575.

Horel, J. D., 1981: A rotated principle component analysis of the interannual variability of the Northern Hemisphere 500 mb heigh field. *Mon. Wea. Rev.,* **109**, 2080–2092.

Horel, J. D., 1984: Complex principal component analysis: Theory and examples. *J. Clim. Appl. Met.,* **23**, 1660–1673.

Huang, R. X., and R. L. Chou, 1994: Parameter sensitivity study of the saline circulation. *Climate Dyn.,* **9**, 391–409.

Hurrel, J. W., J. J. Hack, and D. P. Baumhefner, 1993: Comparison of the NCAR Community Climate Model (CCM) Climates. NCAR Tech. Note NCAR/TN-395+STR, Natl. Cent. for Atmos. Res., Boulder, Co.

Johns, T. C., R. E. Carnell, J. F. Crossley, J. M. Gregory, J. F. B. Mitchell, C. A. Senior, S. F. B. Tett, and R. A. Wood, 1997: The second Hadley Centre coupled ocean-atmosphere GCM: model description, spinup and validation. *Clim. Dyn.,* **13**, 103–134.

Kawamura, R., 1994: A rotated EOF analysis of global sea surface temperatue variability with interannual and interdecadal scales. *J. Phys. Oceanogr.,* **24**, 707–715.

Kiehl, J. T., 1994: Sensitivity of a GCM climate simulation to differences in continental versus maritime cloud drop size. *J. Geophys. Res.,* **99**, 23107–23115.

Kiehl, J. T., and B. P. Briegleb, 1991: A new parameterization of the absorptance due to the 15 μm band system of carbon dioxide. *J. Geophys. Res.,* **96**, 9013–9019.

Kiehl, J. T., J. J. Hack, G. B. Bonan, B. A. Boville, B. P. Briegleb, D. L. Williamson, and P. J. Rasch, 1996: Description of the NCAR Community Climate Model (CCM3). NCAR Tech. Note NCAR/TN-420+STR, Natl. Cent. for Atmos. Res., Boulder, Co.

Kiehl, J. T., J. J. Hack, and B. P. Briegleb, 1994: The simulated Earth radiation budget of the National Center for Atmospheric Research community climate model CCM2 and comparisons with the Earth Radiation Budget Experiment (ERBE). *J. Geophys. Res.,* **99**, 20815–20827.

Killworth, P. D., D. Stainforth, D. J. Webb, and S. M. Patterson, 1991: The development of a free-surface Bryan-Cox-Semtner ocean model. *J. Phys. Oceanogr.,* **21**, 1333–1348.

Knutson, T. R., and S. Manabe, 1997: Simulated ENSO in a global coupled ocean-atmosphere model: Multidecadal amplitude modulation and CO_2 sensitivity. *J. Climate,* **10**, 138–161.

Kushnir, Y., 1994: Interdecadal variations in North Atlantic sea surface temperature and associated atmospheric conditions. *J. Climate,* **7**, 141–157.

Latif, M., 1996: Dynamics of interdecadal variability in coupled ocean-atmosphere models. White paper prepared for the CLIVAR "Ocean Program for DecCen climate variability" workshop, 28-31 October 1996, Villefranche-sur-mer, France. pp. 47.

Latif, M., and T. P. Barnett, 1996: Decadal climate variability over the North Pacific and North America: Dynamics and predictability. *J. Climate,* **9**, 2407–2423.

Latif, M., A. Grotzner, M. Munnich, E. Maier-Reimer, S. Venzke, and T. P. Barnett, 1996: A mechanism for decadal climate variability in *Decadal Climate Variability: Dynamics and Predictability*, D. L. T. Anderson and J. willebrand, eds., Springer. pp. 263–292.

Latif, M., R. Kleeman, and C. Eckert, 1997: Greenhouse warming, decadal variability, or El Nino? an attempt to understand the anomalous 1990s. *J. Climate,* **10**, 2221–2239.

Latif, M., T. Stockdale, J. Wolff, G. Burgers, E. Maier-Reimer, M. M. Junge, K. Arpe, and L. Bengtsson, 1994: Climatology and variability in the ECHO coupled GCM. *Tellus,* **46A**, 351–366.

Levitus, S., 1982: Climatological Atlas of the World's Ocean. NOAA Prof Paper no. 13, NOAA, Washington, DC.

Liu, Z., S. G. H. Philander, and R. C. Pacanowski, 1994: A GCM study of tropical-subtropical upper-ocean water exchange. *J. Phys. Oceanogr.,* **24**, 2606–2623.

Louis, J.-F., M. Tiedtke, and J. F. Geleyn, 1982: A short history of the operational PBL–parameterization at ECMWF. In *Workshop on Planetary Boundary Layer Parameterization, November 25–27, 1981*, ECWMF Workshop Proceedings, Reading UK. ECMWF.

Maier-Reimer, E., U. Mikolajewicz, and K. Hasselmann, 1993: Mean circulation of the Hamburg LSG OGCM and its sensitivity to the thermohaline surface forcing. *J. Phys. Oceanogr.,* **23**, 731–757.

Manabe, S., 1969: Climate and ocean circulation. 1: The atmosphere circulation

and the hydrology of the earth's surface. *Mon. Wea. Rev.,* **97**, 739–773.

Manabe, S., M. J. Spelman, and R. J. Stouffer, 1992: Transient responses of a coupled ocean-atmosphere model to gradual changes of atmosphere CO_2. Part II: Seasonal response. *J. Climate,* **5**, 105–126.

Manabe, S., and R. J. Stouffer, 1988: Two stable equilibria of a coupled ocean-atmosphere model. *J. Climate,* **1**, 841–866.

Manabe, S., and R. J. Stouffer, 1994: Multiple-century response of a coupled ocean-atmosphere model to an increase of atmospheric carbon dioxide. *J. Climate,* **7**, 5–23.

Manabe, S., and R. J. Stouffer, 1996: Low-frequency variability of surface air temperature in a 1000-year integration of a coupled atmosphere-ocean-land surface model. *J. Climate,* **9**, 376–393.

Manabe, S., R. J. Stouffer, M. J. Spelman, and K. Bryan, 1991: Transient responses of a coupled ocean-atmosphere model to gradual changes of atmosphere CO_2. Part I: Annual mean response. *J. Climate,* **4**, 785–818.

Marotzke, J., 1989: Instabilities and multiple steady states of the thermohaline ciculation. in *Oceanic Circulation Models: Combining Data and Dynamics*, D. L. T. Anderson and J. Willebrand, eds., Kluwer Academic. pp. 501–511.

Marotzke, J., P. Welander, and J. Willebrand, 1988: Instability and multiple steady states in a meridional-plane model of the thermohaline circulation. *Tellus,* **40A**, 162–172.

Matthews, E., 1983: Global vegetation and land use: New high-resolution data

bases for climate studies. *J. Clim. Appl. Meteor.,* **22**, 474–487.

McFarlane, N. A., 1987: The effect of orographically excited wave drag on the general circulation of the lower stratosphere and troposphere. *J. Atmos. Sci.,* **44**, 1775–1800.

Mechoso, C. R., *et al.*, 1995: The seasonal cycle over the Tropical Pacific in coupled ocean-atmosphere general circulation models. *Mon. Wea. Rev.,* **123**, 2825–2838.

Meehl, G. A., 1990: Development of global coupled ocean-atmosphere general circulation models. *J. Phys. Oceanogr.,* **21**, 1372–1385.

Meehl, G. A., 1995: Global coupled general circulation models. Scripps meeting 10-12 October 1994, La Jolla CA. *Bull. Am. Meterol. Soc,* **76**, 951–957.

Meehl, G. A., and J. Arblaster, 1997: The Asian-Australian Monsoon and ENSO in the NCAR CSM. *submitted to J. Climate,*.

Mikolajewicz, U., and E. Maier-Reimer, 1990: Internal secular variability in an ocean general circulation model. *Climate Dyn.,* **4**, 145–156.

Miller, A. J., D. R. Cayan, T. P. Barnett, N. E. Graham, and J. M. Oberhuber, 1994: Interdecadal variability of the Pacific ocean: model response to observed heat flux and wind stress anomalies. *Clim. Dyn.,* **9**, 287–302.

Miller, J. R., G. L. Russell, and G. Caliri, 1994: Continental-scale river flow in climate models. *J. Climate,* **7**, 914–928.

Milliman, J. D., and R. H. Meade, 1983: World-wide delivery of river sediment to the oceans. *J. Geol.,* **91**, 1–21.

Moore, A. M., and C. J. C. Reason, 1993: The response of a global ocean general circulation model to climatological surface boundary conditions for temperature and salinity. *J. Phys. Oceanogr.,* **23**, 300–328.

Mysak, L. A., T. F. Stocker, and F. Huang, 1993: Century-scale variability in a randomly forced, two-dimensional thermohaline ocean circulation model. *Climate Dyn.,* **8**, 103–116.

Nakamure, H., G. Lin, and T. Yamagata, 1997: Decadal climate variability in the North Pacific during the recent decades. *Bull. Am. Meterol. Soc,* **78**, 2215–2225.

Namias, J., 1959: Recent seasonal interaction between the North Pacific waters and the overlying atmospheric circulation. *J. Geophys. Res.,* **64**, 631–646.

Neelin, J. D., *et al.*, 1992: Tropical air-sea interaction in general circulation models. *Climate Dynamics,* **7**, 73–104.

Neelin, J. D., and H. A. Dijkstra, 1995: Ocean-atmosphere interaction and the tropical climatology. Part I: The dangers of flux correction. *J. Climate,* **8**, 1325–1342.

Neelin, J. D., M. Latif, and F.-F. Jin, 1994: Dynamics of coupled ocean-atmosphere models: The Tropical Problem. *Annu. Rev. Fluid Mech.,* **26**, 617–659.

O'Brien, J. J., 1986: Time integration schemes. In *Advanced Physical Oceanographic Numerical Modelling*, O'Brien, Ed., D. Reidel. pp. 155–164.

Oppenheim, A. V., and R. W. Schafer, 1975: *Digital Signal Processing.* New

Jersey: Prentice-Hall.

Osborn, T. J., 1997: Thermohaline oscillations in the LSG OGCM: Propagating anomalies and sensitvity to parameterizations. *J. Phys. Oceanogr.,* **27**, 2233–2255.

Pacanowski, R., K. Dixon, and A. Rosait, 1991: The GFDL Modular Ocean Model users guide. GFDL Ocean Group Tech. Rep. 2, GFDL, Princeton, NJ.

Pacanowski, R. C., and S. G. H. Philander, 1981: Parameterization of vertical mixing in numerical models of tropical oceans. *J. Phys. Oceanogr.,* **11**, 1443–1451.

Peixoto, J. P., and A. H. Oort, 1992: *Physics of Climate.* New York: American Institute of Physics.

Peters, H., M. C. Gregg, and J. M. Toole, 1988: On the parameterization of equatorial turbulence. *J. Geophys. Res.,* **92**, 1199–1218.

Philander, S. G., 1990: *El-Niño, La Niña, and the Southern Oscillation.* San Diego: Academic Press.

Pickard, G. L., and W. J. Emery, 1990: *Descriptive Physical Oceanography: An Introduction. 5th edition.* Oxford: Paragon Press.

Pierce, D. W., T. P. Barnett, and U. Mikolajewicz, 1995: Competing roles of heat and freshwater flux in forcing thermohaline oscillations. *J. Phys. Oceanogr.,* **25**, 2046–2064.

Pollard, R. T., and R. C. Millard, 1977: Comparsion between observed and

simulated wind-generated inertial oscillations. *Mon. Wea. Rev.,* **9**, 813–821.

Rasch, P. J., and D. L. Williamson, 1990: Computational aspects of moisture transport in global models of the atmosphere. *Quart. J. Roy. Meteor. Soc.,* **116**, 1071–1090.

Robertson, A. W., 1996: Interdecadal variability over the North Pacific in a multi-century climate simulation. *Clim. Dyn.,* **12**, 227–241.

Rooth, C., 1982: Hydrology and ocean circulation. *Prog. Oceanog.,* **11**, 131–149.

Russell, G. L., J. R. Miller, and D. Rind, 1995: A coupled atmosphere-ocean model for transient climate change studies. *Atmos-Ocean,* **4**, 683–730.

Sarachik, E. S., M. Winton, and F. L. Yin, 1996: Mechanisms for decadal-to-centennial climate variability. in *Decadal Climate Variability: Dynamics and Predictability*, D. L. T. Anderson and J. Willebrand, eds., Springer. pp. 157–210.

Sausen, R., K. Barthel, and K. Hasselmann, 1988: Coupled ocean-atmosphere models with flux correction. *Clim. Dyn.,* **2**, 145–163.

Sausen, R., and M. Ponater, 1990: Reducing the initial drift of a GCM. *Beitr. Phys. Atmosph.,* **63**, 15–24.

Shea, D. J., K. E. Trenberth, and R. W. Reynolds, 1990: A global monthly sea surface temperature climatology. NCAR Tech. Note NCAR/TN-345+STR, Natl. Cent. for Atmos. Res., Boulder, Co.

Simmons, A. J., and R. Strufing, 1983: Numerical forecasts of stratospheric warming events using a model with a hybrid vertical coordinate. *Quart. J.*

Roy. Meteor. Soc., **109**, 81–111.

Slingo, A., 1989: A GCM parameterization for the shortwave radiative properties of water clouds. *J. Atmos. Sci.,* **46**, 1419–1427.

Slingo, J. M., 1987: The development and verification of a cloud prediction scheme for the ECMWF model. *Quart. J. Roy. Meteor. Soc.,* **113**, 899–927.

Stocker, T. F., 1996: An overview of century time-scale variability in the climate system: Observations and models. in *Decadal Climate Variability: Dynamics and Predictability*, D. L. T. Anderson and J. Willebrand, eds., Springer. pp. 379–406.

Stocker, T. F., and L. A. Mysak, 1992: Climatic fluctuations of the century time scale: a review of high-resolution proxy data and possible mechansms. *Clim. Change,* **20**, 227–250.

Stommel, H., 1961: Thermohaline convection with two stable regimes of flow. *Tellus,* **13**, 224–230.

Stouffer, S. M. . R. J., 1995: Simulation of abrupt climate change induced by freshwater induced by freshwater input to the North Atlantic Ocean. *Nature,* **378**, 165–167.

Sundqvist, H., 1988: Parameterization of condensation and associated clouds in models for weather prediction and general circulation simulation. in *Physically Based Modelling and Simulation of Climate and Climatic Change*, Schlesinger, Ed., Kluwer Academic. pp. 433–461.

Tobis, M., 1996. *Effect of Slowed Barotropic Dynamics in Parallel Ocean Climate*

Models. Ph. D. thesis, University of Wisconsin-Madison.

Trenberth, K. E., and J. W. Hurrell, 1994: Decadal atmosphere-ocean variations in the Pacific. *Clim. Dyn,* **9**, 303–319.

Troen, I., and L. Mahrt, 1986: A simple modle of the atmospheric boundary layer; Sensitivity to surface evaporation. *Boundary-Layer Meteor.,* **37**, 129–148.

Tziperman, E., J. R. Toggweiler, Y. Feliks, and K. Bryan, 1994: Instability of the thermohaline circulation with respect to mixed boundary conditions: Is it really a problem for realistic models? *J. Phys. Oceanogr.,* **24**, 217–232.

Vogelezang, D. H. P., and A. A. M. Hotslag, 1996: Evaluation and model impacts of alternative boundary-layer height formulations. *Boundary-Layer Meteorol.,* **81**, 245–269.

von Storch, J.-S., V. V. Kharin, G. C. Hegerl, D. Schriever, H. von Storch, and E. Zorita, 1997: A description of a 1260-year control integration with the coupled ECHAM/LSG general circulation model. *J. Climate,* **10**, 1525–1543.

Walin, G., 1985: The thermohaline circulation and the control of ice ages. *Palaeogegr., Palaeoclimatol, Palaeoecol.,* **50**, 323–332.

Warren, B. A., 1981: Deep circulation of the world ocean in *Evolution of Physical Oceanography*, Warren and Wunsch, eds., MIT Press. pp. 6–40.

Washington, W. M., and G. A. Meehl, 1989: Climate sensitivity due to increased CO_2: experiments with a coupled atmosphere and ocean general circulation

model. *Clim. Dyn.,* **4**, 1–38.

Weaver, A. J., J. Marotzke, P. F. Cummins, and E. S. Sarachik, 1993: Stability and variability of the thermohaline circulation. *J. Phys. Oceanogr.,* **23**, 39–60.

Weaver, A. J., and E. S. Sarachik, 1991a: Evidence for decadal variability in an ocean general circulation model: An advective mechanism. *Atmos.-Ocean,* **29**, 197–231.

Weaver, A. J., and E. S. Sarachik, 1991b: The role of mixed boundary conditions in numerical models of the ocean's climate. *J. Phys. Oceanogr.,* **21**, 1470–1493.

Weyl, P. K., 1968: The role of the oceans in climate change: a theory of the ice ages. *Meteor. Monographs,* **8**, 37–62.

Williamson, D. L., J. T. Kiehl, and J. J. Hack, 1995: Climate sensitivity of the NCAR Community Climate Model (CCM2) to horizontal resolution. *Climate Dynamics,* **11**, 377–397.

Williamson, D. L., J. T. Kiehl, V. Ramanathan, R. E. Dickinson, and J. J. Hack, 1987: Description of NCAR Community Climate Model (CCM1). NCAR Tech. Note NCAR/TN-285+STR, Natl. Cent. for Atmos. Res., Boulder, Co.

Williamson, D. L., and P. J. Rash, 1994: Water vapor transport in the NCAR CCM2. *Tellus,* **46A**, 34–51.

Winton, M., 1996: The role of horizontal boundaries in parameter sensitivity and decadal-scale variability of coarse-resolution ocean general circulation

models. *J. Phys. Oceanogr.,* **26**, 289–304.

Winton, M., 1997: The damping effect of bottom topography on internal decadal-scale oscillations of the thermohaline circulation. *J. Phys. Oceanogr.,* **27**, 203–208.

Winton, M., and E. S. Sarachik, 1993: Thermohaline oscillations induced by strong steady salinity forcing of ocean general circulation models. *J. Phys. Oceanogr.,* **23**, 1389–1410.

Yin, F. L., and E. S. Sarachik, 1995: Interdecadal thermohaline oscillations in a sector ocean general circulation model: Advective and convective processes. *J. Phys. Oceanogr.,* **25**, 2465–2484.

Zebiak, S. E., and M. A. Cane, 1991: Natural climate variability in a coupled model in *Greenhouse-Gas-Induced Climatic Change*, M. E. Schlesinger, ed., Elsevier. pp. 457–469.

Zhang, G. J., 1994: Effects of cumulus convection on the simulated monsoon circulation in a general circulation mode. *J. Geophys. Res.,* **122**, 2022–2038.

Zhang, G. J., and N. A. McFarlane, 1995: Sensitivity of climate simulations to the parameterization of cumuls convection in the Canadian Climate Center general circulation model. *Atmo-Ocean,* **33**, 407–446.

Zhang, R.-H., and S. Levitus, 1997: Structure and cycle of decadal variability of upper-ocean temperature in the north pacific. *J. Climate,* **10**, 710–727.

Zhang, S., R. J. Greatbatch, and C. A. Lin, 1993: A reexamination of the polar halocline catastrophoe and implications for coupled ocean-atmosphere

modeling. *J. Phys. Oceanogr.,* **23**, 287–299.

Zhang, S., C. A. Lin, and R. J. Greatbatch, 1995: A decadal oscillation due to the coupling between an ocean circulation model and a thermodynamic sea-ice model. *J. Mar. Res.,* **53**, 79–106.

Zorita, E., and C. Frankignoul, 1997: Modes of North Atlantic decadal variability in the ECHAM1/LSG coupled ocean-atmosphere general circulation model. *J. Climate,* **10**, 183–200.